THESIS FOR THE DEGREE OF DOCTOR OF PHILOSOPHY

Surface Integrity of Case-hardened Gears – with Particular Reference to Running-in and Micropitting

DINESH MALLIPEDDI

Department of Industrial and Materials Science
CHALMERS UNIVERSITY OF TECHNOLOGY
Gothenburg, Sweden 2018

Surface Integrity of Case-hardened Gears-with Particular Reference to Running-in and Micropitting

DINESH MALLIPEDDI

ISBN 978-91-7597-796-6
Doktorsavhandlingar vid Chalmers tekniska högskolan
Ny serie Nr 4477
ISSN: 0346-718X

Department of Industrial and Materials Science
Chalmers University of Technology
SE-412 96 Gothenburg
Sweden
Telephone +46(0)31-7721000

Printed by Chalmers Reproservice

Gothenburg, Sweden 2018

To my parents
Dhanalakshmi and Ramoji

Surface Integrity of Case-hardened Gears – with Particular Reference to Running-in and Micropitting

Dinesh Mallipeddi
Department of Industrial and Materials Science
Chalmers University of Technology

Abstract

A gearbox with gears of different sizes is part of a vehicle transmission system and plays an important part in transmitting the engine power to the wheels. The efficient energy transmission highly relies on the performance of gears. Together, the mesh efficiency and durability determines the performance of gears.

The hard finishing of gear surfaces by means of different methods; grinding, honing and superfinishing etc., produces unique characteristics in terms of surface roughness, microstructure and residual stresses. These characteristics of tooth affect the gear performance. Running-in process is known to alter them along with surface chemistry and presets the gear for service. This fact creates an interest to understand the initial running-in with the purpose to improve the performance of gears. Thus, this study addressed, the influence of running-in on the evolution of surface characteristics generated by the mentioned methods, and how they developed further during initial usage, represented by efficiency test. Gears tested in a FZG back-back test rig were characterized by combining different analytical techniques. These included scanning electron microscopy (SEM), transmission electron microscopy (TEM), X-ray diffraction (XRD) and X-ray photoelectron spectroscopy (XPS). Surface roughness was found to be the most influential factor and virtually all changes were confined to ~5 μm below the surface. The running-in process smoothened the surface asperities through plastic deformation and the severity of deformation increased with load. Micropitting was also associated with asperity deformation and hence only seen in ground and honed gears, while being absent for superfinished gears. Micropitting was promoted by higher running-in load and this trend continued for subsequent efficiency testing. The running-in load also promoted the deformation bands frequently found in connection with the cracks. Compressive residual stresses beneficial for fatigue life varied between finishing methods, highest stresses recorded for honed gears. The stresses differed between profile and axial direction after manufacturing and, reached similar levels after efficiency testing, but remained compressive throughout the test. The initial increase in compressive residual stresses was linked to retained austenite transformation and its later decrease to crack formation. The indicated tribofilm formation was connected to the surface roughness and promoted by running-in load.

Micropitting is a surface contact fatigue failure that occurs in all types of gears. This failure mechanism was also investigated from material perspective. Gears were tested in a sequence from 200 to 2.2 x 10^7 cycles. The micropitting initiated due to the deformation of asperities and associated microstructural changes; plastically deformed regions (PDR) and deformation bands (thin martensite lath with epsilon carbides precipitated at boundaries). These structural changes started already within 200 cycles and cracks occurred after 2000 cycles, signifying that micropitting can initiate already after short period of operation. Thus, the running-in of gears from materials perspective can be as short as 2000 cycles. The findings presented are expected to contribute to the technical and industrial aims for optimized gear preparation.

Keywords: Gears, running-in, micropitting, surface asperities, residual stresses, surface chemistry, plastic deformed regions (PDR), deformation bands

Preface

This thesis is based on the work performed at the Department of Industrial and Materials Science, Chalmers University of Technology. The work has been carried out under the supervision of Senior Lecturer Mats Norell and Professor Lars Nyborg.

This thesis consists of an introductory part followed by the appended papers:

Paper I: **Stress distribution over gear teeth after grinding, running-in and efficiency testing**
D. Mallipeddi, M. Norell, M. Sosa, L. Nyborg
International Conference on Gears in VDI-Berichte 2255.2, (2015) pp. 973- 984, 2015.

Paper II: **Influence of running-in on the surface characteristics of efficiency tested ground gears**
D. Mallipeddi, M. Norell, M. Sosa, L. Nyborg
Tribology International, Vol. 115, (2017), pp. 45-58

Paper III: **Effect of running-in load and speed on surface characteristics of honed gears**
D. Mallipeddi, M. Norell, M. Sosa, L. Nyborg
Submitted for publication in Tribology Transactions

Paper IV: **The effect of manufacturing method and running-in load on the surface integrity characteristics of efficiency tested ground, honed and superfinished gears**
D. Mallipeddi, M. Norell, M. Sosa, L. Nyborg
Submitted for publication in Tribology International

Paper V: **Localized deformation in nano-sized martensite laths associated with micropitting in case carburized gears**
D. Mallipeddi, X. Zhang, H. Alimadadi, M. Norell, L. Nyborg, M. Näslund
Submitted for publication in Scripta Materialia

Paper VI: **Micropitting and microstructural evolution during contact fatigue testing of gears-from initial cycles to failure**
D. Mallipeddi, M. Norell, L. Nyborg, V.M. Subbaramaiah Naidu, M. Näslund
Manuscript

Paper not appended to the thesis:

Paper A: **Effect of shot peening on the residual stress and mechanical behaviour of low-temperature and high temperature annealed martensitic gear steel 18CrNiMo7-6.**
R. Yang, X. Zhang, D. Mallipeddi, N. Angelou, H. L. Toftegaard, Y. Li, J. Ahlström, L. Lorentzen, G. Wu, X. Huang.
IOP conference series: Materials Science and Engineering, Vol 219, (2017

Contribution to the appended papers

My contribution to the appended papers is as follows:

Paper I: The planning of gear testing and actual testing were done by co-author M. Sosa. I performed all the stress measurements. The first draft of the paper was written by me and finalised in close collaboration with co-author Mats Norell.

Paper II: The planning of the tests and actual testing were done by co-author M. Sosa. I performed all the characterization work. The first draft of the paper was written by me and finalised in collaboration with co-authors.

Paper III: The work was planned in collabration with co-authors. The testing was performed by co-author M. Sosa. I performed all the characterization work. The first draft of the paper was written by me and finalised in close collabration with the co- author Mats Norell.

Paper IV: The work was planned in collabration with co-authors. The testing was performed by co-author M. Sosa. I performed all the characterization work. The first draft of the paper was written by me and finalised in close collabration with co-authors Mats Norell and Lars Nyborg.

Paper V: The test matrix was designed by me and optimized with the co-authors Mats Norell and Matti Näslund. I performed the gear testing together with Master's thesis student V.M. Subbaramaiah Naidu. Initial microstructure characterization using SEM was performed by me. The preparation of the TEM specimens using FIB was done by co-author Hossein Alimadadi. All the TEM characterization was performed by co-author Xiaodan Zhang. Both me and Xiaodan Zhang wrote the first draft of the paper together and finalised it with co-authors Mats Norell and Lars Nyborg.

Paper VI: The test matrix was designed by me and optimized with the co-authors Mats Norell and Matti Näslund. I performed the testing together with Master's thesis student V.M. Subbaramaiah Naidu. I performed all the surface and material characterization, except residual stress measurements that were done by V.M. Subbaramaiah Naidu under my supervision. The first draft of the paper was written by me and was finalised with the co-author's Mats Norell and Lars Nyborg.

Transmission Cluster

Scania CV, AB Volvo, Chalmers University of Technology and KTH (Royal Institute of Technology) together have started a research network called “Transmission cluster” with the aim to improve overall drive train efficiency. As the name indicates the network is a cluster of sub-projects where individual projects address a particular area of drive train challenges. The work presented in this thesis is a part of transmission cluster project that is connected to the performance of gears. The main goal of this PhD thesis project has been to contribute to the improved efficiency and longevity of transmission gears by characterizing, understanding and optimizing the running-in process. This project was first funded by **Swedish Energy Agency** and then **Swedish Innovation Agency** (Vinnova**)**, and sponsored two PhD students, one at KTH and one at Chalmers. The work has been distributed in such a way that the PhD student, M. Sosa at KTH, has focused on gear testing and development of the simulation models to predict the running-in process. To develop real time knowledge and experimental data, KTH has FZG back-back gear test rig that can measure energy losses for varied test parameters. The test rig is also equipped with profilometer giving the possibility to capture the surface topography in-situ. In parallel, the PhD student D. Mallipeddi at Chalmers, has focused on surface and material characterization of tested gears. To characterize surface characteristics of gears, Chalmers has analytical instruments such as high resolution scanning electron microscope (SEM), X-ray photoelectron spectroscopy (XPS) and X-ray diffraction (XRD). The work has also included co-operation with Technical University of Denmark (DTU), regarding dedicated TEM characterization.

Nomenclature of spur gears

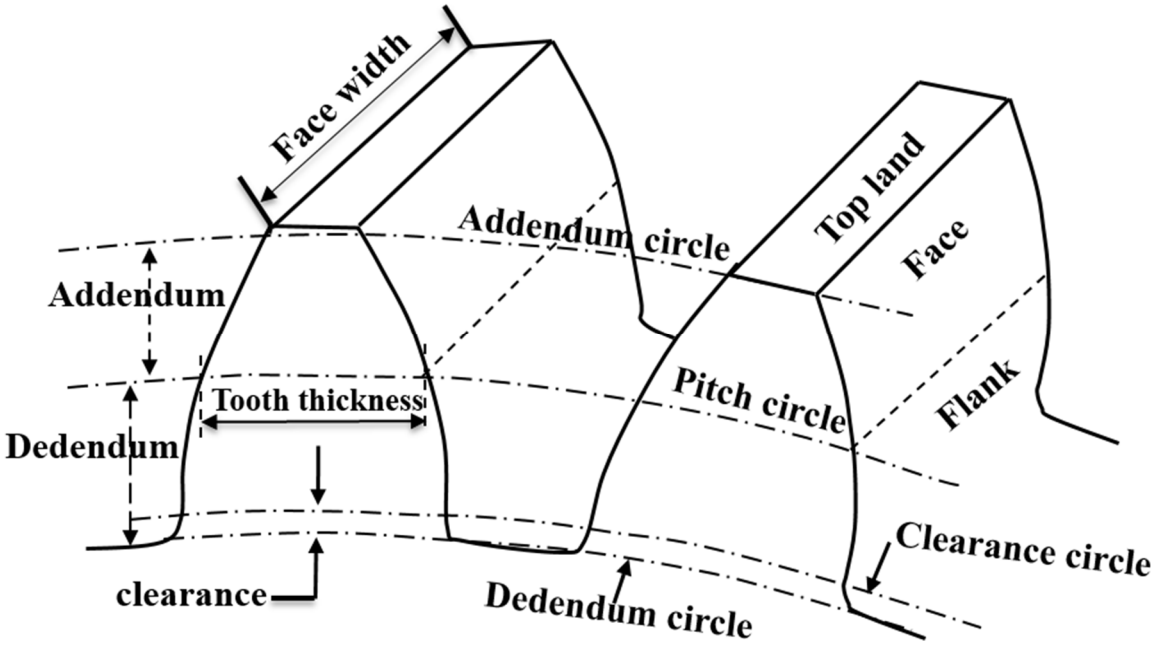

Pitch circle: A normal section of the pitch surface

Addendum circle: A circle bounding the ends of the teeth, in a normal section of the gear.

Dedendum circle: The circle bounding the space between the teeth, in a normal section of the gear.

Pitch surface: The surface of the imaginary rolling cylinder that replaces the toothed gear.

Addendum: The radial distance between the pitch circle and the addendum circle.

Dedendum: The radial distance between the pitch circle and the root circle.

Face of a tooth: The part of the tooth surface lying outside the pitch surface.

Flank of a tooth: The part of the tooth surface lying inside the pitch surface.

Top land: The top surface of a gear tooth.

Clearance: The difference between the dedendum of one gear and the addendum of the mating gear.

Width of space: The distance between adjacent teeth measured on the pitch circle.

Tooth space: The space between successive teeth.

Pressure angle: Angle between the line of action and a line perpendicular to the line of centres.

Back lash: The difference between the tooth thickness of one gear and the tooth space of the mating gear

Table of Contents

1 Introduction 1

1.1 Research objective 1

1.2 Research methodology 2

1.3 Limitations 3

2 Background 5

2.1 Gear geometry 5

2.2 Surface contact related gear failures 5

2.2.1 Micropitting 5

2.2.2 Pitting 6

2.2.3 Spalling 7

2.2.4 Wear 7

2.3 Stress conditions in a gear tooth 8

2.3.1 Contact stress 8

2.4 Lubrication 9

2.5 Gear box efficiency and power losses 11

3 Running-in: a literature survey 13

3.1 Running-in by definition 13

3.2 Running-in mechanisms 13

3.3 Running-in of gears 15

4 Micropitting: a literature survey 17

5 Overview of gear surface characteristics 19

5.1 Topography 19

5.2 Residual stresses 20

5.2.1 Thermal stresses 21
5.2.2 Transformation stress 21
5.3 Microstructure 22
5.4 Surface chemistry 24
6 Deformation mechanisms 27
6.1 Slip 27
6.2 Twinning 28
6.3 Plastic deformation of polycrystals 29
7 Gear manufacturing and work material 31
8 Experimental details and analysis techniques 33
8.1 Back- to- back test rig 33
8.1.1 Running-in 33
8.1.2 Efficiency testing 33
8.1.3 Micropitting testing 34
8.1.4 Gear geometry 34
8.2 Microstructure characterization 35
8.2.1 Scanning electron microscopy (SEM) 35
8.2.2 Sample preparation 35
8.2.3 Transmission electron microscopy (TEM) 36
8.2.4 Sample preparation for TEM 36
8.3 X-ray diffraction 37
8.3.1 Theoretical background of X-ray diffraction – Residual stress measurements 37
8.3.2 Gear flank mapping for surface residual stress measurements 39

8.3.3 In-depth measurements 40
8.3.4 Retained austenite measurements 43
8.4 X-ray photoelectron spectroscopy 43
9 Summary of results and discussion 45
9.1 Surface integrity characteristics of as-manufactured gears 45
9.2 Running-in and efficiency testing 49
9.3 Micropitting 53
10 Conclusions 61
11 Suggestions for future work 63
12 Acknowledgements 65
13 References 67

1 Introduction

Gears are toothed wheels that transmit power from one shaft to another by meshing one another without any slip. The origin of gears can be traced back to 27th century BC. Primitively, they were made of wood and commonly greased with animal fat. The industrial revolution in 19th century escalated the usage of metallic gears in different applications like clocks, water mills, irrigation devices and powered machines, etc. Since then, the science and technology regarding gear manufacturing, design and materials have shown continuous development. Today, gears are used in nearly all power transmission applications. Modern technological advancements have increased the efficiency and durability of gears especially in automotive industry. Still, strive for greater performance enhancement is increasing due to stringent global demands on sustainability and energy consumption.

In heavy duty vehicles, the gearbox is comprised of various combinations of gear drives for attaining different torques and speeds. Of course, not all gears are engaged at the same time for transmitting load, only some are engaged and others roll freely. However, both load carrying and non-load carrying gears, along with bearings, seals and lubricant constitutes for the overall energy losses of a gearbox [1]. Therefore, minimizing energy losses by addressing load dependent and no-load dependent losses can be helpful to further improve the efficiency of a gearbox. Load dependent losses mainly originate from friction between mating gears and are greatly affected by surface topography and chemistry developed from additives in the lubricant.

Gears fail in many ways but primarily due to fatigue [2]. Typically, fatigue failure starts with crack initiation that later progresses into the surface with repeated loading and finally ends by separating a micro- or macro-section from the bulk material. Amongst different modes of surface contact failures, micropitting has been increasingly observed in automotive gear industry. Progression of micropitting creates profile degradation, elevates noise and vibration levels, and further continuation can eventually lead to catastrophe in the form of macro-pitting, spalling and tooth fracture.

The performance of gears is determined by both the efficiency and durability. It is well known that the surface roughness, generated by the hard finishing process has significant influence on the performance of gears. This undesirable surface roughness can be further smoothened before usage via running-in process. However, depending on the running-in conditions used, the surface characteristics topography, residual stresses, microstructure and tribo chemistry evolve differently, which can be beneficial or detrimental during the service.

1.1 Research objective

The main aim of this thesis study is to understand the running-in process in the context of enhancing the performance of gears. Many research studies have previously investigated running- in process from different perspective such as friction, wear and surface transformation (roughness), etc., while from material perspective it was seldom studied. This thesis study focuses on understanding the running-in process from a material point of view. To address this overall goal, the present study is divided into the following questions:

Hard Finishing

- What are the differences in surface characteristics generated by different manufacturing methods; ground, honed and superfinished?
- How the generated characteristics do responds to the running-in process?

Running-in

- How will surface characteristics topography, residual stresses, microstructure and surface chemistry evolve during running-in for different finishing methods?
- How is the evolution influenced by the running-in parameters load and speed?
- How have these characteristics further developed and influences, gear behaviour during initial usage, here represented by efficiency testing?

Micropitting?

- What is the root cause of micropitting mechanism from microstructure perspective?
- Which microstructural changes occur during gear testing?

1.2 Research methodology

To the authors knowledge the term surface integrity was first coined by Field and Kahles [3]. They attributed this to the alteration of both surface and subsurface properties of the surface region affected by machining. Likewise, the surface integrity of gears is also poised by different characteristics. However, topography, microstructure, residual stresses and chemistry are considered as major influential characteristics. The detailed analysis of these characteristics is necessary to understand the variations induced by different manufacturing methods as well as their response to testing. To do so, a characterization methodology was developed by combining different analytical techniques as shown in Fig.1. By combining different techniques, the evolution of individual characteristics and the correlation between them can be studied in detail.

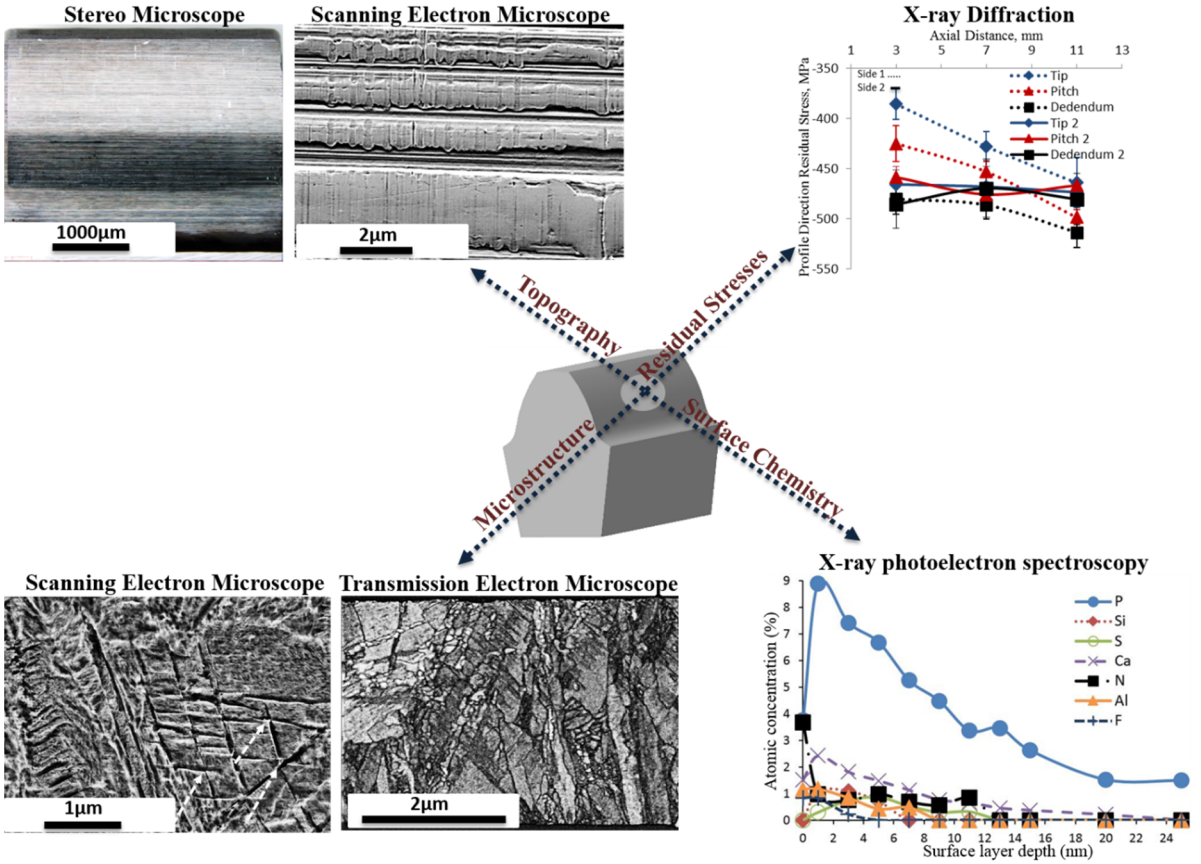

Figure 1. Overview of the analysing techniques used to characterize gear surface characteristics.

1.3 Limitations

Certain limitations are inevitable in any research work, likewise, the author has also faced few during the course of this thesis work. Some important limitations are presented below.

- The planning regarding running-in cycles and load parameters was designed by twin PhD student at Royal Institute of Technology (KTH) before the author has started his doctoral studies.
- The details regarding finishing processes are unknown.
- Likewise, the information regarding lubricant chemistry is also unknown for detailed understanding of the surface chemistry. Hence, only certain clear trends has been possible to depict.

2 Background

In this chapter, a brief overview of important topics that comprise the background knowledge needed to understand the insights of this thesis study are presented.

2.1 Gear geometry

The possibility of maintaining constant angular velocity throughout the meshing (law of gearing) made gear drives more reliable in power transmission applications. Different profiles of gear teeth like involute, cycloidal and circular arc can satisfy the law of gearing. However, the ease of manufacturing, high nominal efficiency and capability of providing constant velocity ratio irrespective of center distance, predominated the usage of involute profiled gears compared to other profiles.

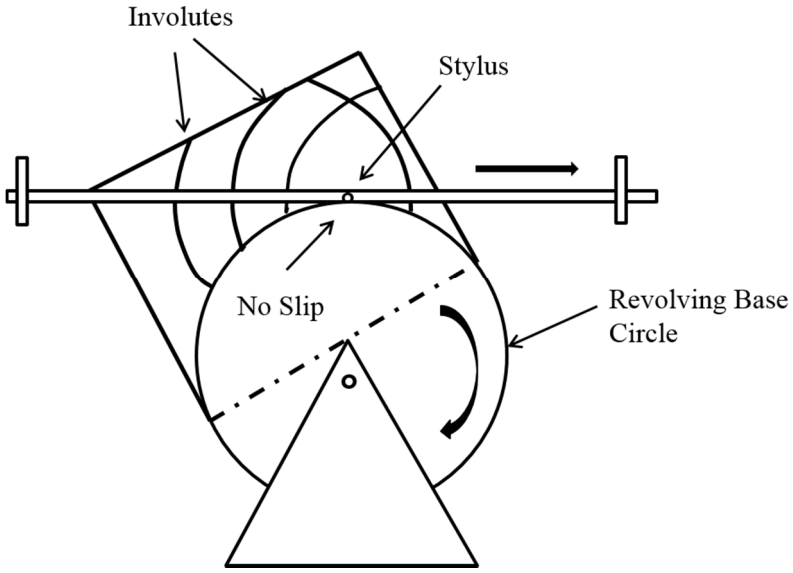

Figure 2. Revolving base circle (reproduced after [4]).

Simply defining, an involute curve is the path traced at the end of thread while unwinding it from a cylinder. For mechanically generating involute, fixed base circle and revolving base circle methods are used. Operations like hobbing, shaping, shaving etc. generate involute teeth based on revolving base circle method [4]. A schematic representation of revolving base circle method is shown in Fig. 2. In this method, an involute profile is generated from a straight beam and base circle that roll with one another without any slip, details are explained elsewhere [4].

2.2 Surface contact related gear failures

Prominent contact failures encountered on the active gear flank surfaces are discussed in this section.

2.2.1 Micropitting

Micropitting appears like dull matte or grey stained to the naked eye. The major difference of this damage mechanism in comparison to macro-pitting is that it initiates on the surface asperity level. Interaction of asperities under high tractional forces generate a multitude of surface cracks. Thus generated cracks, then grow into the surface at a shallow angle [5] and break off

material forming a pit in the microns range i.e. around 5-10 μm in depth. The detailed mechanism of micropitting will be discussed in a later section of the thesis.

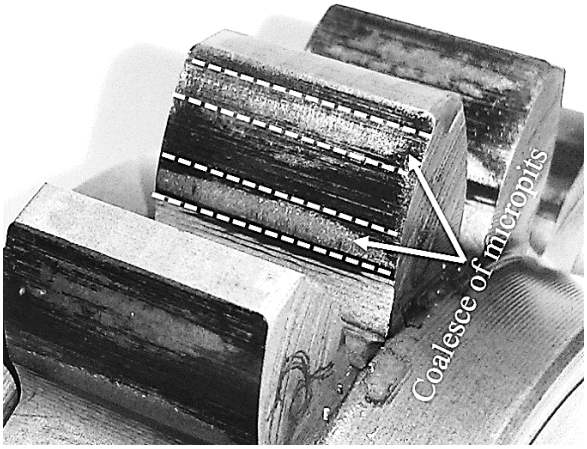

Figure 3. Micropitting on a gear tooth.

2.2.2 Pitting

In simple words, pitting can be described as a shallow crater on the gear surface. The repeated stresses acting on near-surface region deform segments of the material plastically and elastically. High internal stresses are developed depending on plasticity difference and grain orientation, which eventually leads to the initiation of a crack [2]. The initiated crack, then progresses through the weak zones and separates the particles from the surface forming a pit. Figure 4 shows an example of pitted gear surface.

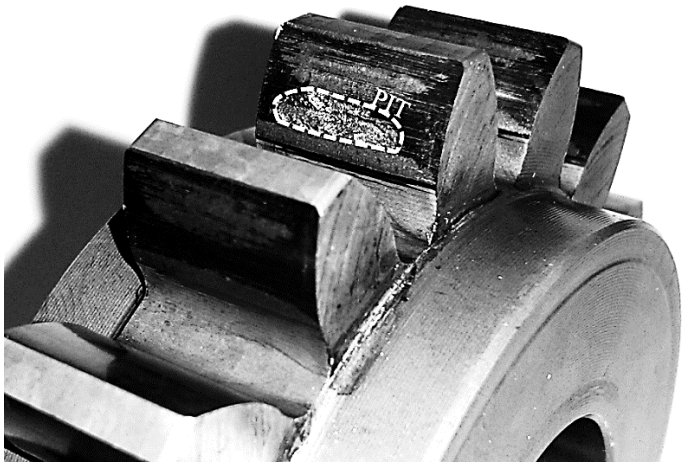

Figure 4. Pitting on a gear tooth.

Due to negative sliding, pitting usually initiates at the dedendum region. Later it develops over the entire surface of the gear flank. Extensive pitting degrades tooth profile and causes a malfunction of the gear drive in terms of efficiency, vibrations and audible noise. The pitting life of gears is highly correlated to a specific film thickness of lubrication, which is dependent on the gear surface roughness [6].

2.2.3 Spalling

Spalling is generally regarded as a propagation of macro-pitting that occurs when a series of pits coalesce due to failure of the intermediate metal. According to ASM (American Society for Metals) committee of failure of gears [2], this mode of failure occurs only after numerous cycles of operation. However, it can also take place after relatively few operating cycles. This mode of failure originates from the subsurface-defects that are typically 20-100μm deep from the contact surface [7].

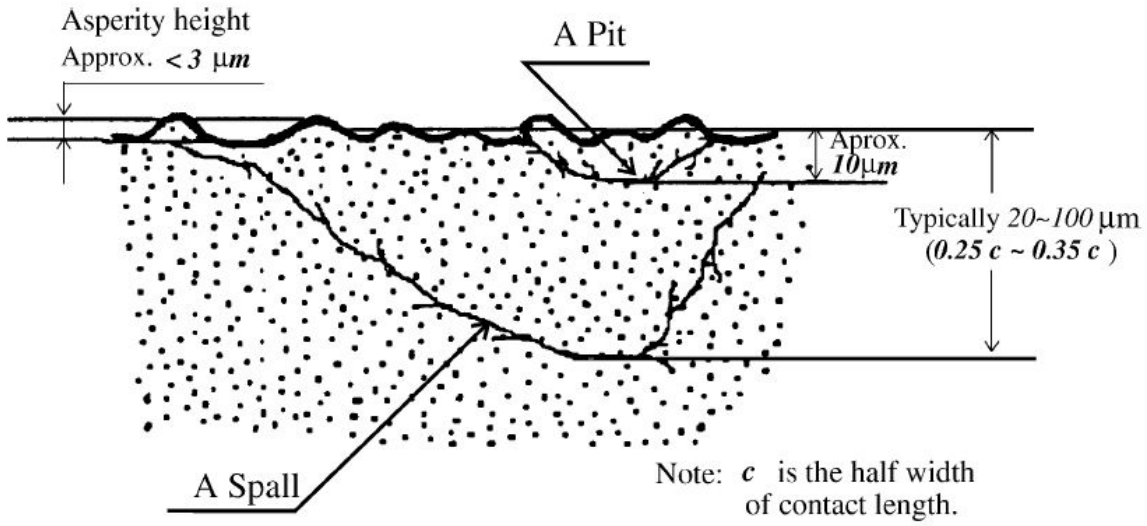

Figure 5. Schematic illustration showing the origins of pitting and spalling (published with permission from Elsevier [7]).

2.2.4 Wear

Wear of a gear tooth can be described as local surface deterioration created by surfaces sliding against one another or by impurities present in the lubricant. It is classified majorly into two types, abrasive and adhesive wear [2], [8].

Abrasive wear – during sliding, shearing off surface takes place due to the existence of hard foreign abrasive particles in the lubricant. The detrimental effects of abrasive wear summarized by Louis Faure [9] are presented below:

- Gear backlash is increased by abrasive wear, thereby altering the dynamic behaviour;
- Excessive erosion by abrasive wear creates pointed teeth;
- Severe abrasive wear diminishes the thickness of hardened layer.

Adhesive wear – ample pressure between the mating asperities of gear pair during sliding causes localized plastic deformation or micro-welding. Due to the deformation there is an energy storage which results in overheating the surface. As a consequence of raise in frictional heat, the surface become soft and promotes more adhesion and plastic deformation, this in turn causes further increase in local temperatures that leads to microstructural changes at the surface [2]. Adhesive wear is categorized into three different types, polishing, hot scuffing and cold

scuffing. The influential factors that are responsible to activate the different modes of adhesive wear are presented below [8]:

- Polishing occurs due to low operational speed (< 20 m/sec) that fails to yield sufficient film thickness.
- Hot scuffing occurs due to breakage of oil film caused by high pressure between mating surfaces, high sliding speeds and excessive contact temperatures.
- Cold scuffing occurs due to breakage of oil film caused by extremely low sliding velocity (linear speed not exceeding over 4 m/s).

2.3 Stress conditions in a gear tooth

Gear teeth under the influence of induced stress may fail in the form of root breakage or surface contact fatigue. Hence, reliable calculations and test methods are essential to estimate the level of bending and contact stresses arising from the contact surfaces. In this section the generalised mathematical equation used to predict contact stresses is described.

2.3.1 Contact stress

In general, the contact between gear pair is nonconformal. Hence, the applied load is carried only by a small fraction of area. Increasing load expands the contact area, but always remains smaller than the contact area that exist between conformal contacts. The contact stress between gear pair can be predicted by using Hertzian theory. The Hertzian equation is postulated based on the following assumptions [10]:

- The materials of contacting bodies are homogenous and yield stress is not exceeded anywhere. This means the materials are approximated as linear elastic solids;
- No friction exists within the contact;
- The solid bodies are continuous without any cracks or discontinuities in their surfaces;
- Contact is limited to a small portion of the surface i.e. the dimensions of the contact area is small compared to radii of curvature of the surfaces.

With these assumptions the maximum Hertzian pressure or contact stress existing within the contact is given as:

$$\sigma_C = E' \left(\frac{w'}{2\pi}\right)^{\frac{1}{2}} \quad 2.1$$

where E' = effective elastic modulus = $\frac{2}{\frac{1-v_a{}^2}{E_a}+\frac{1-v_b{}^2}{E_b}}$ 2.2

and w' = dimensionless load = $\frac{W}{E' R_x \ b_w}$ 2.3

In eq.2.3, b_w is contact face width, W is the load per unit length along the contact and R_x is the effective radius, for spur gears R_x is a function of pinion diameter, gear diameter and pressure angle and is given as:

$$\frac{1}{R_x} = \left(\frac{1}{d_p} + \frac{1}{d_g}\right)\frac{2}{sin\emptyset} \quad 2.4$$

However, during service the induced stress can be slightly higher than predicted from eq.2.1. This is due to different operational conditions used. To correct for additional factors, American Gear Manufacturing Association (AGMA) has recommended modifications to the existing equation. The AGMA contact stress equation is described as:

$$\sigma_c = E' \left(\frac{W' k_o k_s k_m k_v}{2\pi}\right)^{\frac{1}{2}} \quad 2.5$$

where, k_o is the over load factor, k_s is the size factor, k_m is the load distribution factor and k_v is the dynamic factor.

Usually, the contact between mating spur gears is considered as rectangular and the Hertizan half width is give as:

$$b^* = R_x \left(\frac{8w'}{\pi}\right)^{\frac{1}{2}} \quad 2.6$$

Noteworthy that the Hertizan theory applies to perfectly smooth surface. In reality, gear surface has some roughness and the real area of contact is dependent on the asperities in contact. This implies that apart of the Hertizan stresses, mating asperities also generate stresses that act very close to the surface. To sum up there are two active regions where shear stress reaches the maximum value. One is geometry dependent i.e. Hertizan contact and the other is due to asperity contact.

2.4 Lubrication

The functionalities of lubricant interposed between non conformal contacts (specifically in gears) include reducing friction and wear, heat dissipation and suspension of contaminants. To minimize friction which decides the degree of wear and heat evolution, the interacting surfaces are either separated by a fluid film created by pressure or by formation of a protective tribofilm.

The Stribeck curve obtained by plotting coefficient of friction against the product of dynamic viscosity and angular velocity divided by the normal load enables us to classify the different regimes of fluid film; hydrodynamic, mixed and boundary lubrication. In practise, for gears, cams and rolling element bearing, the classical hydrodynamic lubrication proposed by Reynolds predicts negligible fluid film [11]. Still, the gears manage to function satisfactorily without any wear/damage for prolonged time. This confirmed that the standalone hydrodynamic theory falls short to predict or explain the fluid film mechanisms of high pressure non-conforming contacts. Later, it was understood that sufficient thickness of fluid film needed to separate the mating gear teeth contact occurs as a result of the following effects:

- Piezo viscous effect: Viscosity of lubricant oil increases enormously at the high pressure region of mating gear tooth contact [12].
- With an increased viscosity, lubricant acts as a solid leading to elastic deformation of mating surfaces, where the smallest deformation corresponds to two or three times the minimum film thickness [13].

The regime developed based on the above mentioned effects is called as elastohydrodynamic lubrication (EHL). Figure 6 depicts the pressure distribution and contact shape of EHL contact, which also resembles the contact between mating gear teeth. The occurrence of the pressure spike at the outlet of contact is related to the elastic deformation induced by high viscous lubricant resulted from exerting high pressure on the lubricant in the Hertizan contact region. This characteristic pressure spike at the outlet zone was first observed by Petrusevich and hence sometimes is referred as "Petrusevich spike".

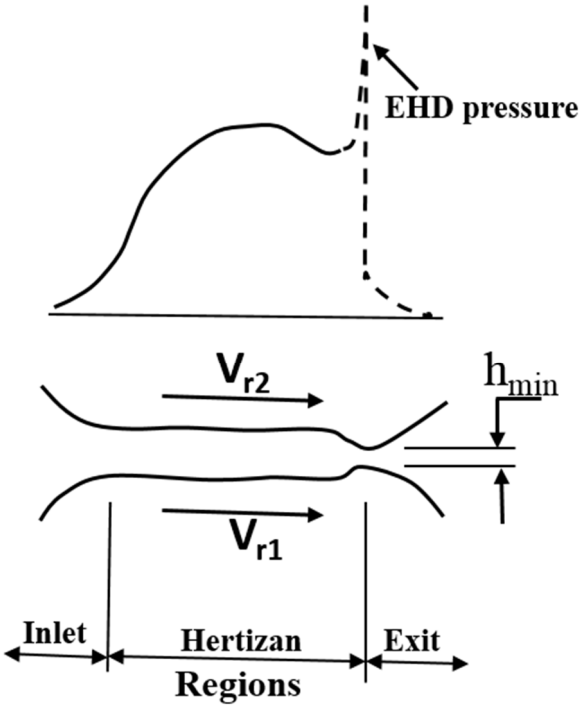

Figure 6. Schematic illustrating regimes of elastohydrodynamic contact between the mating gear teeth of the gear set (reproduced after [14]).

The following empirical equation postulated by Dowson and Higginson cited by Sosa [15] best predicts the minimum film thickness for a non-conformal contact

$$h_{min} = R(1.654U^{0.7}G^{0.54}W^{-0.13}) = 1.654\ \frac{(\eta_0\ v_+)^{0.7}\ R^{0.43}\ \alpha^{0.54}\ b^{0.13}}{E_r^{0.03}\ F_c^{0.13}} \qquad 2.7$$

where, η_0 is the absolute viscosity, $\boldsymbol{v}_+$ is the entrainment speed of the gear contact, R is the composite radius, α is the pressure viscosity coefficient, b is the gear face width, E_r is the reduced young's modulus and F_c is the contact force.

Using the equation 2.7, the specific film thickness is calculated as follows

$$\lambda = \frac{h_{min}}{\sqrt{R_{q1}^2+R_{q2}^2}} \qquad 2.8$$

where, R_{q1} and R_{q2} are the root mean square roughness parameters of pinion and gear.

The above mentioned Dowson and Higginson equation predicts minimum EHL films of the order of 1 µm with the assumption of perfectly smooth surface and ideal operating conditions of gears. However, in practice, the average roughness of a ground gear tooth is about 0.4 µm

and peak-to-valley asperity features are around 2-4 μm. This indicates that the EHL film fails to exceed the height of asperity peaks, and this effect of roughness on EHL film is referred as micro-elastohydrodynamic lubrication [12], [16]. The pressure ripples created by these asperity peaks induces high principal stresses very close to the contact surface and this highly influences the fatigue damage at the asperity level in the form of micropitting.

2.5 Gear box efficiency and power losses

The efficiency of gear box is defined as the ratio of output power to the input power

$$\eta_{total} = \frac{P_{Output}}{P_{input}} \quad 2.9$$

The difference between input and output arises from different sources such as gears, bearings, seals, synchronizers and auxiliary losses [1]. In addition, the losses from gears and bearings can be subdivided into load-dependent and no-load losses. Load-dependent losses mainly originate from the friction in the gear mesh and rolling element bearings. No-load losses can occur even without any power transmission and are mainly associated to lubricant properties; viscosity and density, immersion depth of the gears in sump lubricated gearboxes and dimensions of the gear box. The total losses are hence commonly summarized as shown below.

$$P_{Total} = P_{Gears,Load} + P_{Gears,No\ load} + P_{Bearings,Load} + P_{Bearings,No\ load} + P_{seals} + P_{Synchronizers} + P_{Auxiliary} \quad 2.10$$

3 Running-in: a literature survey

3.1 Running-in by definition

To the author's perception, running-in is involved with various aspects of the surface such as friction, wear, surface roughness, mechanical properties, microstructure and chemical composition etc. Several researchers have defined running-in but none have proposed a generic one covering all the aspects. To introduce the reader to the topic of running-in, prominent definitions are presented below.

- According to Gosudarstvennyy standard (GOST – Russian standard) [17] running-in is defined as "The change in geometry of the sliding surfaces and in the physicomechanical properties of the surface layers of the material during the initial sliding period, which generally manifests itself, assuming constant external conditions, in a decrease in the frictional work, the temperature, and the wear rate"
- Summer-Smith [18] defined running-in as "The removal of high spots in the contacting surfaces by wear or plastic deformation under controlled conditions of running giving improved conformability and reduced risk of film breakdown during normal position"
- Blau [19] defined run in (with no hyphen) as " To impose a set of conditions on a tribosystem to reduce the time required to achieve a steady state, improve long-term performance, and/or to cause a state of geometric conformity to exist at the contact surfaces in that system"

Other definitions/concepts that author has come across during literature survey include:

- smoothening or flattening of asperity peaks in a defined number of cycles,
- first part of the life period of rolling or sliding contact elements,
- reaching steady state in terms of friction and wear,
- initial operating cycles of the virgin surfaces,

3.2 Running-in mechanisms

In general, running-in is considered as an initial conditioning process that helps to improve the conformity between surfaces. The contacts between surfaces can be pure rolling, pure sliding or rolling-sliding. Hsu et al. [20] stated that with the help of running-in process a steady state condition can be achieved between contact pressure, surface roughness and interfacial layer. The aforementioned parameters reach steady state condition due to the change in surface topography obtained during the running-in. The two dominant mechanisms responsible for topography changes are plastic deformation and wear [21].

Mikhin and Dobychin proposed a theoretical model of running-in process, cited by Kragelsky [17], describing how an individual spherical asperity sliding against a smooth surface reaches its equilibrium state. Figure 7 illustrates the model. According to the model, the contact area formed between the spherical asperity and the smooth surface is divided into two parts; frontal half space of spherical asperity (section ABC in Fig. 7) and bottom half space of spherical asperity, i.e. region behind the spherical asperity (section CAD in Fig. 7). The frontal half space

is related to the plastic deformation region (denoted by A_{PL} in Fig. 7) that forms during sliding and is governed by normal load and tractional force. The bottom half space is related to elastic restoration region (denoted by A_{eL} in Fig. 7) of sliding material, which belongs to unloaded state. Mikhin and Dobychin suggested that running-in process is characterized by the redistribution of this contact region. Repetitive action of sliding varies the ratio of these two regions by decreasing the plastic deformation and increasing the elastic restoration regions respectively. Finally, the system approaches equilibrium when the ratio of these two regions becomes equal.

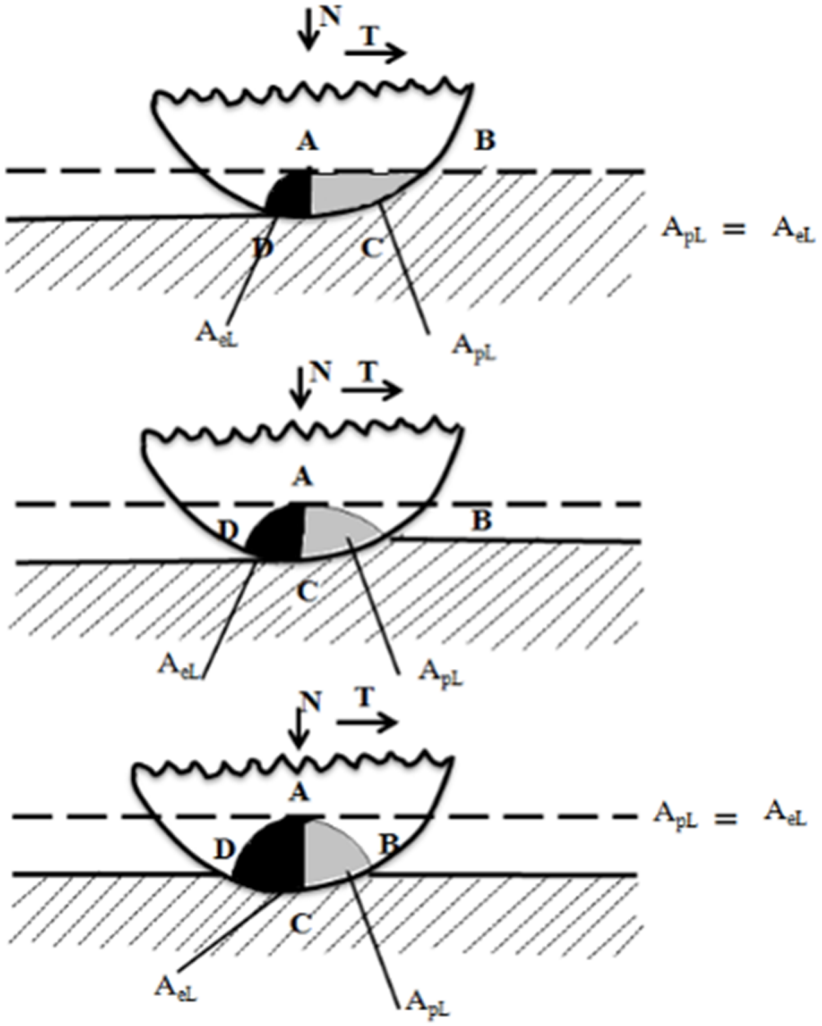

Figure 7. Sliding of spherical asperity over smooth surface (reproduced after [17]).

Several factors such as load, speed, physicomechanical properties of the material and lubrication medium influence the effectiveness of the running-in process [17]. Some studies that addressed the effect of influential factors on running-in behaviour are summarized below.

- By increasing running-in load the percentage of deformed asperities increases [17], [22].
- High running-in velocity produces a more negative skewness [22].
- The formation of lubricating film that prevent wear is highly dependent on the magnitude of running-in velocity/speed [23], [24].

- Contact temperature greatly influences the performance of lubricant and its additives [25].
- Higher load yields lower surface roughness after running-in [26].

Not only the influential factors related to the actual conditions employed, but also the initial surface roughness created by means of manufacturing process affects the behaviour of the running-in process. Conclusions from some important studies with respect to the initial surface characteristics are as follows.

- Higher surface roughness increases the weight loss [24].
- The change in roughness is higher for rougher initial surface [26].
- After running-in, the surface roughness is increased for smooth surface, while opposite behaviour occurred for rough surface [27].
- The wear rate is also influenced by roughness pattern i.e. orientation of roughness lay [28].

3.3 Running-in of gears

To the author's knowledge, little has been published about running-in process with respect to gears. Possibly, the first experimental work on gears was performed by Andersson [29]. In that study, it was observed that the running-in process decreased the surface roughness of both hobbed and shaved gears. However, the decrease in roughness was higher for hobbed gears due to its rougher initial surface. Also, the wear of gear surfaces accelerated with increasing speed and contact load. Sjöberg [30] studied how surface topography set by different manufacturing methods (green shaving, grinding and honing) responded to running-in process. The results showed that real contact area of gear surfaces is increased by means of running-in. This was true for all the manufacturing methods.

Recently, Sosa [15] presented his study on "Running-in of gears from a surface and efficiency transmission point of view". Note that the same gears from that study were examined in this thesis. The outcome of his work is summarized below.

- In-situ surface roughness measurements showed reduction of tips after first cycles. However, valleys remained the same.
- For ground gears, higher running-in load yielded higher efficiency for all speed ranges.
- The surface roughness characteristics of ground gears are largely affected by high running-in load compared to low running-in load. In other words, higher running-in load produced smoother surface.
- For superfinished gears, running-in did not affect surface topography and efficiency.
- In general, superfinished gears exhibited higher overall efficiency compared to ground gears, but only for high speeds. Opposite phenomena was observed for low speeds (below 2 m/s).

4 Micropitting: a literature survey

Micropitting has long been recognized as the prevailing failure in rolling and sliding contact elements such as gears, roller bearings and cams. In gears, the process is characterized by the initiation of micro-cracks at or near the surface opposite to the sliding direction, followed by their propagation into the surface at a shallow angle and the breakoff of material, forming a pit with characteristic depth and diameter in the range of microns or tens of microns [5], [16], [31]. Most often, micropitting occurs during the first 10^5-10^6 stress cycles. Nevertheless, a gear pair runned with unfavourable conditions, for example when using low load carrying capacity lubricant, micropitting can initiate after a short running time [32]. An example of micropitting is shown in Fig. 8.

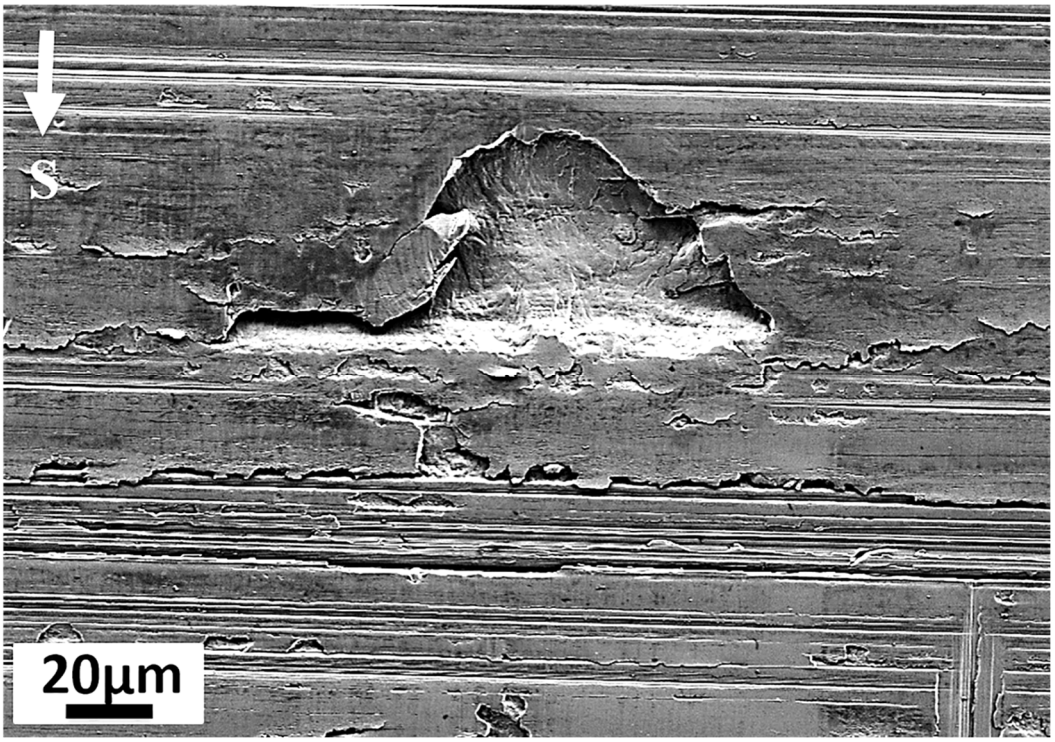

Figure 8. Micropit on ground gear tooth after efficiency testing. “S” in the image indicates the sliding direction.

In general, micropitting can initiate all over the gear tooth surface. However, dedendum region is more prone to micropitting due to negative sliding [33]. The micropits grow opposite to the sliding direction and its initiation is associated with the surface irregularities. Olver [34] using a simple slip line field theory proposed plastic deformation of asperity as a fundamental cause for micropitting. Moorthy and Shaw [31] based on their observations suggested that micropits are produced as a consequence of initiation and progression of micro-cracks from a notch-like micro-valleys, which are oriented favourably against the sliding direction.

Although it is commonly known that micropitting is associated with surface irregularities, a complete mechanism depicting micropitting has not been established due to the involvement of diverse influential factors such as surface roughness, residual stresses, microstructure, lubricant properties and operating conditions. With the aid of a fractional factorial design Oila and Li [35], [36] identified contact pressure as the most significant factor influencing micropitting in rolling and sliding contact. Interestingly, both the studies suggested that reducing surface

roughness amplitude alleviates micropitting. Other investigations [37]–[39] have also confirmed that rougher gear surface is more prone to micropitting. By producing smooth surface via superfinishing process Winkelmann et al. [40], Zhang and Shaw [41], as well as Krantz et al. [42] showed that this results in improved resistance to micropitting. Moorthy and Shaw [43] tested the surface durability of coated and uncoated ground helical gears. Their results showed lowest visible micropitting for coated gears compared to uncoated.

Residual stresses also affect the surface integrity and hence influence micropitting and thereby fatigue failure. Batista et al.[44] performed contact fatigue testing of automotive gears made with two different surface treatments (carbo-nitrided and carbo-nitrided + shot peening) to study the influence of residual stresses. The results showed that damage initiated after the same time, however, the progression to spalling was delayed in carbo-nitrided + shot peened gears due to the higher level of compressive residual stresses. Townsend et al. [45] also investigated pitting resistance of carburized and ground spur gears with and without additional shot peening process. The results showed that the pitting fatigue lives of shot-peened gears with higher compressive residual was 1.6 times higher than that of normal gears.

Some experimental studies investigated micropitting mechanisms in relation to microstructural changes. In particular, Oila et al. [46], [47] linked micropitting to phase transformations induced by cyclic contact fatigue. The authors identified development of so-called plastic deformed regions (PDR) beneath the asperities, and proposed that the microcracks initiate at the intersection point between surface and the softer boundary of PDR. The boundary of PDR was depicted as dark etching regions (DER), and suggested be newly formed structure as a result of recrystallization. Hoeprich [48] also observed dark etching alterations (DEA) beneath the contacting surfaces and related them to accumulation of dislocation densities rather than phase transformation. Another study by Venkatesh and Krishnamurthy [49] proposed transcrystalline and intergranular cracking as a reason for metal removal and pit formation in contact fatigue tested pearlite/ferrite dual-phase soft gears (hardness ~230HV).

Other studies focused on the influence of lubricant additives on micropitting. Winter and Oster [50] found that the micropitting resistance of carburized gears increased when tested with lubricant containing S-P additives. In contrary, Cardis and Webster [51] reported negative effect on micropitting with the gear oils blended with anti-scuffing additives. Martins and Seabra [52] performed micropitting tests to compare mineral oil and biodegradable ester oils. Their study suggested that micropitting performance of two lubricants was similar and thus encouraging the usage of non-toxic biodegradable gear oils.

The literature presented above focused on one specific characteristic and studied its influences on the micropitting mechanism. However, to elucidate the complete mechanism, the evolution of each individual characteristic and correlation between them needs to be understood in detail from initial stage to complete failure. This has been addressed in the present thesis study by combining different analytical techniques.

5 Overview of gear surface characteristics

This chapter provides a brief background of the characteristics that, hold the integrity of gear surface. The evolution of these characteristics was addressed in this thesis and studied in detail in order to understand the running-in process as well to be able to depict the underlying mechanism responsible for micropitting phenomena.

5.1 Topography

Topography is the three-dimensional representation of surface geometry. Any deviations with respect to the desired nominal surface are generally referred as surface irregularities. These irregularities are generally categorised as form, waviness and roughness. Whitehouse [53] defined these terms as follows:

- Roughness relates to irregularities of short wavelengths left on a surface from the finishing processes, for example, the impression left by grinding or honing processes.
- Waviness relates to irregularities of longer wavelengths left on a surface due to improper manufacturing, for example, deflections or vibrations in an individual machine
- Form relates to the general shape of a surface and usually represented as a very long wave. The deviation from the general shape can result from thermal distortion or insufficient rigidity in supporting sample during production etc.

Together, roughness and waviness constitute the surface texture, and are superimposed on the nominal surface, see Fig. 9a. For applications like gears, the position of maximum surface stresses, plastic deformation and surface contact fatigue are greatly influenced by the surface roughness. Hence, roughness need to be separated carefully in order to assess its influence. Figure 9b illustrates an example of the stress profiles caused by waviness and roughness.

The factor that differentiates roughness from waviness is called sampling length or cut-off length. This has to be chosen carefully in a way that it includes enough surface to obtain a reliable value of the desired roughness parameter, and at the same time it should exclude waviness. There are certain recommendations to select a proper sampling length, and specific details can be found in ref [54]. In addition, the term “lay”, which is the predominant direction of the surface pattern is also a function of surface texture. In practise, 2D surface measurements are usually measured perpendicular to the characteristic lay direction. The most commonly used surface roughness parameters with respect to gear surfaces both in industry and scientific research are: R_a (arithmetic average height), R_z (ten point height), R_p (maximum height of peaks) and R_q (root mean square roughness). A detailed description of these parameters can be found in ref [55].

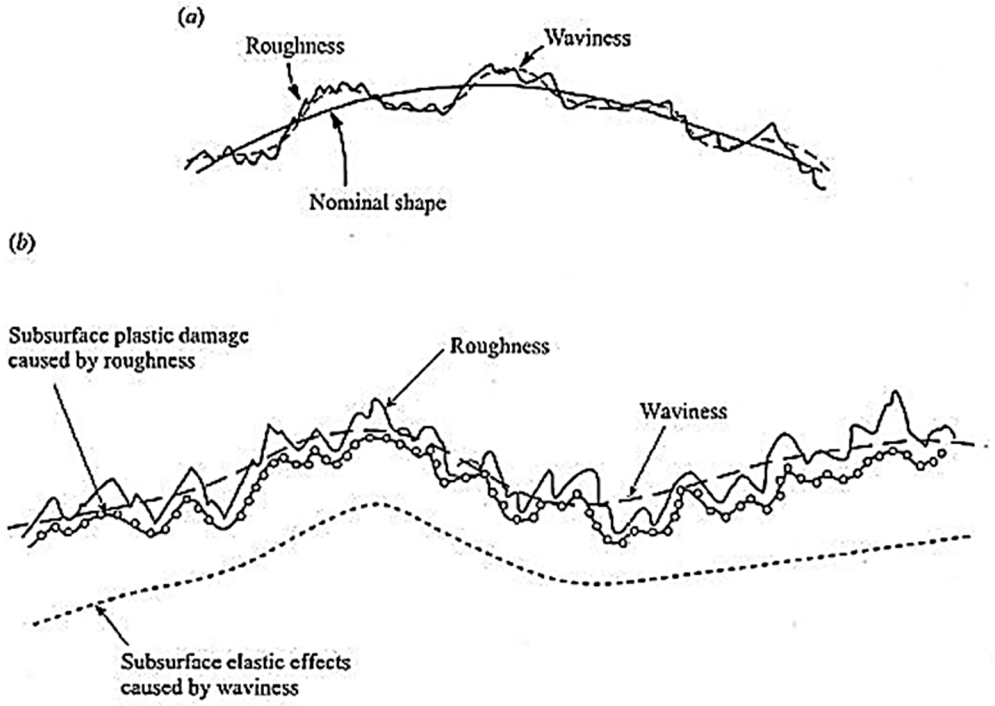

Figure 9. Waviness and roughness superimposed on nominal shape (a) and stress profiles with respect to roughness and waviness (b), (published with permission from Taylor and Francis Group LLC Books [53]).

The main advantage of profilometer measurements is the quantification of the results. However, in the present study, the main aim is to understand the deformation of asperities and associated micropitting with respect to operating conditions. Therefore, surface topography in this study refers to the examination of surface plane view with the aid of stereo-light optical microscope and scanning electron microscope. As an example the surface lay and asperities of a ground gear and their deformation due to running-in testing are shown in Fig. 10.

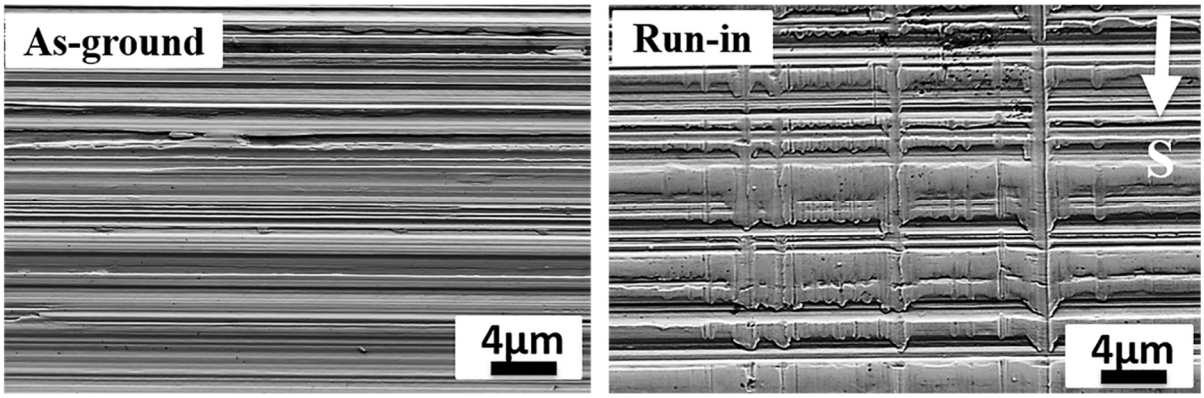

Figure 10. Surface topography of ground gear before and after running-in. “s” indicates the sliding direction.

5.2 Residual stresses

Noyan and Cohen [56] defined residual stress as “the self-equilibrating internal stress existing in a free body when no external tractions are applied”. It is a well-known fact that the performance of gears is greatly affected by residual stresses. Presence of surface tensile residual

stresses is undesirable, while compressive residual stresses are beneficial for contact fatigue strength. In general, residual stresses originate from the physical deformation induced either by thermal gradients or by phase transformation during the cooling process of the heat treatment [57].

5.2.1 Thermal stresses

At the beginning of quenching the core has higher temperature in comparison to the surface. This results in higher specific volume in the core than the case, which resists the volume contraction of the surface. As a consequence, surface compressive stresses will develop in the core and tensile stresses in the case. When the stresses exceed the yield stress during cooling the plastic deformation takes place, then the specific volume in the surface becomes greater than the core. Gradually, when the temperature difference between core and case decreases the stress states will be reversed resulting in compressive stresses in the case and tensile stresses in the core [58].

5.2.2 Transformation stress

Transformation stresses mainly originate from the transformation of austenite to martensite that is accompanied by the volumetric expansion. Importantly, the final state of the surface residual stresses is dependent on when the surface austenite transforms to martensite i.e., prior to or after the transformation in the core. If the martensite forms first at the surface, the associated volume expansion is restrained by the untransformed core and as a result compressive stresses develop initially at the surface. Later, when the core transforms to martensite or to any other microstructure, its volume expands and keeps the surface in tension. The representation of this phenomena is shown in Fig. 11.

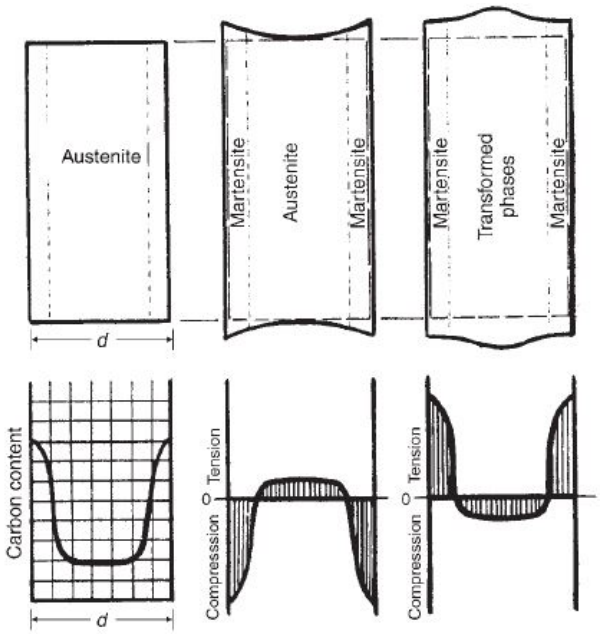

Figure 11. Development of residual stresses in carburized steels when the surface transforms to martensite prior to the core (published with permission from ASM International [57]).

However, for case-carburized gears, the core transforms first at high temperature ~ 500 to 600°C depending on the steel grade. Then, the case transformation takes place below 200 to 300°C, resulting in surface compressive stresses. According to ref [59], high-carbon case with

approximately 0.8 % of carbon (as for the gears used in this research work) expands nearly 1.2 % and low carbon core containing 0.2% C expands only 0.3 %. This carbon gradient determines the sequence of phase transformation and thereby residual stress levels from the surface and inwards into the quenched material.

Overall, it should be remembered that the transformation stresses play a key role in any heat treatment where the cooling process starts from the austenite phase, while thermal stress are dominant in subcritical heat treatments. Nevertheless, for machine elements like gears, these stresses were further altered during the final hard finishing process.

5.3 Microstructure

Martensite (α') is a crystal structure that is obtained by rapid quenching of steels from the austenite (γ) phase to room temperature. The salient feature of this peculiar transformation is that it takes place in an athermal and diffusionless manner involving coordinated atomic movements to a distance less than an atomic diameter [60]. The diffusionless nature indicates no occurrence of compositional change after transformation, i.e. carbon content remains the same for both the phases. This means the shape transformation of face centered cubic structure (fcc) to body centred tetragonal (bct) structure takes place by change in volume as well as a large shear. Nevertheless, phenomenological theory of martensite crystallography (PMTC) emphasised that the lattice strain associated with shape change is not sufficient enough to attain the martensite transformation. It suggested that the second shear in the form of lattice invariant strain contributes to the completion of martensite transformation by bringing the required change in crystal structure. This invariant strain is invisible and being thought to occur by slip or twinning.

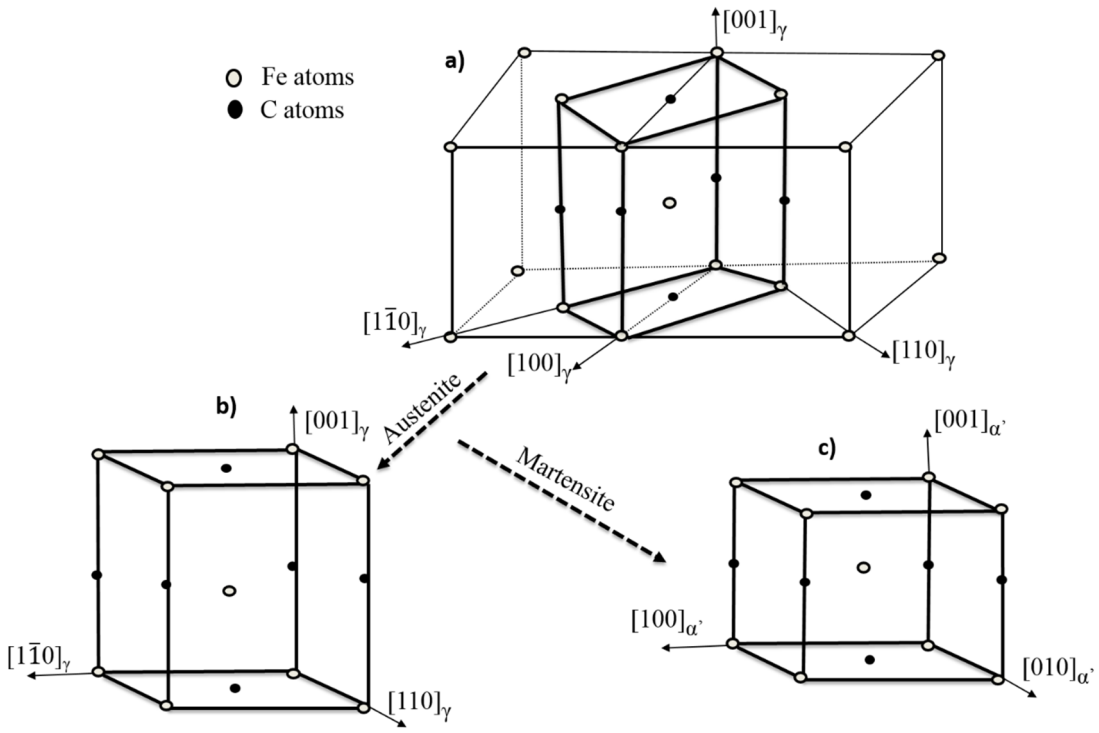

Figure 12. Martensite transformation.

Bain proposed a simple path of correspondence for martensitic transformation. Figure 12 shows the Bain correspondence illustrating the transformation of face centered cubic structure (fcc) to body centered tetragonal (bct) structure. The bct silhouette in Fig. 12a is constructed by joining two fcc unit cells on their (010) planes. However, to convert into bct martensite, deformation (Bain strain) is required, which involves 25% contraction along $[001]_\gamma$ to transform into $[001]_{\alpha'}$, and 13% elongation along $[1\bar{1}0]_\gamma$ and $[110]_\gamma$ directions to transform into $[100]_{\alpha'}$ and $[010]_{\alpha'}$. This figure and description are reproduced from ref [60].

As a consequence of the austenite-martensite transformation the carbon atoms will occupy the octahedral interstitial sites and makes unit cell a tetragonal. The tetragonality of martensite is dependent upon the carbon content, and the axial ratio c/a, is given by [61]:

$$\frac{c}{a} = 1.000 + 0.045 \text{ wt\% C} \quad 5.1$$

This equation indicates a linear relationship between axial ratio and carbon content. In other words, with zero carbon content the crystal structure would be bcc instead of bct. The lattice parameters *a* and *c* varies slightly with presence of Ni, Cr or Mn in the steel. However, the actual axial ratio c/a is only affected by carbon content [61]. Not only the lattice parameters but also the M_s and M_f temperatures can be influenced by alloying elements. The empirical relationship proposed by Andrews [62], as given in equation (5.2), best describes the relative effect of alloying elements on martensitic start temperature.

$$M_s(°C) = 539 - 423(\%C) - 30.4\ (\%Mn) - 17.7\ (\%Ni) - 12.1\ (\%Cr) - 7.5\ (\%Mo) \quad 5.2$$

It is obvious from the equation (5.2) that the carbon level has the largest effect on M_s temperature compared to that of any other alloying elements. Therefore, the carbon content act as a prime factor to set M_s temperature, which in turn decides the amount of retained austenite. Hence, for gears it is important to choose right tempering temperatures, which decides the mechanical properties via carbon content and retained austenite percentage.

The other important characteristic of martensite is its morphology. Maki [63] classified the morphologies of martensite (bcc or bct) into five different types; lath, butterfly, lenticular (plate), $\{225\}_\gamma$-plate and thin plate based on the alloy composition and M_s temperature. However, the lath and plate morphologies are the common ones observed in ferrous alloys. The lath forms in the carbon range of 0-0.6 wt%, whereas plate forms above 1 wt%. Importantly, there is no sharp transition between lath and plate martensite. Hence, mixed martensite exist between 0.6 to 1 wt% C [64]. The width of an individual lath is of the order of 0.2-0.5 μm. These fine laths align themselves parallel to one another in regions of the parent austenite grain. Unlike laths, plates form nonparallel to one another. Figure 13 shows an example of the mixed martensite structure along with retained austenite, which is obtained by tempering the spur gears (hard finished by grinding after tempering) at about 185°C. The carbon content is around 0.8 wt%.

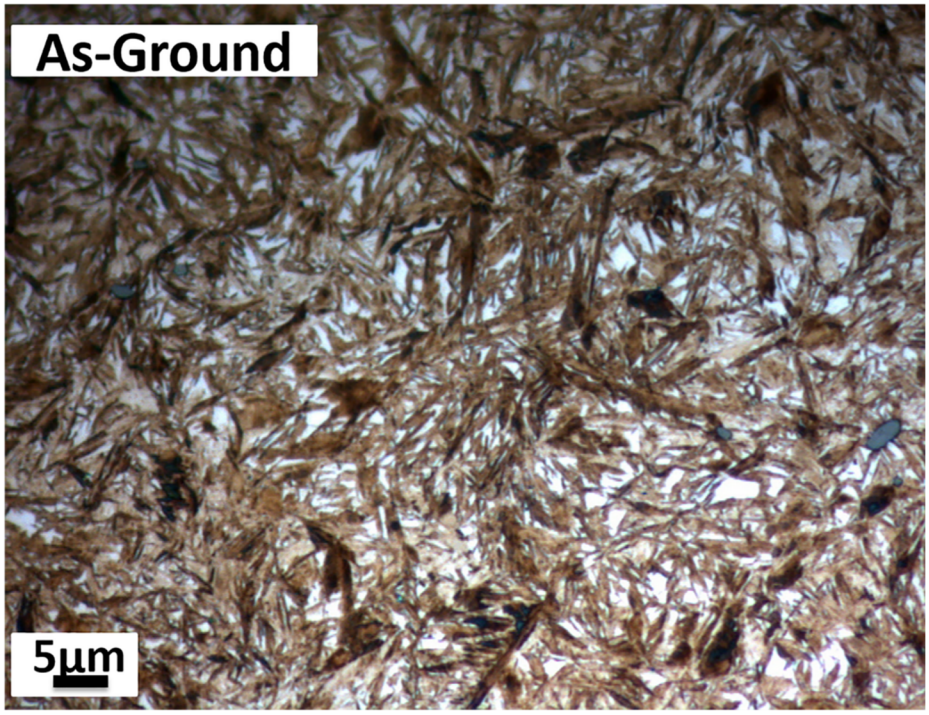

Figure 13. Light optical micrograph showing case microstructure of as-ground spur gear; mixed martensite and retained austenite can be seen (etched with 1.5% Nital).

The tempering of martensite in the temperature range 100 to 250°C results in the precipitation of extremely small (~ 2nm) transition carbides [65]. Two different types of crystal structures have been reported for transition carbides. Jack [66] first proposed a hexagonal structured epsilon carbide (ε) having a stoichiometry of $Fe_{2.4}C$. Later, Hirotsu and Nagakura [67] proposed an orthorhombic structured eta (η) carbide having a stoichiometry of Fe_2C. However, the stoichometries proposed above are still being questioned, and the exact structure and composition are left as open questions up till now.

5.4 Surface chemistry

It is a well-known fact that the adhesive or frictional wear resulting from asperity-to-asperity contact between mating gears is a serious threat to gear performance. Apart from the initial higher surface roughness, unfavourable operating conditions like higher load or lower speed also generates higher temperatures via increased friction and consequently lead to the welding of asperities. To counteract this wear mechanism lubricant oil blended with antiwear (AW) or extreme pressure (EP) additives are usually employed as they contribute to forming a protective film (in the order of few nm) over interacting metal surfaces. Both these additives form protective films by a similar mechanism, however, the activation of EP additives typically requires higher temperature and load compared to AW additives [68].

The protective film formation is supposed to take place in two stages. At the start, the protective film is formed purely by adsorption. Then a chemical reactive layer is formed either by thermal decomposition or by hydrolysis [69]. The shear modulus of the reaction layer formed by additives is generally low. This ensures a removal of the reaction layer during sliding. However, to protect the surface, the rate of layer formation should be higher than the rate of layer removal

[70]. This is only possible if the additives in the lubricant both decompose and react with the metal surface readily at extreme conditions.

The commonly used EP and AW additives based on the compound type are summarized in the below table [71].

Table 1. Typical EP/AW additives blended with base oil

Sulphur compound type	Sulfurized fatty oil Sulfurized terpene Sulfurized olefin Sulfide
Chlorine compound type	Chlorinated paraffin Chlorinated fatty oil
Phosphorous compound type	Phosphite Phosphate Amine phosphate
Organo-metallic compound type	Dialkyldithiophosphate Dialkyldithiocarbamate Naphtanate

It should be noted that in the present study, the main focus regarding surface chemistry is to understand how testing influences tribo film formation rather than studying the effect of lubricants on gear performance.

6 Deformation mechanisms

Surface plastic deformation plays a significant role in sliding and rolling-sliding contact fatigue failure, which is also the case for active gear tooth flanks. An example of plastically deformed material at the surface and close to the surface caused by severe sliding friction is shown in Fig. 14.

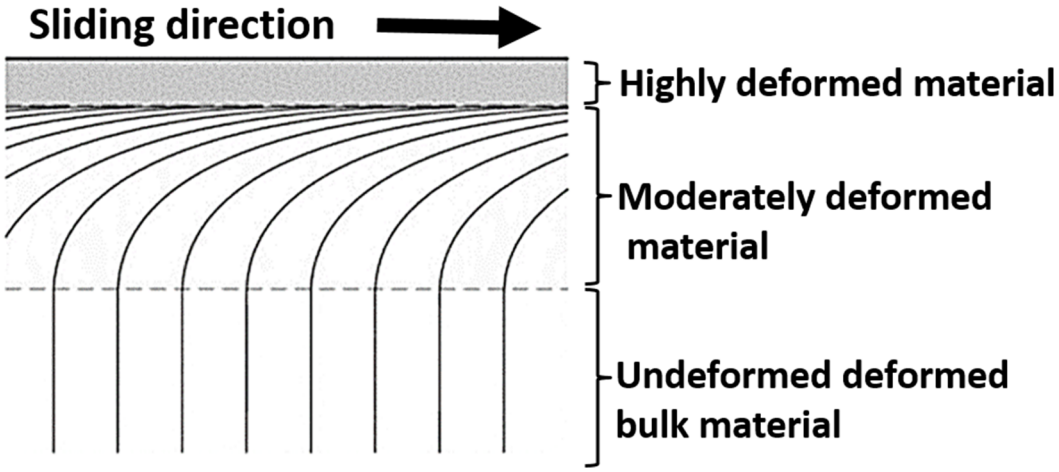

Figure 14. Sliding induced plastic deformation (edited version, published with permission taken from Elsevier [72]).

From the above figure it can be seen that the surface material is deformed and reoriented towards the sliding direction. Depending on the strain levels induced by sliding process the severity of deformation also varied from the surface to the bulk material. Such plastic deformation in metallic materials generally takes place by slip or twinning. A brief overview of these mechanisms is presented below.

6.1 Slip

Slip is the most dominant plastic deformation mechanism in metals. The process of slip involves sliding of one atomic plane over another by dislocation movements [73]. A simple model illustrating the slip process is shown in Fig. 15. When the applied shear stress exceeds the critical shear stress, the atoms advances over an integral number of atomic distances via the motion of dislocations. The dislocation here is nothing but a boundary between the slipped and unslipped portions of the plane of a partly glided crystal lattice [74]. The definite crystallographic plane along which dislocation line moves is called a slip plane. As a consequence of the slip process a slip step is formed at the free surface, which can be observed under microscope. The slip usually occurs in the plane with the closest atomic packing and the slip direction is the closed-packed direction in the slip plane. The combination of slip plane and slip direction constitute slip system. In case of the fcc structure, the close-packed planes and directions are {111} and <110> respectively. This means there are four possible individual planes and three directions, which together gives a total of 12 slip systems. On the other hand, bcc structures have 48 slip systems resulting from the combination of slip planes {110}, {112} and {123} with <111> slip direction [75].

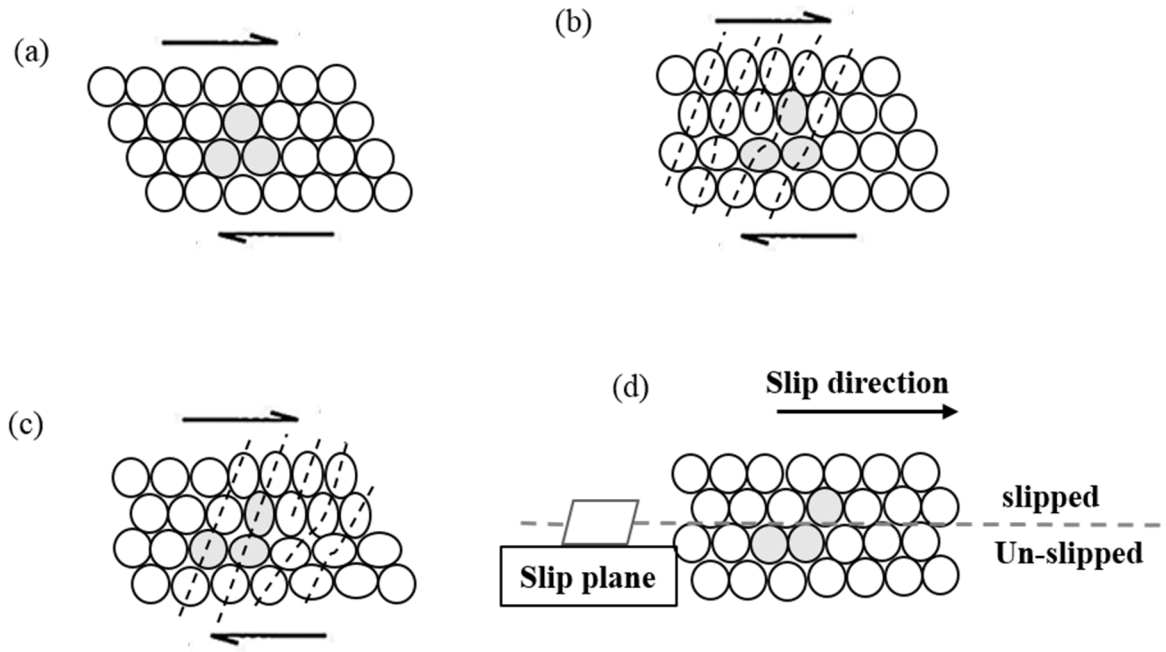

Figure 15. Schematic illustration of slip process (reproduced after [76]).

6.2 Twinning

Twinning is dominant when the deformation by the dislocation slip is limited. Nevertheless, both slip and twinning can occur simultaneously [77]. The twinning mechanism involves rearranging a portion of the crystal lattice with an orientation that is exactly in mirror symmetry with respect to the untwinned lattice. The plane of symmetry between the two orientations is termed as twinning plane [73]. Similar to slip mechanism, twinning also takes place in a definite crystallographic directions. In fcc structure, the twinning system takes place in combination of {111} plane and <112> direction, whereas for bcc the twinning system corresponds to {112} plane and <112> direction [75]. Twinning usually occurs in two different modes; mechanical twins and annealing twins. Mechanical twins result from rapid mechanical loading at low temperatures and are commonly seen in bcc and hcp structures. While, annealing twins are formed during annealing of fcc structures [73]. An example illustrating a twinned and parent matrix separated by a twin boundary plane is shown in Fig. 16.

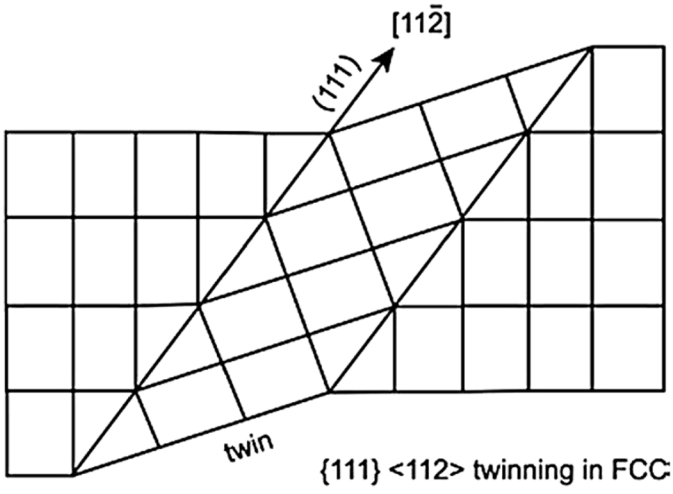

Figure 16. Twinning in a fcc structure (published with permission taken from Springer [75]).

6.3 Plastic deformation of polycrystals

Slip process in single crystals can be categorized into two different stages. During the first stage of deformation the dislocations glide over long distance across the crystal. This movement is restricted in the next stage due to the formation of dislocation cells as a result of intersection of two slip planes. The cell walls are impenetrable and act as a barrier, hence, the gliding of dislocations is limited to the inside regions of the cell [77].

In the case of polycrystals, this limitation exists from the beginning due to the presence of grain boundaries. As dislocations cannot slip via grain boundary, new dislocations nucleates in the surrounding grain as a result of a build-up of stresses at grain boundary from imposing dislocations. Consequently, the activation of slip with different orientation takes place on either side of the grain boundary. This can break the continuity of the grain boundary. However, to overcome this constraint, slip activates on multiple systems within the grain. Thus, each grain deform individually and at the same time maintains the continuity of the grain boundary. For polycrystalline material when subjected to plastic deformation, slip can simultaneously take place on five different systems. In general, this could be a limitation for hcp structures, hence twinning occurs commonly in hcp compared to bcc and fcc metals [75], [77].

The crystals usually avoid the necessity of simultaneous activation of five slip systems by sub-diving into different regions. By sub-division crystal can accommodate a similar deformation as activating five slip systems. Figure 17 shows the hierarchy of microstructure deformation with sub-divisions.

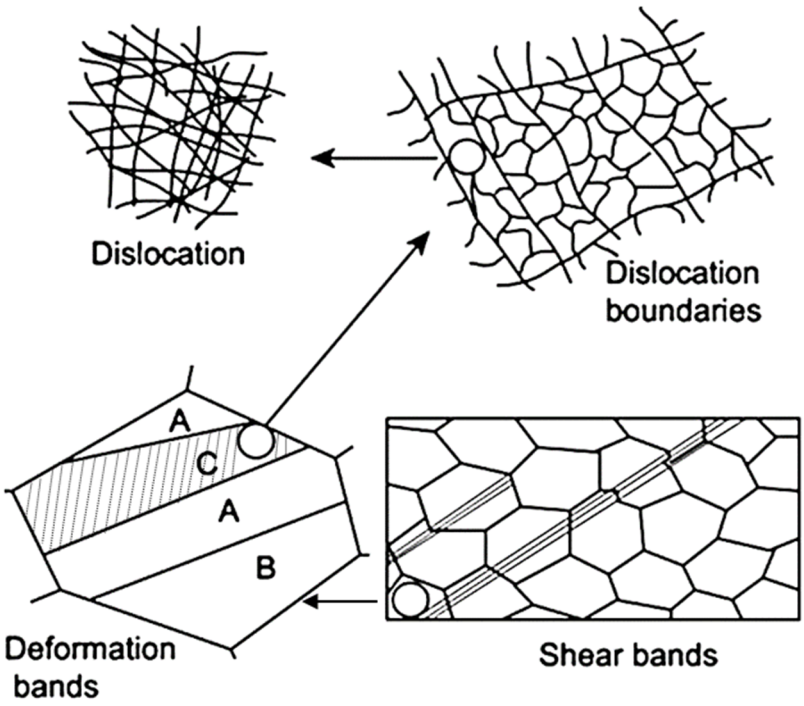

Figure 17. Dislocations and deformation bands formed during deformation (edited version, published with permission from Springer [75]). Note that the figure illustrates the deformation hierarchy of pure Al, other metals may show similar or different structures.

On the finest level, dislocation cells are formed with low dislocation density confined to the cell and high densities appearing at the cell boundaries (or simply referred as cell wall). The

dislocations are mobile within the cell, but are immobile at the boundary of the cell. Importantly, they exist in different signs, but never annihilate and leads to a misorientation of about 1-2° across the cell boundary. At the next step, the dislocation cells organises in bands. These bands are in the range of a few cell-blocks thick with thicker walls. The misorientation also increases consequently as compared to the previously formed dislocation cell walls. At the next hierarchical stage, both cell boundaries and bands together constitute deformation bands. These deformation bands form in clusters and the border of these micro bands (see dotted lines) are fine regions, called as transition bands. Finally, at the highest level, shear bands are formed under high strain levels. These bands are the consequence of severe plastic deformation and can pass through several grains. In simple words, shear bands represent the weakest regions of the material and can form independent of grain structure and normal crystallographic considerations [75], [77].

7 Gear manufacturing and work material

The generation of gear teeth demands consistency and accuracy with respect to geometrical aspects like tooth size, shape and runout etc. [78]. The technology has advanced in recent times to produce gears with specified tight geometrical tolerances in less production time. For example, this includes generating gear teeth by using hob tool instead of form milling-cutters on milling machines. The flow chart representing the sequence of steps involved in manufacturing spur gears used in this study is shown in Fig. 18.

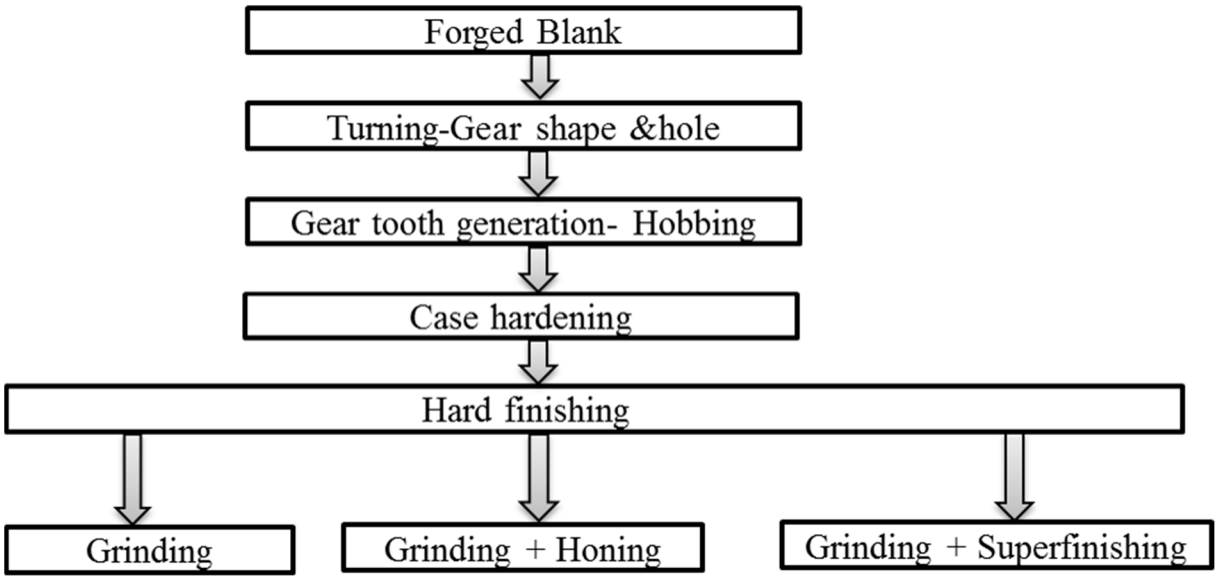

Figure 18. Flow chart representing manufacturing steps in gear manufacturing.

After turning the blank into the required diameter, the teeth are generated by hobbing. Thus produced gears undergo heat treatment (case hardening) for improving surface hardness and also to gain compressive residual stresses. The details regarding heat treatment cycles are discussed in the subsequent section. Nevertheless, surface distortions are created as a result of heat treatment and quenching. Due to the alterations in microgeometry the degree of contact stresses can increase up to 5 – 10% [79]. Therefore, as a last step, gears are usually hard finished to attain required geometrical tolerances. The gears used in this thesis study were hard finished by means of three different processes. One set of gears were hard finished by generating grinding that produced a surface with a R_a value (arithmetic average height) of 0.3 µm. These stages were common for all gears. Additionally, one set was honed and one was superfinished. The respective R_a values for the two later conditions were 0.16 and 0.08 µm. The three gear sets are referred with respect to the final finishing process, namely ground, honed and superfinished. The topographic features and residual stresses set by these finishing processes are considered to have a significant influence on the contact fatigue.

The spur gears used in this study were made from two different alloy steels; DIN 16MnCr5 and DIN 17NiCrMoS6-4. The nominal composition of these steels are presented in Table 2.

Table 2. Nominal chemical composition (in wt %) of the alloy steels 16MnCr5 and 17NiCrMoS6-4

	C	*Si*	*Mn*	*Cr*	*P*	*S*	*Ni*	*Mo*	*Fe*
16MnCr5	*0.13-0.19*	*0.15-0.40*	*1-1.30*	*0.80-1.10*	*≤ 0.035*	*0.020-0.040*	*-*	*-*	*bal*
17NiCrMoS6-4	*0.14-0.20*	*≤ 0.40*	*0.60-0.90*	*0.80-1.20*	*≤0.025*	*0.020-0.040*	*1.20-1.50*	*0.10-0.20*	*bal m*

In service, gears typically experience bending stresses at the root of the tooth and shear stresses on the flank surfaces. Cyclic events of these stresses can lead to two different failure mechanisms:

- fatigue crack initiation at the root of tooth
- surface and subsurface contact fatigue cracks

To restrain these mechanisms, the steel should be enriched with enhanced toughness in the core and a hard, wear resistant surface at the case [80], [81]. These properties can be embedded into the steel through heat treating either by through-hardening or by case-hardening. Case-hardened gears possess higher load carrying capacity compared to through-hardened gears [82]. Figure 19 depicts the specific heat treatment cycles followed for carburization case-hardening process. After tempering, the gears attain a case depth of about 1 mm with 0.8wt% carbon content at the surface. Regarding microstructure, martensitic structure is obtained, but with approximately 20% retained austenite (for the case-hardened steels in this study).

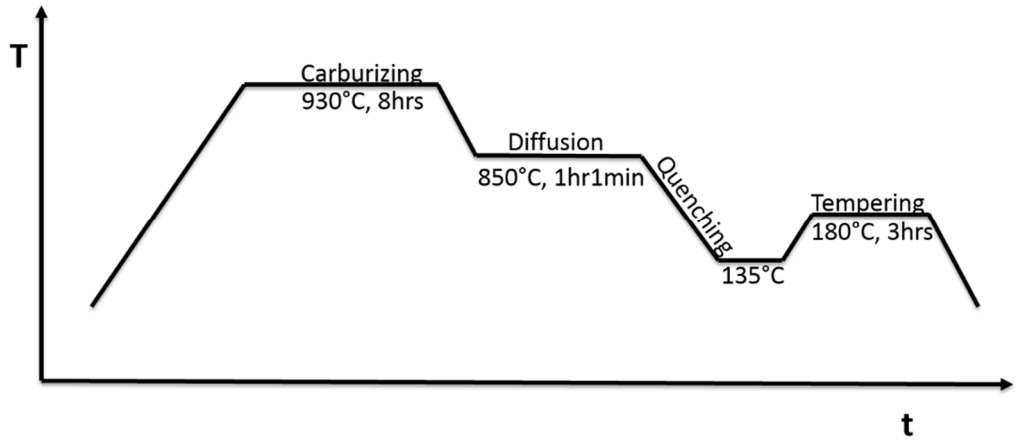

Figure 19. Heat treatment process followed for case hardening the gears used in this study.

8 Experimental details and analysis techniques

In this section a detailed description of the test rig and procedures used for testing gears are provided. Also, the analytical methods employed to study the gear surface are presented.

8.1 Back- to- back test rig

The FZG back-to-back gear test rig at KTH, see Fig. 20, was used throughout this research work. It consists of two gearboxes, slave and test gearbox. Two shafts are used to connect both the gearboxes by connecting gear to gear and pinion to pinion, thus forming a power loop. The power loop is driven by a motor that is connected to the slave gear box on gear side. Any losses occurring in the loop due to friction are measured by a loss torque sensor which is situated between motor and slave gearbox. Additional power needed to compensate energy losses during testing is constantly supplied by the motor. Static torque is applied to the system by twisting the torque clutch with the help of lever and dead weights. Gears with the same geometry were used in both the slave and test gearbox for running-in and efficiency testing. Similar test rig located at Scania CV AB was used for micropitting tests. However, for micropitting tests helical gears were used in the slave gear box.

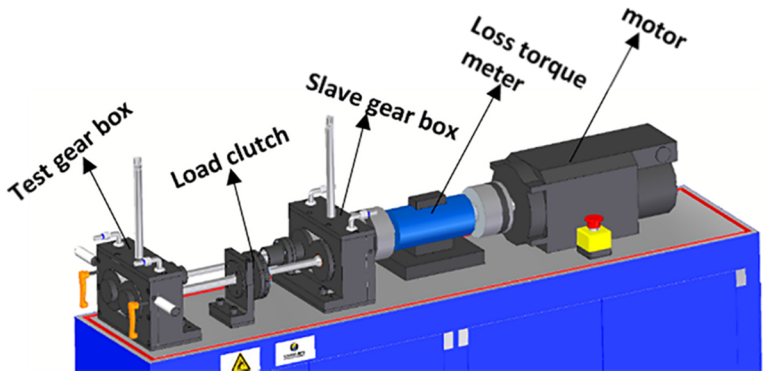

Figure 20. Schematic of FZG back-to-back gear test rig (Paper II).

8.1.1 Running-in

To study the effect of running-in process, load and speed were selected as experimental parameters. The running-in cycles were 20880 revolutions of the wheel, as a standard for FVA efficiency test procedure [83]. Two different loads of 302 or 94 Nm (referred as load stage 5 (LS5) and load stage 9 (LS9), respectively, according to FZG manual guide [83] were used. The speeds (0.5 and 8.3 m/s pitch velocities corresponding to 87 and 1444 rpm of the wheel) were used for investigation. In case of ground and superfinished gears the running-in tests were performed only at low speed, while honed gears were tested at both the speeds. The gears were fully dipped in a synthetic polyalphaolefin (PAO) lubricant controlled at 90 °C.

8.1.2 Efficiency testing

The efficiency testing following after running-in consisted of 32 different conditions, i.e. four loads and eight speeds. The test started with an inside power loop torque of 0 Nm, sweeping through speeds of 0.5, 1, 2, 3.2, 8.3, 10, 15 and 20 m/s pitch velocity for 5 minutes at each speed, using the same lubricant and temperature control as in the running-in procedure. Once

the highest speed was tested, the same speeds were swept at 94 (LS5), 181 (LS7) and 302 (LS9) Nm. This amounts to 208800 revolutions. The temperature was maintained at 90°C or 120°C.

Noteworthy that all the running-in and efficiency tests were performed by twin PhD student (M. Sosa) at KTH. All the surface and material characterization of the tested gears were performed by the author. It is important to note that new pair of gears were used in each test and all the analyses have been done on the driven gear wheel.

8.1.3 Micropitting testing

To systematically follow the evolution of micropitting and corresponding changes in surface characteristics, 12 gear pairs belonging to the same batch were tested to different length, from 200 to 2.6×10^7 cycles in a sequence with logerthermic increment. The full details of test matrix can be found in the appended paper VI. All these tests were carried out with a set torque of 239.3Nm corresponding to 2.4GPa Hertizan pressure at pitch. The speed of the wheel was 1500 rpm and the temperature of the lubricant (75W-80 MTF) was maintained at 85°C. It should be noted that the last test in the matrix, which was planned for 2.6×10^7 cycles of the wheel was stopped after 2.2×10^7 cycles due to heavy vibrations created by severe pitting.

The micropitting tests were performed by the author, along with master thesis student (V.M. Subbaramaiah Naidu) at Scania CV AB, Södertälje.

8.1.4 Gear geometry

Standard FZG C-PT type spur gears modified with tip relief were used for running-in and efficiency testing, and FZG C-PTX type spurs gears were used for the micropitting tests. The geometrical characteristics of the tested gears are presented in Table 3.

Table 3. Geometrical parameters of tested gears

	FZG C-PT	FZG C-PTX
Material	16MnCr5	17NiCrMoS6-4
Center Distance, a (mm)	91.5	91.5
Module, m (mm)	4.5	4.5
Pressure angle, α (°)	20	20
Pinion		
No of teeth Z_1	16	16
Face width, b_1 (mm)	14	14
Pitch diameter, d_{w1} (mm)	73.2	73.2
Tip diameter, d_{a1} (mm)	82.45	82.45
Tip relief Ca_1 (µm)	20	-
Root relief C_{f1}	-	-
Wheel		
No of teeth Z_2	24	24
Face width, b_2	14	14
Pitch diameter, d_{w2} (mm)	109.8	109.8
Tip diameter, d_{a2} (mm)	118.35	118.35
Tip relief Ca_2 (µm)	20	50
Root relief C_{f2} (µm)	-	50
Crowning C_{b2} (µm)	-	30

8.2 Microstructure characterization

8.2.1 Scanning electron microscopy (SEM)

The scanning electron microscopy (SEM) is a resourceful technique for characterizing materials in different aspects. Its high spatial resolving capabilities (1-5 nm) and depth of field helps to explore finer details present in bulk object. The schematic, illustrating the working principle of SEM instrument is shown in Fig. 21. The beam of electrons emitted from the electron gun is focused down to nanometer width on to a sample surface by using condenser and objective lenses. The interaction of electrons with surface results in a "pear" shaped interaction volume [84], from which back scattered electrons, characteristic X-rays and secondary electrons are emitted. Thus emitted electrons and X-rays are then detected by using different detectors. The size of interaction volume is dependent on the accelerating voltage and sample density, but typically of the size of up to 1 μm for the X-ray emission.

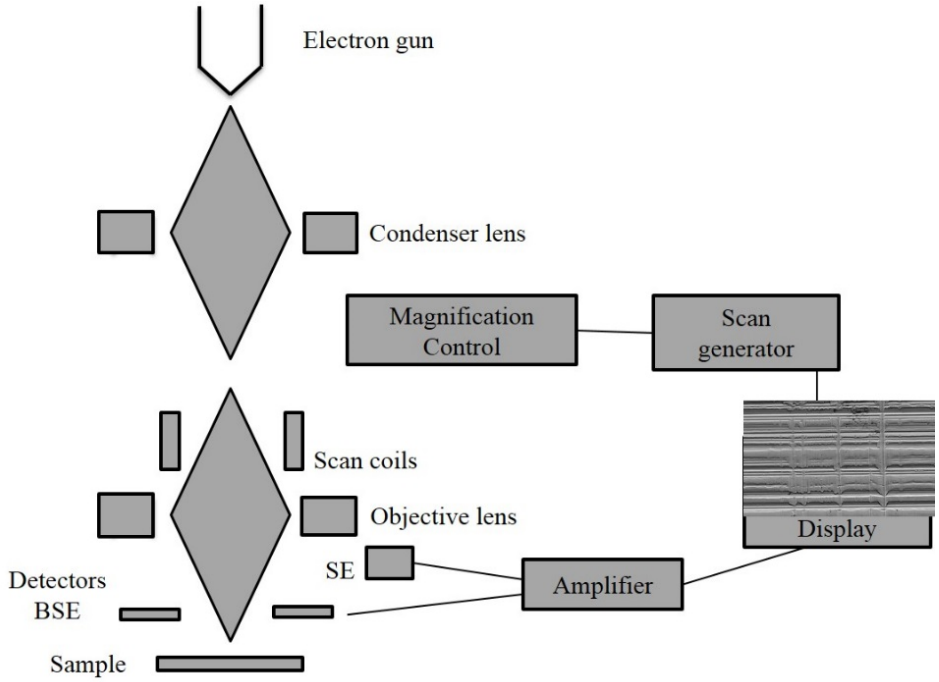

Figure 21. Working principle of a scanning electron microscope.

The instrument used in this work was a LEO Gemini 1550 equipped with field emission gun. Surface structure can be resolved down to the order of 10 nm or better by using secondary electrons [85]. Hence, these electrons were used for imaging both surface topography and microstructural features. The image of topography can be enhanced by limiting the beam interaction to a region very close to the sample surface. This is achieved by using low beam energies i.e. in the range between 5 keV to below 500 eV. Therefore, an accelerating voltage of 5 keV was used for all the microscopic investigations. Prior to topographical studies, the gear teeth samples were dipped in a solution of xylene for about 24hrs in order to dissolve all the lubricant residues.

8.2.2 Sample preparation

To perform microstructural and surface crack investigations by means of scanning electron microscopy (SEM), a gear tooth was cut out from the wheel by using mechanical cutting. Some

of the individual teeth were sectioned along profile direction and some in axial direction (particularly at dedendum). The cross sections were then mounted in a hot resin (Polyfast). After mounting, the samples were finished by grinding and final polishing down to 1 μm finish using diamond suspension. To delineate the microstructure the polished samples were chemical etched by using either 1.5% Nital or a mixture of 2%Nital and 4% Picral.

Since the details at the surface of the tooth are of the greatest importance, some samples were nickel plated prior to mounting in order to prevent edge retention during grinding and polishing. Nickel plating was performed by using 20-25% $NiSO_4$ – 10% $NiCl_2$ solution as electrolyte and pure nickel plate as anode. The cross sectioned samples were dipped into the electrolyte solution that was maintained at a temperature of 50°C. A constant voltage 2.9 V was applied between sample and nickel plate for around 90 min. The thickness of the plating is directly proportional to the time.

8.2.3 Transmission electron microscopy (TEM)

Typical operating voltages used in transmission electron microscopy (TEM) are in the range of 100-300 kV, which is much higher in comparison to a maximum voltage of 30kV used in SEM [86]. The construction of TEM typically consists of the electron gun, electromagnetic lenses and a viewing screen, which are all enclosed in a vacuum system. The lenses are separated based on their placement i.e., pre-specimen lenses or post-specimen lenses [87]. The electrons from the electron gun passes through the pre-specimen lenses, which include one or more condenser lenses and form the initial beam that targets the very thin specimen (thickness < 200 to 300 nm). Thus the electrons undergo several interactions with the specimen, and as a result, some electrons are diffracted (based on the periodic array of the atomic planes) and some still remain parallel to the direction of the incident beam. These interacted electrons are then passed through a series of post-specimen lenses that include objective lenses, intermediate lenses and a projection and finally produce a magnified image either on a fluorescent screen, photographic film or on a CCD camera. The images formed based on transmitted electrons and diffracted electrons are referred to as bright-field and dark-field image respectively. The TEM used in this work was a JEOL 3000 operated at an acceleration voltage at 300 kV, located at Technical University of Denmark (DTU).

8.2.4 Sample preparation for TEM

In this research work, the TEM analyses were used for characterizing the thin deformation bands that are often found in connection with the micro-cracks. Since, these bands are seen on cross-sections and found only after etching, site specific preparation is essential. Hence, in-situ lift out technique by means of focused ion beam (FIB) milling was used to prepare electron transparent foil for TEM investigations. The equipment used was a FEI Helios Nanolab^{TM} 600 dual beam microscope at DTU.

Once the site of interest with deformation bands was selected, the surface was deposited with thin layer of Pt (c.f. Fig.22b) in order to protect the microstructure from ion milling. Then, the material was removed by ion milling down to a depth of approx. 20 μm on both sides of the Pt-protected area with a thickness around 1 μm (c.f. Fig.22c). Thereafter, this foil was further thinned to ~ 500 nm (c.f. Fig.22d), lifted and attached to a Cu grid, and further thinned to 100 nm for the TEM observation.

All the TEM analyses and associated sample preparation presented in this thesis study were performed by Xiaodan Zhang (co-author of paper V) at DTU (Technical University of Denmark).

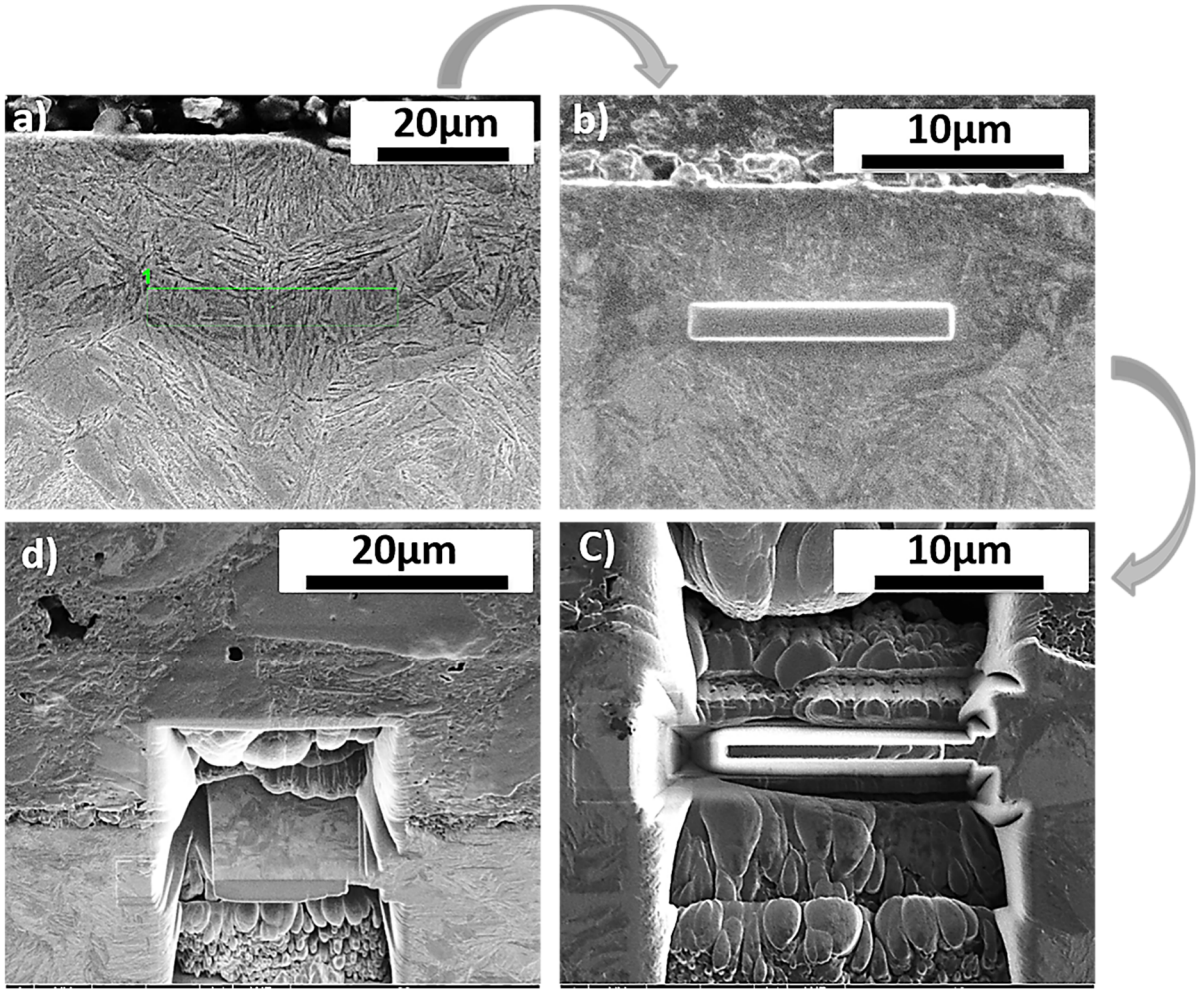

Figure 22. FIB sample preparation a) selecting site of interest, b) Pt-deposition on selected area for protection, c) removal of material adjacent to the area of interest d) further thinning to < 100 nm.

8.3 X-ray diffraction

In this study, both residual stresses and retained austenite were determined by using X-ray diffraction analysis.

8.3.1 Theoretical background of X-ray diffraction – Residual stress measurements

In 1912, English physicists, W.H. Bragg along with his son W.L. Bragg developed an expression (referred as Bragg's law), see in equation 8.1, to elucidate why the periodic atomic planes of crystals diffract X-ray beams at certain angles of incidence θ.

$$n\lambda = 2d_{hkl}\sin\theta \qquad 8.1$$

In equation 8.1, λ is the wavelength of the X-ray, d_{hkl} is the interplanar spacing of the reflecting planes, θ is the reflection angle and n is an integer number [88]. Stress is an extrinsic property

and cannot be measured directly. Therefore, elastic strain is measured and computed into stress by using values of elastic constants. Strain free crystalline material with defined inter-planar spacing produces a characteristic diffraction pattern when exposed to X-rays [88]. Under the influence of external forces, the inter-planar spacing d_{hkl} of the crystal lattice will change, which in turn causes a shift in diffraction pattern. This shift can be captured by using equation (8.2), which in its differentiation form yields:

$$\Delta\theta = \frac{-\Delta d_{hkl}}{d_{hkl}} tan\theta \qquad 8.2$$

Thus by measuring the shift $\Delta\theta$, the elastic strain i.e. $\Delta d_{hkl} / d_{hkl}$ within the material is estimated and thereby the associated stress value can be determined. Figure 23 depicts the mathematical relationship between interplanar spacing and elastic strain. A plane stress condition is assumed in the surface layer exposed to X-ray radiation. This means, the stress (σ_3) perpendicular to the surface is supposed to be zero. However, the strain (ε_3) component is not equal to zero due to Poisson's contractions created by principle stresses, and it can be obtained from equation (8.3) as follows:

$$\varepsilon_3 = \frac{d_n - d_0}{d_0} \qquad 8.3$$

where d_n is strained inter-planar spacing measured from peak shift and d_o is unstrained inter-planar spacing. Of course, it is also possible to measure the planes oriented at different angles of ψ by simply scanning the specimen for various tilt angles. The strains for lattice planes with respect to angles ψ and ϕ [89] can be expressed as:

$$\varepsilon_{\phi\psi} = \frac{d_{\phi\psi} - d_0}{d_0} \qquad 8.4$$

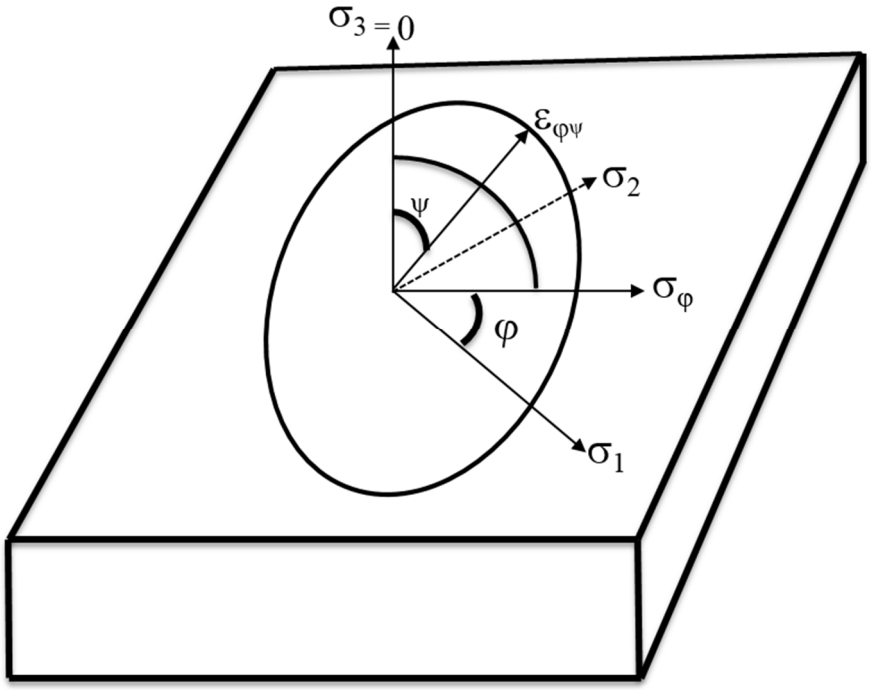

Figure 23. Schematic showing plane stress condition at the surface, $\sigma_3 = 0$. Whereas both σ_1 and σ_2 lie in the plane of the surface.

From Hooke's law, which relates the elastic stress – strain of an isotropic solid material, the strain $\varepsilon_{\phi\psi}$ along ψ and ϕ angles [89] is given by:

$$\varepsilon_{\phi\psi} = \frac{d_{\phi\psi} - d_0}{d_0} = \left[\frac{1+\upsilon}{E}\,\sigma_\phi\, sin^2\psi\right] - \left[\left(\frac{\upsilon}{E}\right)(\sigma_1 + \sigma_2)\right] \quad 8.5$$

where υ is Poisson's ratio, E is the modulus of elasticity. By rearranging equation (8.5), we get:

$$d_{\phi\psi} = \left[\left(\frac{1+\upsilon}{E}\right)\sigma_\phi d_0 sin^2\psi\right] - \left[\left(\frac{\upsilon}{E}\right) d_0(\sigma_1 + \sigma_2)\right] + d_0 \quad 8.6$$

Equation (8.6) shows the linear relationship between lattice spacing $d_{\phi\psi}$ and $\sin^2\psi$, and by measuring lattice spacing at multiple ψ tilt angles, the surface residual stress σ_ϕ can be determined by calculating the slope of a line fitted between $d_{\phi\psi}$ and $\sin^2\psi$ as shown in eq. (8.7):

$$\sigma_\phi = \frac{E}{1+\upsilon} \times \frac{1}{d_0}\left(\frac{\partial d_{\phi\psi}}{\partial sin^2\psi}\right) \quad 8.7$$

However, the value of d_0 is generally unknown, but because the Young's modulus is much greater than the summation of principal stresses (E>> $\sigma_1 + \sigma_2$), the d_0 can be substituted by the interplanar spacing value measured at ψ = 0 ($d_{\phi 0}$) with less than 1% inaccuracy [89]. The technique, where multiple ψ tilts are used to determine σ_ϕ is popularly known as the "$\sin^2\psi$ technique". An example of graph recorded in this thesis study using $\sin^2\psi$ technique is shown in Fig. 24.

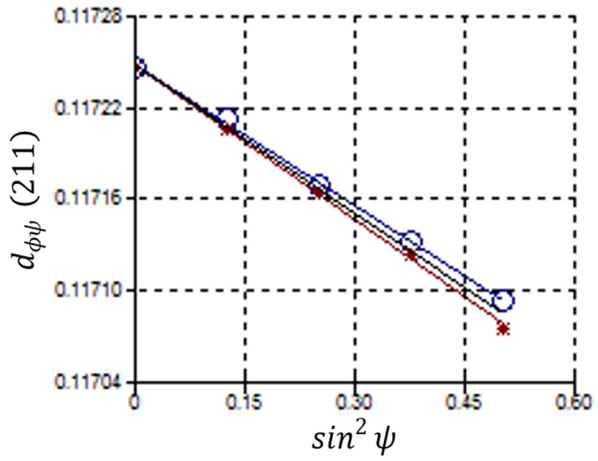

Figure 24. The $d_{\phi\psi}$ Vs $\sin^2\psi$ plot (recorded in this work).

In this work, the residual stresses were performed on a XSTRESS 3000 G2R with CrKα X-ray source. Five equi- sin2 (ψ) tilts from -45/+45 and lattice deformations for {211}α –Fe peak were used for determining the stress values. To measure surface residual stress, X-rays were irradiated through either a circular 3mm or 2mm collimator respectively.

8.3.2 Gear flank mapping for surface residual stress measurements

Measuring residual stress on involute gear teeth is complex and there is a high risk for interference of incident and diffracted beam by the adjacent teeth. In order to avoid these complexities, gear tooth was cut out from gear wheel by mechanical cutting. The stresses were

measured both in the profile and axial direction of the gear tooth. Due to contact mechanics, see Fig. 25, regions of gear flank experiences different kinds of stresses. Pure rolling exists along the pitch-line, positive sliding along the addendum and negative sliding along the dedendum regions [90]. To evaluate the effect of contact stresses separately, residual stresses were measured along three different lines in profile direction, and at three positions along each line in axial direction. The exact positions for the measurements along with their designations are illustrated in Fig. 26.

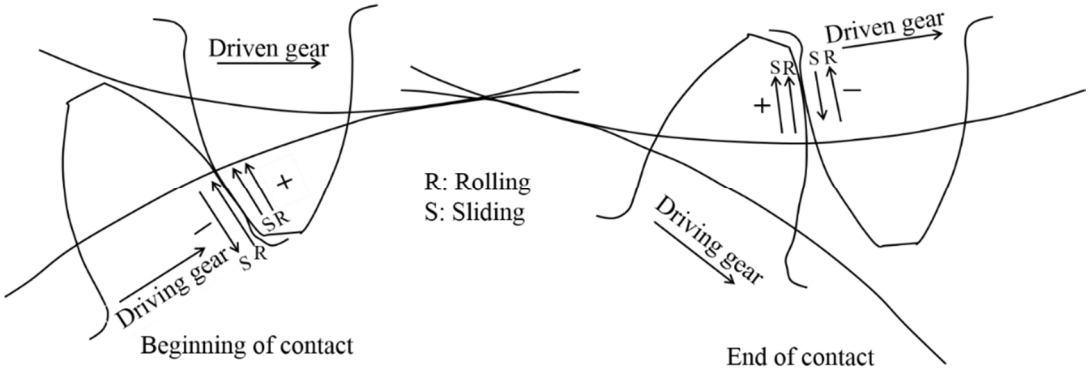

Figure 25. Contact conditions of sliding and rolling between gear pair.

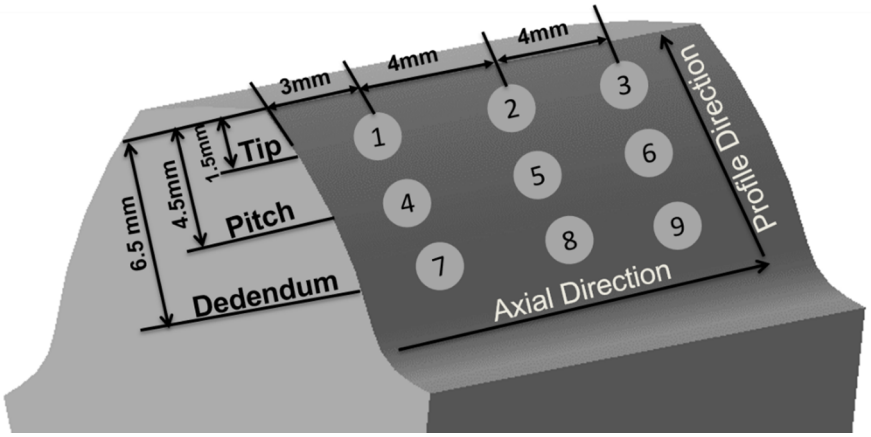

Figure 26. Gear tooth mapping for surface residual stress measurements.

8.3.3 In-depth measurements

It is a well-known fact that the average sampling depth of X-rays (used in XRD), which is defined as the distance from the surface where 63% of the diffracted intensity originates [91], is limited to the outer few micrometers. The important factors that influence the penetration and escape depths of X-rays is the attenuation coefficient of the material and dimensions of the irradiated beam on the analysing surface. According to [91], the penetration depth "x" can be estimated by using the expression:

$$x = \frac{1}{2\mu}\ sin\theta\ COS\psi \qquad 8.8$$

where, μ is the attenuation coefficient (~ 0.08733/m for iron base materials w.r.t Cr-kα source), ψ is the tilting angle of the X-ray beam and θ is the diffraction angle. Based on the above equation, the mean penetration/sampling depth (ψ is 33.21°) for iron base materials is around

5 µm. This leaves us with no option other than removing the surface material for measuring subsurface stresses.

In this thesis study, electrochemical etching was used to expose subsurface for measuring residual stresses. A 3M NaCl solution was used as electrolyte. The experimental setup with electrochemical cell used for etching is shown in Fig. 27. The gear tooth is turned into anodic surface by connecting it to the positive charge. A pencil shaped cathode connected to negative charge is placed over the gear tooth surface to be etched. Etching was carried out by applying a voltage and the material was removed through dissolution of the surface material in the electrolyte.

Similar to surface stress measurements the sub surface stresses were also measured along three different lines in profile direction. However, due to geometrical restrictions only one position along axial direction was measured. The exact locations for the subsurface measurements along with their designations are illustrated in the Fig. 28. The material was removed in a circular area of diameter 3.5 mm and a collimator with diameter 1.5 mm was then used for irradiating X-rays.

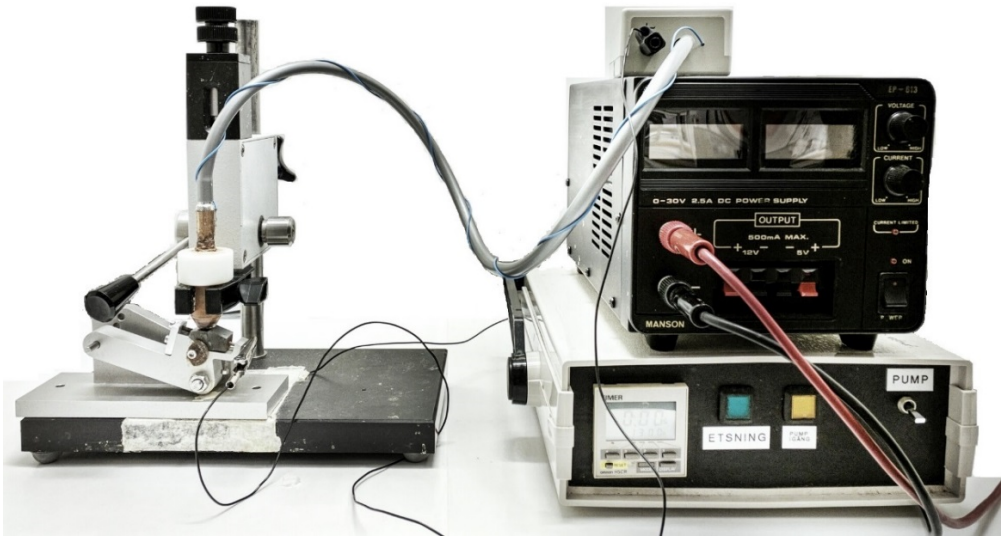

Figure 27. Experimental setup with electrochemical cell used for etching.

Obtaining a flat and smooth surface for every etching step is highly essential for accurate stress measurements and achieving this on involute profile is very difficult. Therefore, a special tool holder was designed (Fig. 29) to make the confined circular region horizontal for etching. To etch, the gear tooth was first fixed over involute base tooth rest. The surface to be etched was brought to flat position by locking the tooth rest arm in a specific hole present in the adjacent block. For example, to etch the tip surface, the tooth rest arm is locked in the hole designated as

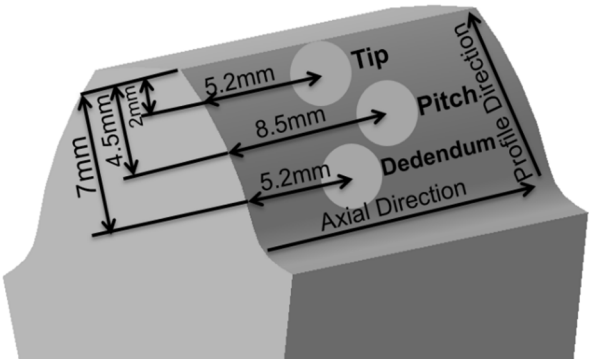

Figure 28. Gear tooth mapping for subsurface stress measurements.

tip. The holes on the adjacent block were made at specific angles that were calculated with respect to involute profile.

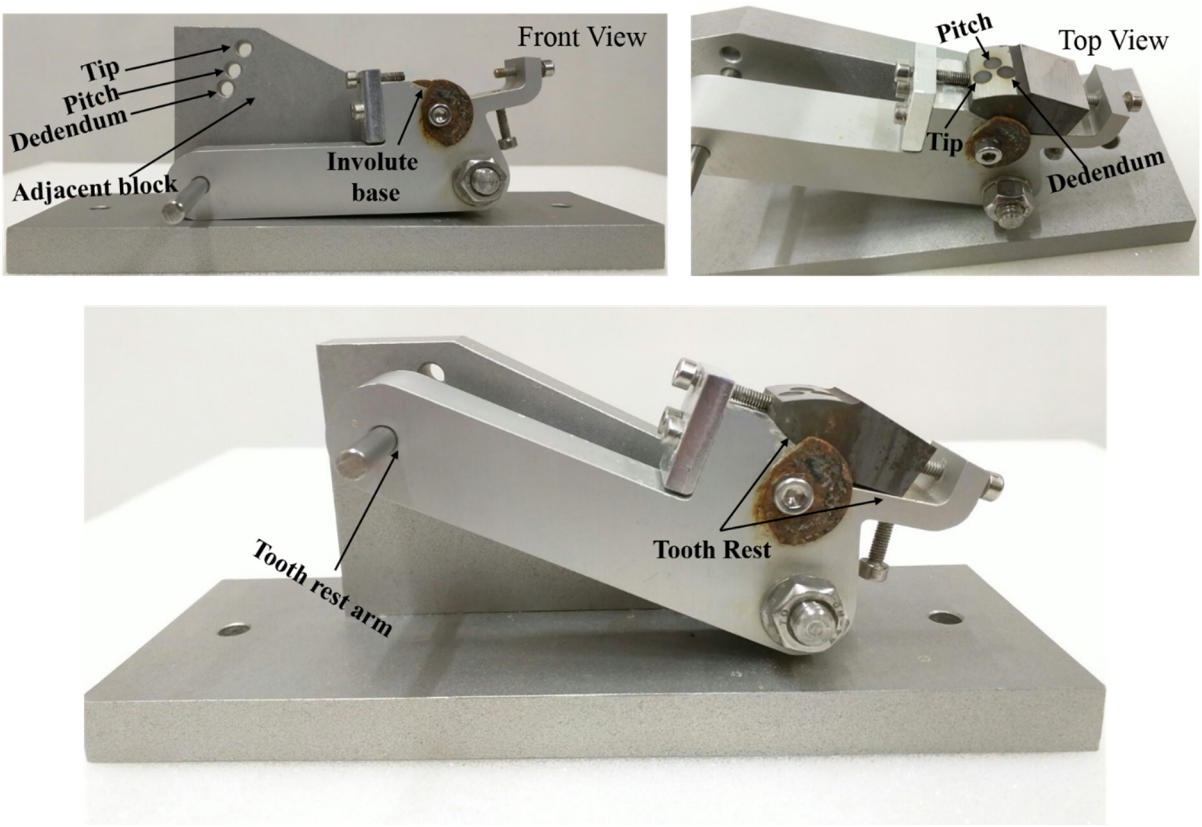

Figure 29. Specially designed tool holder for etching involute gear tooth (developed in this thesis study).

After every step of etching, the etch depth and roughness of the etched hole were confirmed by stylus profilometer. An example of the etch depth measurement is shown in Fig. 30.

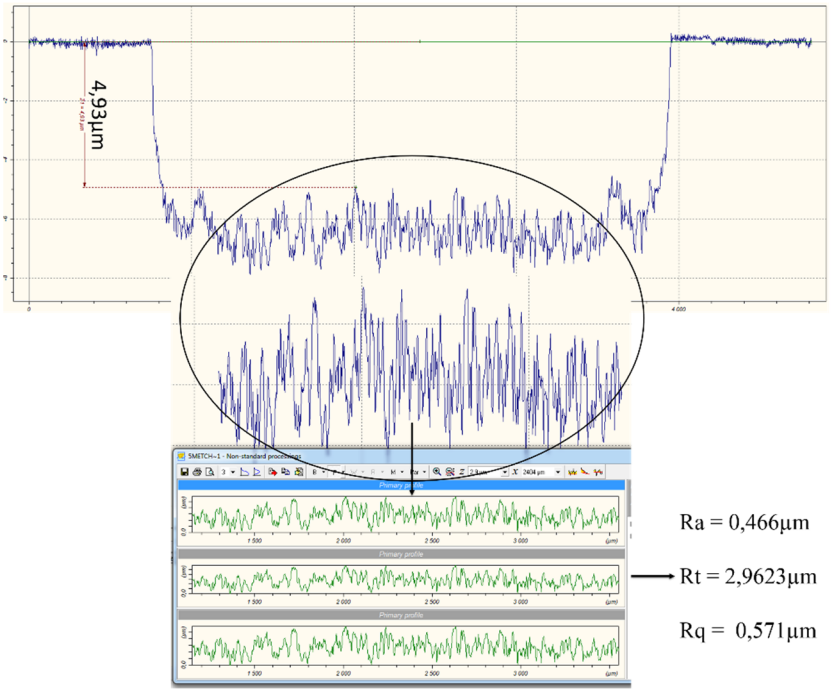

Figure 30. Etch depth verification measurement (recorded in this thesis study).

8.3.4 Retained austenite measurements

Retained austenite measurements were performed by using XSTRESS 3000 G2R. In this technique, the integrated intensity of the austenite and ferrite (martensite) peaks were measured first by using the diffraction planes $\{200\}_{\gamma}$, $\{220\}_{\gamma}$ and $\{200\}_{\alpha}$, $\{211\}_{\alpha}$. Then by comparing measured integrated intensities with theoretical intensities, the volume fraction of retained austenite is determined according to the equation 8.9. The detailed derivation to the equation (8.9) is found elsewhere [92].

$$V_{\gamma} = \left[(1 - v_c) \frac{\frac{1}{q} \sum_{j=1}^{q} \left(\frac{I_{\gamma j}}{R_{\gamma j}} \right)}{\frac{1}{q} \sum_{i=1}^{p} \left(\frac{I_{\alpha i}}{R_{\alpha i}} \right) + \frac{1}{q} \sum_{j=1}^{q} \left(\frac{I_{\gamma j}}{R_{\gamma j}} \right)} \right] \quad 8.9$$

In eq. 8.9, I_{γ} is the integrated intensity for the austenite peak, I_{α} is the integrated intensity for ferritic/martensite peak and v_c is the volume fraction of the carbides present. The parameter R is theoretical integrated intensity for each phase and is dependent on parameters such as interplanar spacing, Bragg angle, crystal structure and phase composition. The influence of carbides is normally small and can be neglected. For measurements, the exposure time was set to 30 sec with an inclination of +45° and scanning ± 85° with 15 steps. For in-depth analysis, same etching procedure as used for stress measurements was followed.

8.4 X-ray photoelectron spectroscopy

X-ray photoelectron spectroscopy (XPS) is a surface sensitive technique that is based on the photoelectric effect [93]. The working principle involves irradiating the material with a monoenergetic beam of X-ray photons having energy hυ. Thus interacted X-rays with surface region causes emission of so called photoelectrons i.e. photo emission. The kinetic energy and the intensity of the emitted electrons are then measured by using a detector. Thereby, the binding energy which is unique for each element is derived from the expression:

$$BE = \mathrm{h}\upsilon - \mathrm{KE} - \varphi \quad 8.10$$

where, BE is the binding energy of the emitted electron, KE is the kinetic energy and φ is the spectrometer work-function.

In this study, surface chemical analysis and compositional depth profiling of the gears tested for different conditions were performed by means of XPS combined with argon ion etching. The XPS spectra were obtained by using both a PHI 5500 spectrometer and PHI 5000 Versaprobe III Scanning XPS Microprobe, operated with monochromatic Al Kα (1486.6 eV) source. For the measurements, a tooth from the gear wheel was cut out. Before introducing into the vacuum chamber, gear tooth was cleaned with xylene for 5 minutes in ultrasonic bath and then with ethanol for 5 more minutes. Argon ion etching was employed for depth profiling with etch rate as calibrated on Ta_2O_5. Both survey spectra and high resolution spectra for specific elements were acquired at each depth. An important characteristic of XPS is the capability of depicting the chemical state of the elements from the high energy resolution positioning of the characteristic BE energy peaks for the elements. This allows for example to distinguish to what extent Fe is present in oxide state compared to its metallic state or if e.g. oxygen is present in the form oxide (O^{2-}) or hydroxide state (OH^-).

According to the instrument setup, both the X-ray source and spectrometer axis are positioned at an angle of 45° with respect to the normal of the sample surface. However, this setup is true only for the flat surface samples. Gear tooth secured to the specially designed holder (surface profile remains same for every gear tooth) gave a surface profile that is only flat at dedendum region, see Fig. 31. Therefore, to ensure same photoelectron emission angle and etch rate for different regions of a gear tooth, the stage remained unchanged for analysing dedendum, tilted to 11° for analysing pitch region and 25° for analysing tip surfaces. The tilt direction is shown in Fig. 30.

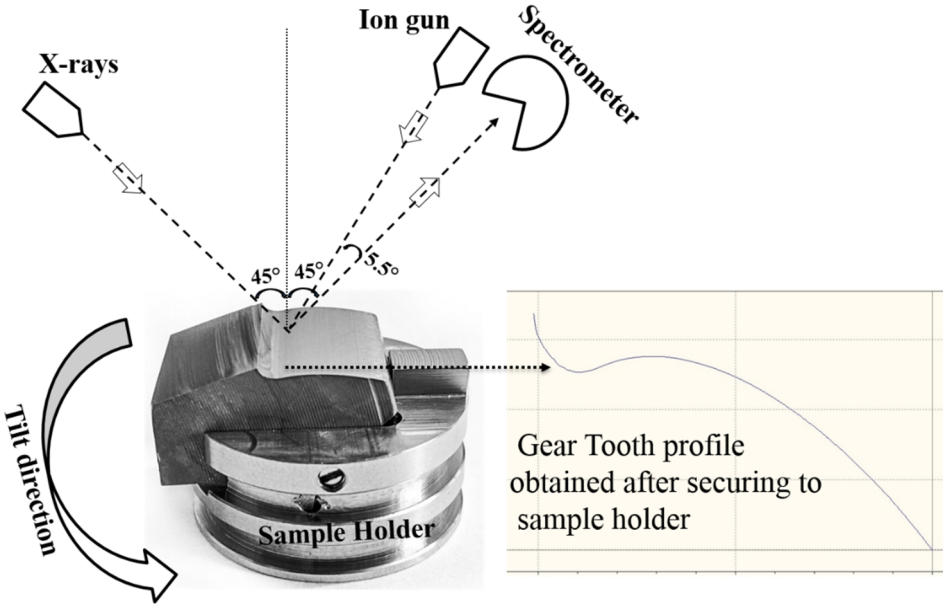

Figure 31 – Gear tooth setup for XPS analysis (developed in this thesis study).

A stainless steel mask with similar involute shape was attached to the tooth flank. Circular holes with 3 mm diameter positioned at the centre of face were made on separate masks at all three regions. The main purpose of the mask was to protect the surface outside the intended analysis area while ion etching. Secondly, it ensures the reproducibility of measurement location for comparing different test conditions.

9 Summary of results and discussion

The performance of the gears highly relies on the surface integrity characteristics such as topography, residual stresses and microstructure that are generated by hard finishing processes. In addition, the contribution of tribo layers from lubricant additives should also be considered. Nevertheless, every finishing process produces unique characteristics, which responds differently to the operating conditions, and in turn influences the surface integrity of gears accordingly. In this context, a detailed investigation has been performed to understand the variances in surface characteristics generated by ground, honed and superfinished gears and their evolution with respect to testing. In addition, micropitting mechanism related to microstructural changes was also studied in detail. In the forthcoming section, a short summary of key results along with the discussion is presented.

In this study, the evolution of surface characteristics was characterized in a holistic way by combining different analytical techniques such as XRD, LOM, SEM, TEM and XPS. The advantage of combining techniques is that the evolution of individual characteristics and correlation between them can be explored in detail.

9.1 Surface integrity characteristics of as-manufactured gears

In this section the following research question will be addressed.

- What are the differences in surface characteristics generated by different finishing methods; ground, honed and superfinished?

Before going into details regarding surface integrity characteristics, it should be noted that all the gear were first hard finished by grinding. Then, after grinding, one set of gears was honed and one set was superfinished. For details, see chapter 7.

The characteristic micro topographical features such as lay and roughness are totally dependent on the final hard finishing process applied. Figure 32 shows dedendum surface topography of differently finished gears. Gear surface finished by grinding process generated roughness lay parallel to the axial direction and the orientation of lay is uniform all over the surface i.e. at tip, pitch and dedendum. While, for honed gears, the lay orientation is different at different regions (not shown here). The lay orientation is similar to ground gear at pitch surface. However, at the tip and dedendum surface the lay is oriented at an angle with respect to the pitch surface, but in an opposite direction. For the detailed image, see Fig. 1 in the appended paper III. Irrespective of the orientation, the lay of both honed and ground gears consist of adjacent peaks and valleys with irregular surface asperities. These surface peaks with asperities determines the real contact area, and thereby acts as localized stress raisers. This in turn influences the surface integrity, and ultimately contact fatigue. On the other hand, superfinished gear tooth surface is smoother and has no roughness lay and asperity peaks. However, irregular isotropic grooves are present all over the surface.

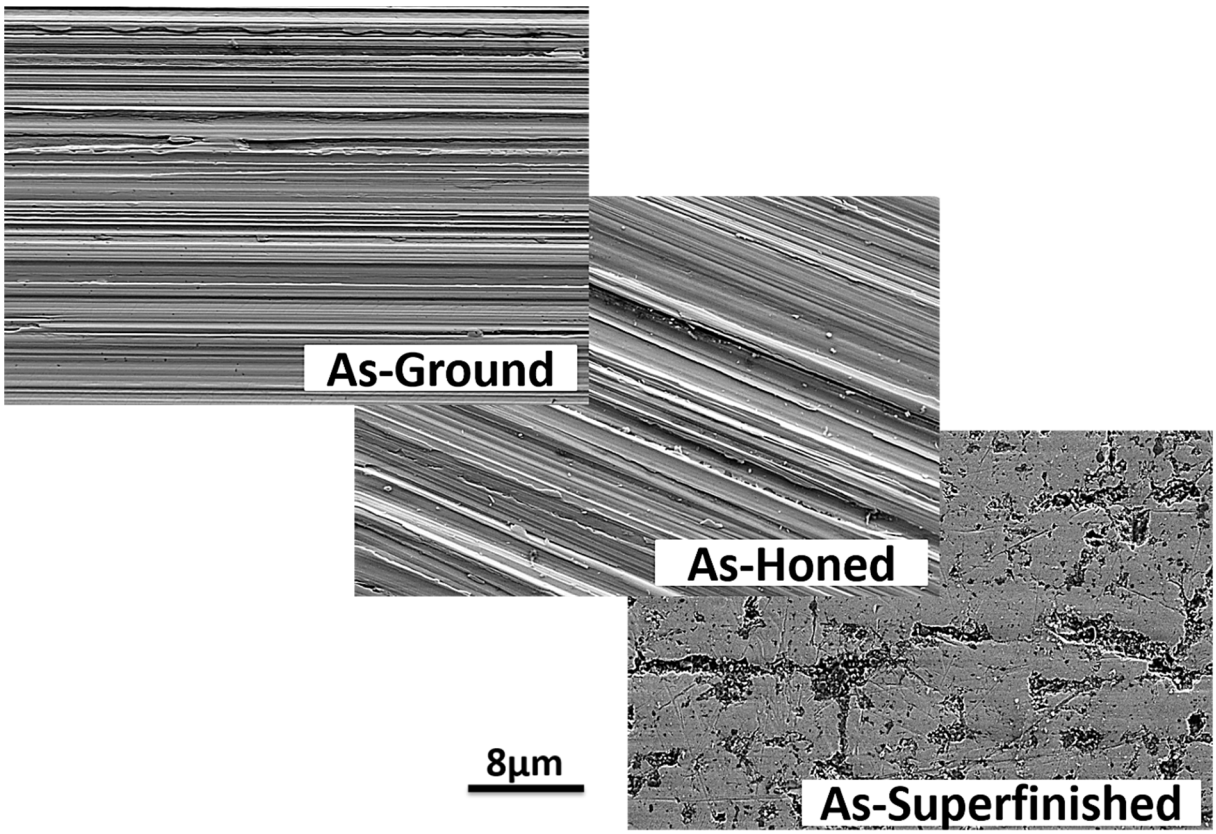

Figure 32. Surface topography of as-manufactured ground, honed and superfinished gears at dedendum.

Residual stresses plays an influential role in enhancing the fatigue life of gears. It is a well-known fact that presence of tensile residual stresses are undesirable, while compressive stresses are beneficial for fatigue.

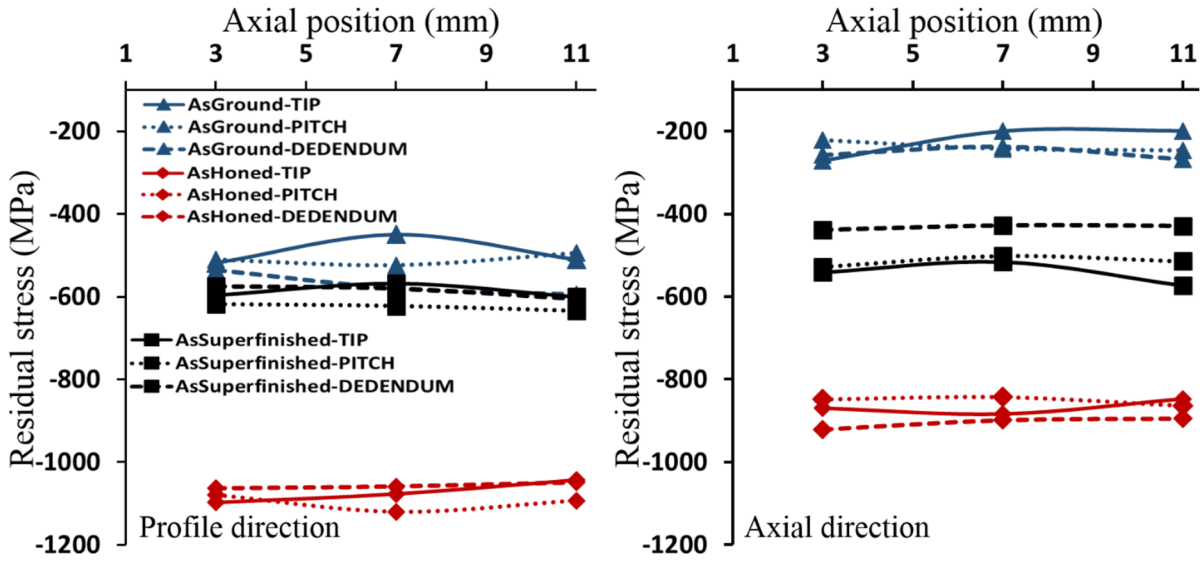

Figure 33. Surface residual stresses of as ground, honed and superfinished (paper IV).

In general, mechanical treatments employed after the carburizing and hardening processes influences the residual stress levels. For example, stresses developed during grinding process can be compressive or tensile depending upon the operating conditions used [94]. Therefore, one should be aware of the stress levels induced by hard finishing prior to the testing. Figure 33

shows residual stress distribution over gear tooth surface of different finishing processes. It is evident from the figure that the stresses were compressive in both directions and for all the finishing methods. However, the honing induced highest compressive stresses followed by grinding and superfinishing. Similar levels of residual stresses for ground and honed gears were previously reported in a robin study [95]. However, unlike in this study, grinding and honing was performed separately after case hardening. The other important observation is that there is no significant variation between tip, pitch and dedendum surfaces, and this is true for every condition. However, there is a difference in stress levels between directions, and this difference is higher for ground gears followed by honed and superfinished. The difference in stress levels between finishing methods was not only limited to the surface, but extended beneath the surface, see Fig. 34. The major difference is that honing induced compressive stresses to a depth of ~ 10 µm, whereas, stresses induced by grinding and superfinishing were limited to the outer layers of 5 µm.

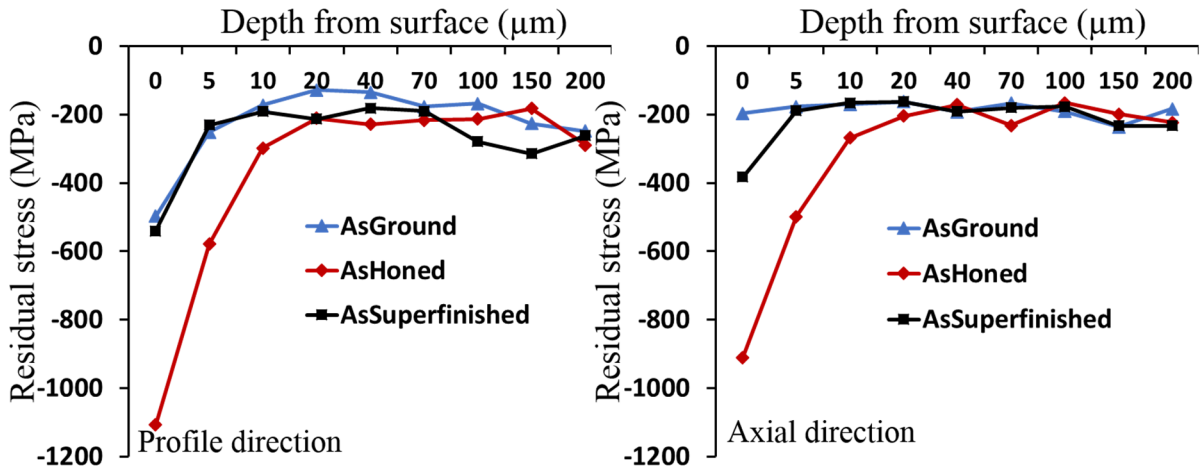

Figure 34. Depth profiles of residual stress measured at center of the dedendum.

Regarding microstructure, the case hardened layer consist of mixed lath and plate martensite along with retained austenite. An example of as-ground gear microstructure is shown in Fig. 35. It should be remembered that with the aid of an SEM image differentiating retained austenite phase from lath and plate martensite is nearly impossible. This differentiation is best seen under light optical microscope, for example see Figure 13. However, the retained austenite content was characterized by using XRD. The results showed that the retained austenite content of as-ground gears was around 22 vol%. Interestingly, additional finishing process honing and superfinishing decreased the retained austenite levels to about 10 vol% and 18 Vol% respectively. This indicates a possible transformation of retained austenite into deformation induced martensite. Moreover, the reduction could be further correlated to the noted higher compressive stresses, which typically develops as a consequence of volume expansion, which takes place during retained austenite transformation [96].

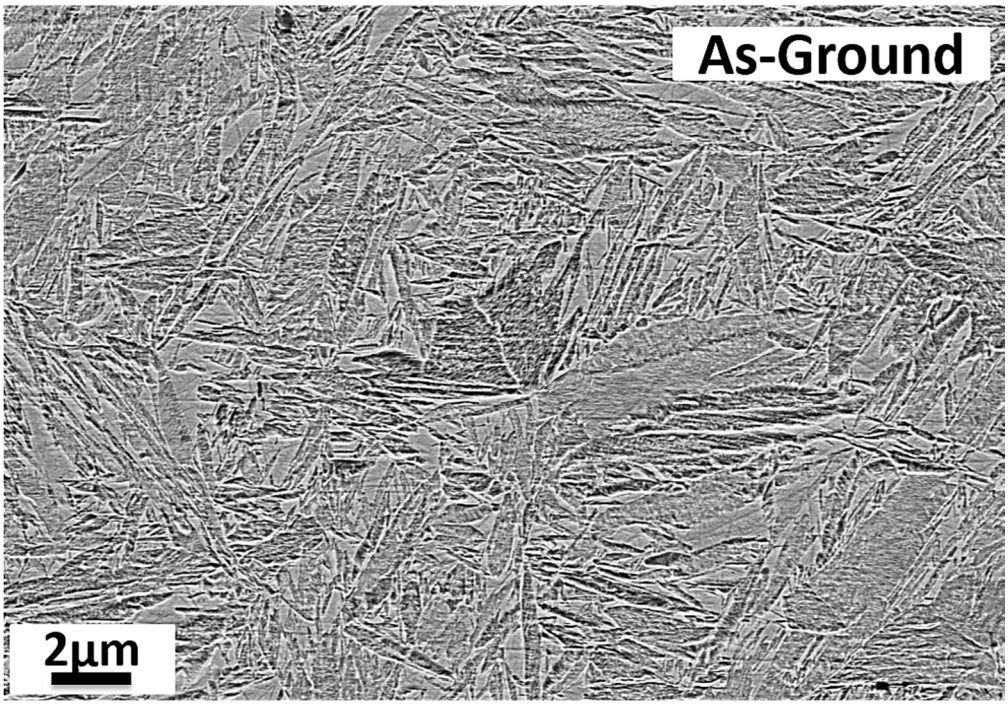

Figure 35. Case microstructure of as-ground gear tooth.

Apart from the above described characteristics, finishing processes also created differences in the chemistry of surface layers. An example of the XPS depth profile of an as-ground gear tooth is shown in Fig. 34. The gear surface was rich in C, O, and Fe for all the finishing methods (see upper part of the Fig. 36). The presence of Fe-oxide along with alloying elements Cr and Mn was limited only to a few nm. The XPS analysis though indicated a possible difference in oxide thickness with superfinished gear having somewhat greater oxide thickness. The C was mostly removed after first ion etching, hence, it can be attributed to the surface contamination. Nevertheless, the main difference comes from the elements that are presumed to originate from the tool materials, cutting fluids or liquids used during the finishing operation. The lower part of Fig. 36 shows such elements present on as-ground gear tooth. The characteristic elements

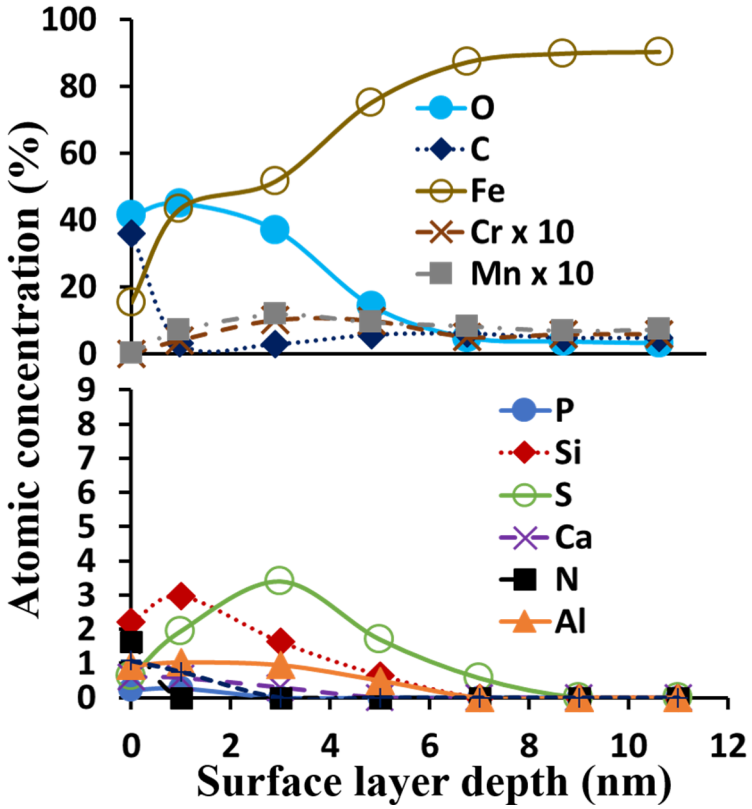

Figure 36. XPS depth profile analysed at dedendum surface of an as-ground gear tooth (paper II).

were S and Si, but minute traces of Ca, N, Al and P were also recorded but in a lower amounts. Here, S and P should be noted as they may originate from the additives present in the lubricant. Whereas, for honed gears, no traces of S and P were found and the profile did reveal low amounts of Si, N and Ca. For the superfinished gears the profile shows the same elements as for the as-honed, but just as the oxide was thicker they were present to a larger depth. In addition, there was some Al of about 2-3 at% and it is not unreasonable to assume that this observation originate from the abrasive slurry used in the superfinishing process.

9.2 Running-in and efficiency testing

Running-in process, in general, is known to improve the conformity between mating gears via smoothening of asperities. However, it will also affect the microstructure, residual stresses and surface chemistry near the surface, factors that will influence the efficiency and durability of the gear. Nevertheless, the detailed understanding of how these surface characteristics evolve and in turn affects the performance has remained as an open question. In this context, the following research questions will be addressed.

- How will surface characteristics topography, residual stresses, microstructure and surface chemistry evolve during running-in for different finishing methods?
- How is the evolution influenced by the running-in parameters load and speed?
- How have these characteristics further developed and influences, gear behaviour during initial usage, here represented by efficiency testing?

Before going into details, it should be noted that the running-in cycles were 20880 revolutions of the wheel. The following summary is based on the testing that was performed at two different running-in loads (0.9GPa and 1.7GPa) with a pitch velocity of 0.5 m/s (corresponding to 87 rpm of the wheel). For better understanding of the results the detailed test matrix with individual test designations is presented in Table 4.

Table 4. Detailed test matrix with designations

Running-in		**Efficiency**	**Test Designation**
LS5(0.9GPa)	LS9(1.66GPa)		
x			GRI5
	x		GRI9
x			HRI5
	x		HRI9
x		x	GE-RI5
	x	x	GE-RI9
x		x	HE-RI5
	x	x	HE-RI9
x		x	SFE-RI5
	x	x	SFE-RI9

The designations GRI5 and GRI9 represents running-in tests of ground gears corresponding to load stages LS5 and LS9. Similarly, GE, HE and SFE represents efficiency tested ground, honed and superfinished gears. The complete formulated test designation, for example, GE-RI5 indicates efficiency tested ground gears with prior running-in performed with LS5. It should also be noted that superfinished gears were examined only after efficiency testing. The

influence of higher running-in speed (8.3m/s) was also studied, but for only honed gears. The most significant conclusion with respect to speed was that micropitting was enhanced by speed more than load.

The surface asperities were plastically deformed in the direction of sliding during running-in and as a consequence, the micropits were formed. As can be expected the deformation was higher for higher running-in load, and thus also the micropits formation. The influence of running-in load was higher for ground gears that had rougher initial surface compared to the honed gears. The efficiency test following running-in continued the trend, and as a result, the degree of micropitting was higher for GE-RI9 and HR-RI9 than GE-RI5 and HE-RI5 test conditions. Nonetheless, the amount of micropits is nearly identical between HE-RI9 and GE- RI5. Moreover, the difference in micropits between HE-RI9 and HE-RI5 is less significant compared to the difference in micropitting between GE-RI5 and GE-RI9. As an example, stitched SEM micrographs of efficiency tested ground gears are shown in Fig. 37.

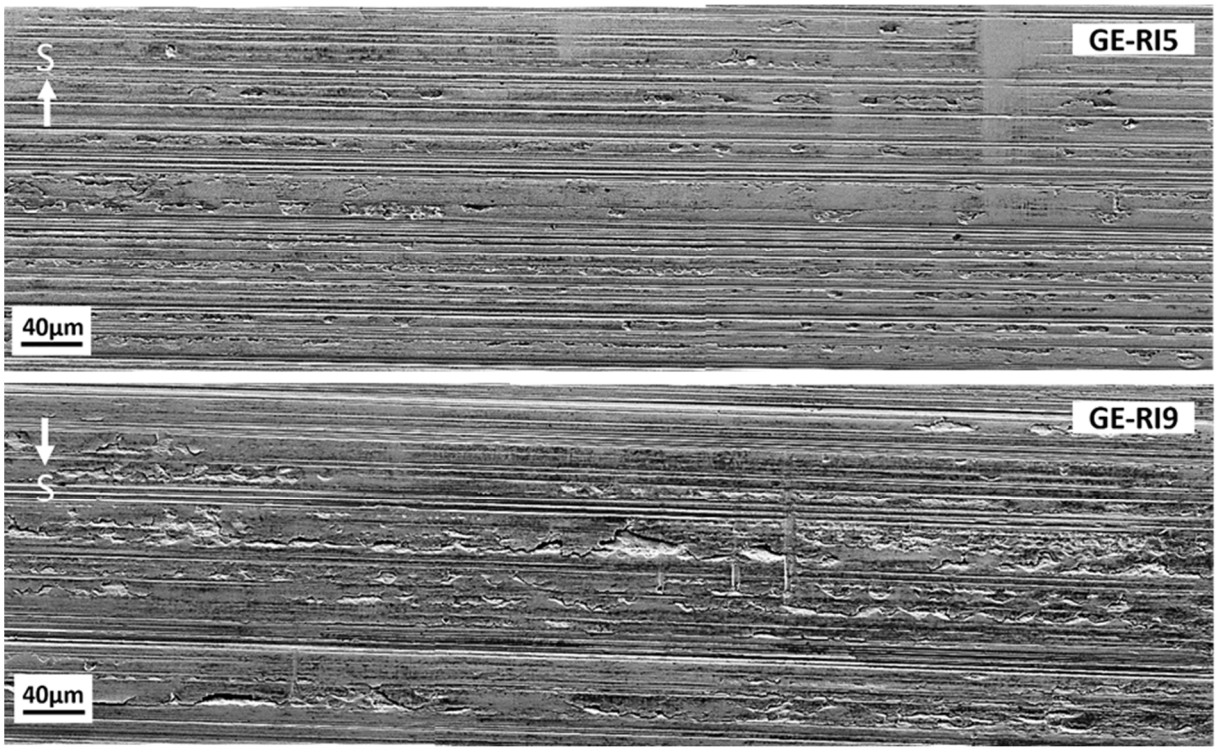

Figure 37. Dedendum surface topography of efficiency tested ground gears. “S” indicates the sliding direction. The shown stitched SEM images were taken at dedendum surface close to EAP (paper IV).

For superfinished gears, micropitting has not occurred even after efficiency testing. The results emphasise that higher surface roughness produced higher amount of micropits. Similar effect of roughness on pitting behaviour was previously reported by Muraro et al [39], who performed pitting testing with spur gear finished by shaving and milling. They observed that pitting was higher for the milled gears that had a higher initial surface roughness and, they attributed the better performance of shaved gears to the uniform load distribution and higher λ (specific film thickness) values to be achieved due to lower surface roughness. Andersson et al. [97], who calculated the λ values of the very same gears presented in this study reported higher values for superfinished gears compared to ground gears. This also means that coefficient of friction was

higher for ground gears compared to superfinished gears. The conclusion is that the surface finish has a significant influence on the initiation and progression of micropitting. Even more importantly, the influence of running-in load is more pronounced for gears with higher roughness.

For ground gears, after running-in, the surface compressive residual stresses increased in both profile and axial direction. The following efficiency test decreased surface compressive stresses in profile direction and increased them in axial direction. As a consequence, the difference in stress levels between the directions induced by grinding was decreased. In contrast, running-in decreased the surface compressive residual stresses in both directions for honed gears. Then, the following efficiency testing further decreased the surface compressive stresses in both directions, but significantly in profile direction. Moreover, this trend was enhanced by higher running-in load. The decrease in profile direction compressive residual stresses of honed gears was attributed to maximum load stresses acting in profile direction created by the combined effect of rolling and sliding [98]. The direction of maximum load stresses applied is the same for ground gears. Still, the stress alteration pattern is different from that of honed gears. This shows that evolution of residual stresses is also dependent on initial stress state. On the other hand, the influence of retained austenite content and its transformation on residual stress evolution should not be neglected. After efficiency testing, the retained austenite content has reduced both in ground and honed gears. Importantly, the reduction was higher for higher running-in load conditions. Shaw et al. [99] reported the transformation of half of the initial retained austenite (which was about 60%) to deformation induced martensite in ground gears after testing for 32 million cycles. It was suggested that the austenite transformation, increased the surface compressive residual stresses in both directions, but significantly in axial direction. Also, in the present study for ground gears, compressive stresses increased in both directions at least after running-in. Although, the retained austenite content has not been characterized after running-in, it is not unreasonable to assume that the actual transformation might have happened during the very initial cycles of testing. This behaviour of early transformation was observed by the author, for details refer appended paper VI. In short, the increase in stresses in both the directions could be attributed to retained austenite transformation. Once this has happened and also the initial deformation of asperities, the maximum load stress acting in the profile direction might come into play and, hence, the reduction in profile direction stresses. Interestingly, for superfinished gears, even after efficiency testing, the residual stresses remained more or less same as that of the initial state. This indicates that the initial surface roughness also had an impact on the evolution of residual stresses. The evolution of sub surface stresses were also characterized and the results showed that the alteration of stresses is confined only to the outer most layers of ~ 5 μm in the surface for all the conditions.

The plastic deformation has also affected the microstructure. After running-in, deformation bands were observed near the teeth surface along the profile. These deformation bands were prominently seen at the dedendum, where micropitting is severe. This is the case for both the ground and honed gears. Though it is hard to quantify, more of these bands were seen for higher running-in load condition. Detailed cross-section analyses revealed the association of these bands with surface cracks that are known to be connected to surface asperities, for example see Fig. 38.

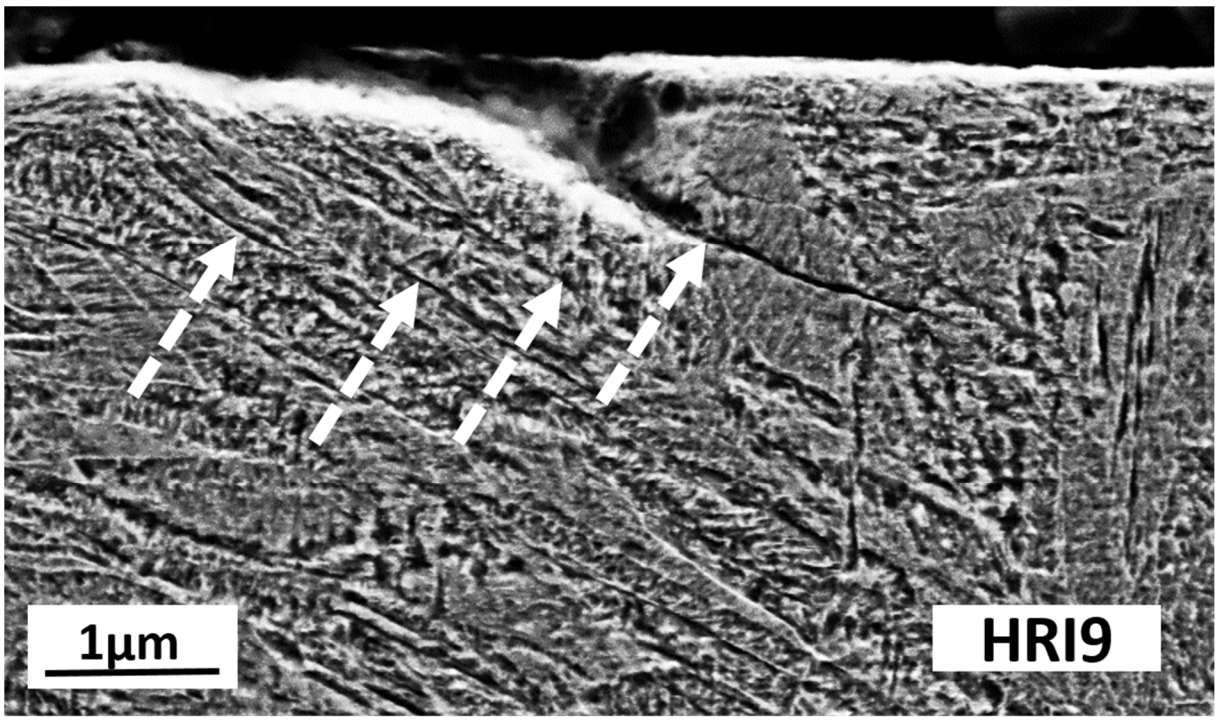

Figure 38. Deformation bands associated with cracks, indicated by arrows (paper III).

The efficiency test following running-in further increased presence of these bands. Furthermore, after efficiency testing, the surface cracks were often found in connection to plastic deformed regions (PDR) that are always associated with the deformation bands (see figure 13 in paper IV for reference). The plastic deformed regions and bands related to surface cracks will be discussed in detail in the subsequent micropitting section. Interestingly, none of these microstructural changes or surface cracks were observed in superfinished gears even after efficiency testing. The observed structural changes can be explained from surface roughness point of view, which is higher for ground and honed gears compared to superfinished gears. The initial real area of contact between mating gears is small for both ground and honed gears due to asperity interaction. This means all the imposed load is carried by the asperities. Together, sliding and normal force deform these asperities, but at the same time elevates the stress concentration within a narrow region beneath the folded asperities. With continuous cyclic loading, the deformation is accumulated leading to the formation of bands that are connected to cracks. Clearly, higher running-in load enhances the described phenomena. Contrary to this, superfinished gears without asperities possess large real area of contact, which means more uniform load distribution and hence no structural changes and cracks.

Regarding surface chemistry, similar oxides (Fe-oxide), C contamination, N, Al and Si distribution remained almost similar even after running-in and efficiency testing. A part from these general chemical characteristics, the most interesting elements to follow are P and S as they are present in EP additives and expected to contribute to tribo film formation. The S which was only found in the as-ground gear, was recorded to similar depths after testing. However, the concentration had slightly decreased and the decrease appeared to be enhanced by higher running-in load. These observations do not represent any significant changes and it is supposed be concluded that S was not active during testing and, hence no contribution in tribo film formation. For ground gears, more P from EP additives was observed after running-in. The XPS depth profile of P was similar for both running-in loads. However, the concentration for high

running-in load condition was found slightly higher up to a etch depth of 10nm. A similar trend was also observed for honed gears. The P profiles recorded after efficiency testing are shown in Fig. 39.

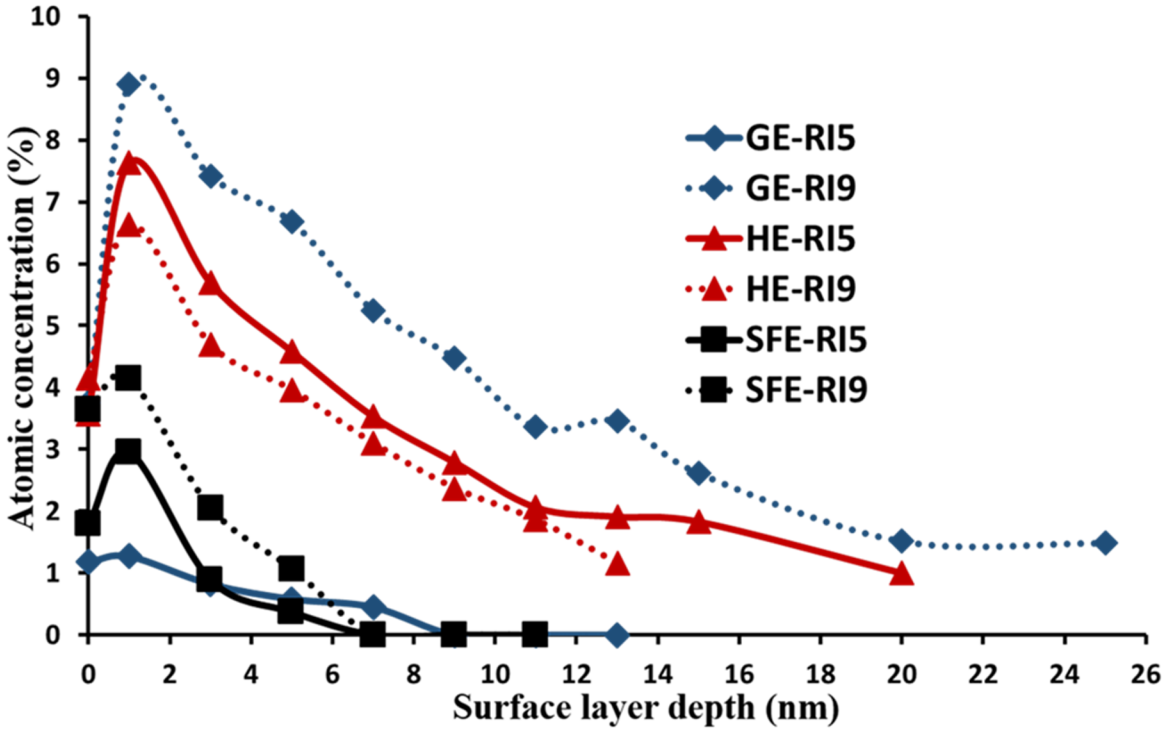

Figure 39. Phosphorous depth profiles after efficiency test for different conditions (paper IV).

As seen from the graph, higher P-levels in thicker layers were recorded for ground gears followed in order by honed and superfinished gears. However, there is a discrepancy for one particular test condition i.e. GE-RI5 that has among the lowest amounts of P for all tests. This trend was confirmed on multiple teeth. Contrarily, the running-in load had no major influence on the efficiency tested honed or superfinished gears. Calcium, known as detergent additive, was also recorded after testing. The trend with respect to the profile shape was similar to that of P but lower amounts. Disregarding GE-RI5, the results show that higher roughness promoted the tribofilm formation.

9.3 Micropitting

The influence of roughness and running-in load on micropitting phenomena has been discussed in earlier sections. Here, micropitting mechanism will be discussed with respect to microstructural evolution and, the following research questions will be addressed.

- Which microstructural changes occur during gear testing?
- What is the root cause of micropitting mechanism from microstructure prospective?

To systematically follow the evolution of micropitting and its relation to microstructural changes, ground spur gears were tested in a sequence from 200 to 2.2 x 10^7 cycles at logerthermic increment. The tests were carried out with a set torque of 239.3 Nm corresponding to 2.4 GPa Hertizan pressure at pitch. This rather high load was selected on purpose to promote

the formation of micropits. The speed of the wheel was 1500 rpm and the lubricant temperature was maintained at 85°C. The detailed test matrix is shown in Table 5.

Table 5. Micropitting test cycles (Paper IV)

S. No	Cycles	
	Pinion	**Wheel**
1	As-ground	As-ground
2	300	200
3	945	630
4	3000	2000
5	9000	6000
6	3×10^4	2×10^4
7	9.45×10^4	6.3×10^4
8	3×10^5	2×10^5
9	9.45×10^5	6.3×10^5
10	3.24×10^6	2.16×10^6
11	9.48×10^6	6.32×10^6
12	3.3×10^7	2.2×10^7

As known, the surface lay of as-ground gear tooth consists of adjacent peaks and valleys with irregular surface asperities. These asperity peaks were plastically deformed in the direction of sliding during testing and, the deformation was evident already after 200 cycles, which are the shortest cycles employed in the test matrix. Therefore, it should be remembered that the actual asperity deformation might have started even earlier than 200 cycles. For example, Sosa et al. [100] performed detailed analysis of the running-in of ground gears using in-situ profilometer measurements. In that study, 44 cycles were reported as run-in cycles required for surface transformation with respect to roughness. Returning to the tests performed in this thesis study, the evolution of micropitting can be outlined as follows. Considering the deformed asperities, these tended to cover the adjacent valleys and this trend continued with further testing. The asperities that cannot accommodate any further deformation started to break off leaving a micropit. This was first noticed for the 2000 cycles tested gear tooth. The micropitting then progressed with further testing along with the smoothening of asperities. Tough it is hard to quantify significant amount of micropits with larger size (> 20μm) was noticed after 2×10^4 cycles, see Fig. 40. The surface smoothening and growth of micropits continued further with increasing number of cycles and as a consequence the grinding lay disappeared (at least at dedendum) after 6.32×10^6 cycles (for reference see Fig. 6 in appended paper VI). Later, the micropits developed into macro-pits. To conclude, asperity deformation has smoothened the tooth surface, but at the same time initiated micropits in less than 2000 cycles.

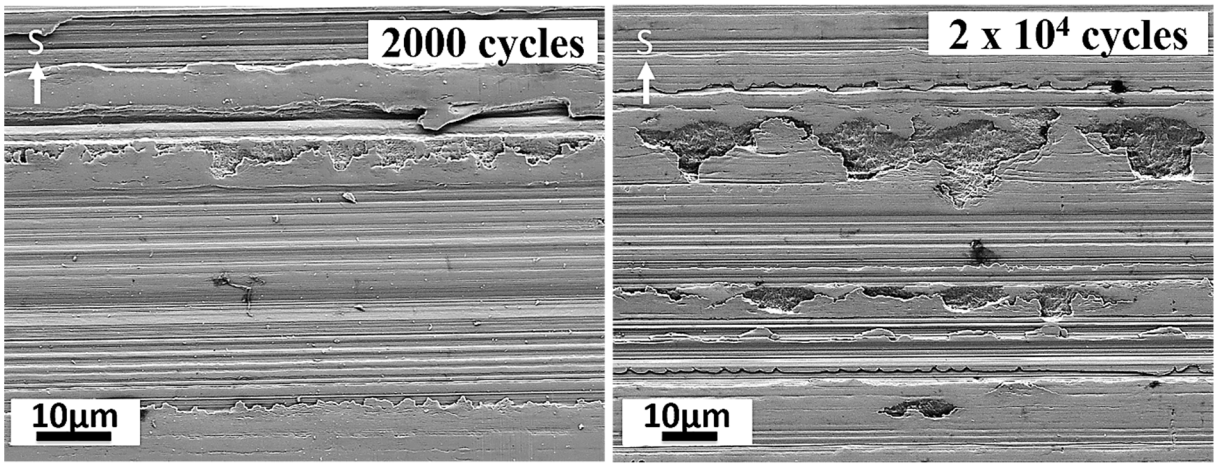

Figure 40. Dedendum surface topography after 2000 and 2 x 10^4 cycles.

The testing also induced changes in the residual stresses. Figure 41 shows the residual stresses induced by grinding and corresponding evolution during testing.

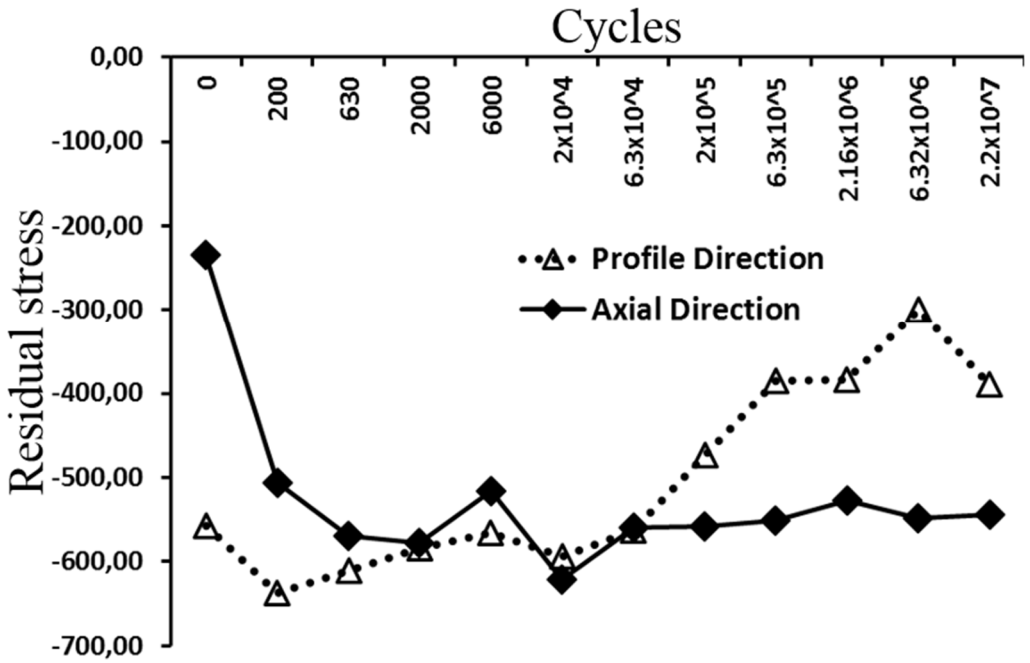

Figure 41. Evolution of surface residual stresses at dedendum for different test cycles of the spur gear testing. Note that the stress in as-ground gear tooth is represented as "0" cycles. Note that the maximum statistical error of these measurements was ± 20 MPa (paper VI)

The non-equal biaxial stresses induced by grinding has adopted to similar levels between directions within 2000 cycles. Prior to this, the compressive residual stresses were first increased in both the directions after testing for 200 cycles, and more so for the axial direction. Then, the profile direction compressive residual stresses progressively decreased slightly, while compressive stresses in axial direction slightly increased. The stresses then reached to similar levels at around 2000 cycles and remained more or less unchanged until 6.3 x $10^{\wedge 4}$ cycles. With further testing, the profile direction compressive stresses decreased significantly with increase in test cycles, while the axial direction stresses remained basically unchanged. This again

created a difference in stress levels between directions, but opposite to that of the as-ground surface. Still, the stress evolution was confined only to the surface zone of ~ 5 µm.

The plastic deformation of asperities also affected the microstructure. The initial retained austenite content of about 20 vol % was decreased to 17 vol % within 200 cycles. During the same number of test cycles, the compressive residual stresses also increased in both directions, but mostly in axial direction. In both cases the changes were confined only to the surface layer ~ 5 µm. Thus, it is reasonable to assume that the retained austenite has transformed into deformation induced martensite, which creates volume expansion and as a result the compressive residual stresses were enhanced in the matrix [96]. Then, the austenite content remained unchanged until 2 x 10^5 cycles. It then further decreased from 17 vol % to ~ 14 vol% and from ~ 14 % ~ 12 % after testing for 6.3 x 10^5 cycles and 6.32 x 10^6 cycles respectively, see Fig. 42. Considering the changes in austenite content during the testing, the stress evolution characteristics can in some way be connected. As said, after 200 cycles the compressive residual stresses tended to decrease and particularly so in profile direction, but remained unchanged for tests between 2000 and 6.3 x 10^4 cycles. This relaxation of compressive residual stress in profile direction could be attributed to the maximum load stress acting in profile direction, micropits and microcracks.

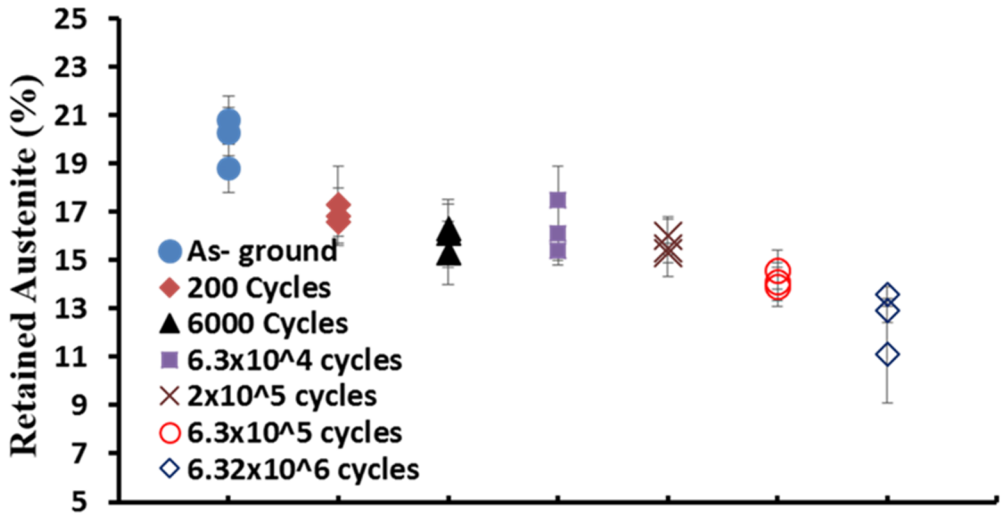

Figure 42. Surface retained austenite content at dedendum for different test cycles (paper VI).

Apart from retained austenite transformation, the etched cross sections revealed plastically deformed regions (PDR) with no initial characteristic martensite laths or plates, see Fig. 43a. These regions were discontinuous and most prominently seen at dedendum where micropitting occurred. In line with the asperity deformation, plastically deformed regions were also present already after 200 cycles. In addition, thin deformation bands associated with plastically deformed regions were also observed, but only after 2000 cycles. These bands were mostly found beneath the plastically deformed regions. However, they were also found independently both at the very surface and beneath the surface, see Fig. 43b. An image illustrating PDR (encircled) and deformation bands (indicated by orange arrows) is shown in Fig. 42a. Importantly, the cracks were found in association with these two microstructural changes; PDR (see red arrow in Fig. 43a) and deformation bands (see red arrow in Fig. 43b).

The detailed structure of a PDR region associated with a crack is shown in Fig. 44. As can be seen, the initial hierarchical lath martensite deformed and reoriented parallel to the sliding direction. Importantly, the thickness of lamellar deformed structure (see orange arrows in Fig. 43) continued to decrease in the sliding direction and disappeared towards the end indicating severity of deformation.

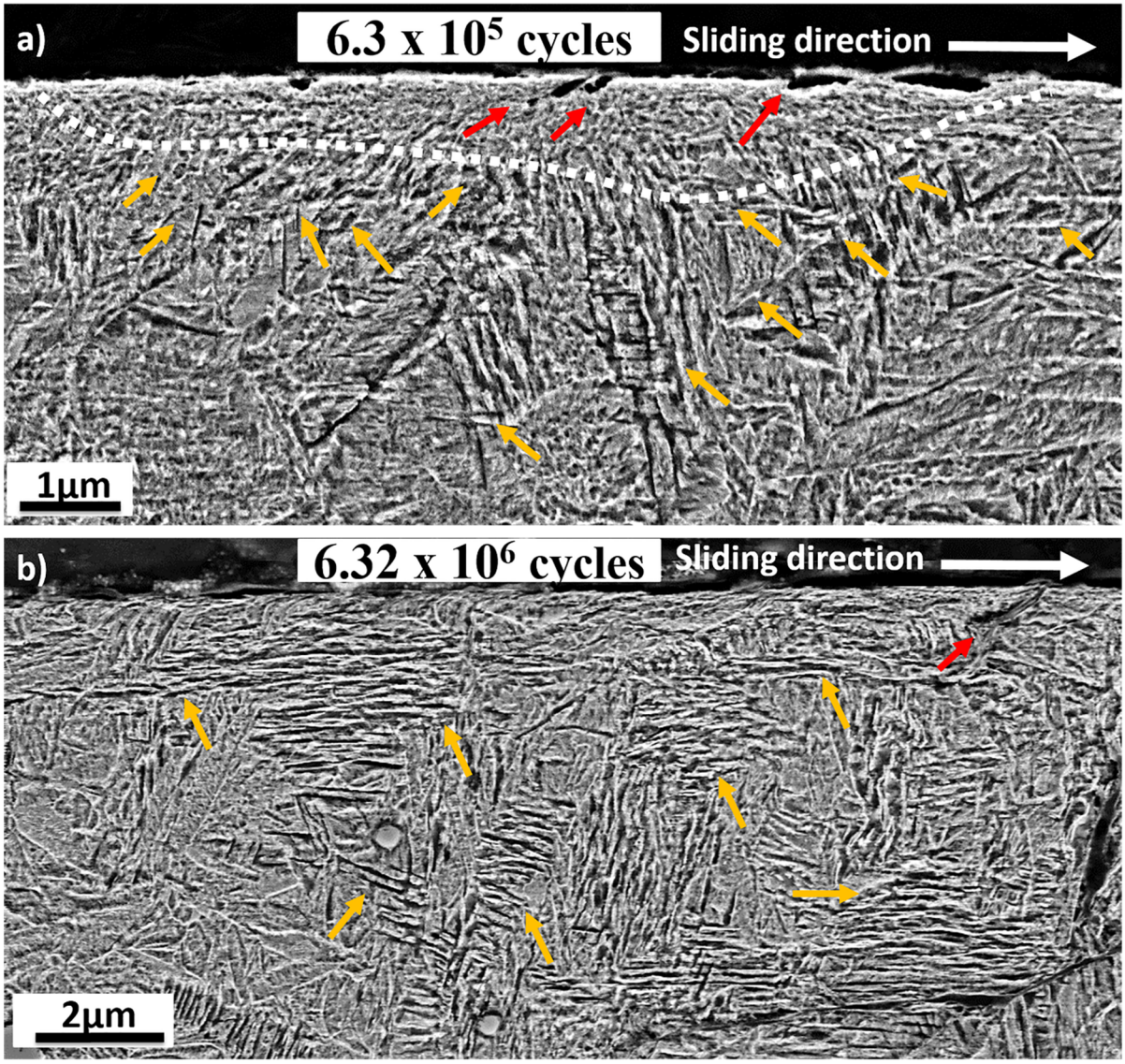

Figure 43. Microstructural changes associated with micropitting after 6.3 x 10^5 cycles a) and 6.32 x 10^6 cycles b). Encircled region illustrate PDR, orange arrows illustrate deformation bands and red arrows indicate cracks (Fig. 43a is from paper VI and 44.b is complementary figure prepared by author for thesis).

Consequently, micro-cracks might have initiated at the end where accommodation of any further deformation might become increasingly difficult with repeated cyclic contacts. However, the local hardness variations might also be responsible for crack initiation. This type of reorientation process to form lamellar deformation structure has been frequently observed in other lamellar structures such as pearlite with alternating ferrite and cementite lamellae [101] [102]. However, further TEM investigations are needed to reveal the true morphology of the

observed lamellar deformation in order to see the similarities or differences in comparison to surrounding deformed bands.

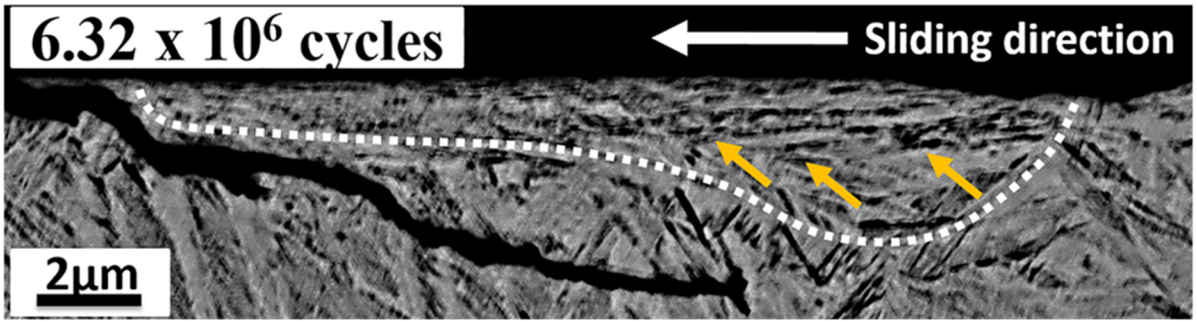

Figure 44. Back scatter electrons image showing the detailed structure of the PDR region, which has a typical lamellar structure at the surface with reducing lamellar thickness in the direction of sliding (paper VI).

To reveal the true nature of deformation bands including the crystallographic and dislocation structures an area with parallel lamellae orienting perpendicular to the surface was selected from the SEM observation and a foil with a thickness of 100 nm has been taken out by FIB in-situ lift-out technique (for more details see appended paper V). The TEM analysis showed that the deformation bands are connected to thin martensite lath lamellae (in nm range) with epsilon carbides precipitated at the lath boundaries. Such lamellae with no or less epsilon carbides within the lath seems to be more prone to local deformation as they offer least resistance to gliding compared to the coexisting adjacent coarse lath structure with internally precipitated epsilon carbide. The trace analysis also showed that these deformed thin lath lamellae are parallel to the {110} slip plane, which is the most common slip plane for bcc steel. In addition, the dislocation density of thin lath martensite was above the normal range, and the dislocation morphology in the martensite showed a typical deformation configuration with dislocations bulging from the martensite/carbide interface, see Fig. 45. This characteristic deformation behavior is quite different from the typical deformation of lath martensite without precipitated carbides at the lath interfaces, which transforms into a cell block structure when experience small to medium strains and then refines further with increasing strain [103].

Based on the observations with respect to the evolution of surface integrity characteristics, the micropitting mechanism has been divided into three different stages; running-in, steady progression and breakdown. A schematic representation of these three stages is shown in Fig. 46.

In short, micropitting was mainly associated with asperity deformation and microstructural changes; PDR and deformation bands. Depending upon the operating conditions used, these structural changes can develop within 2000 cycles. Therefore, from materials and microstructural point of view the running-in period is limited to 2000 cycles for the conditions tested.

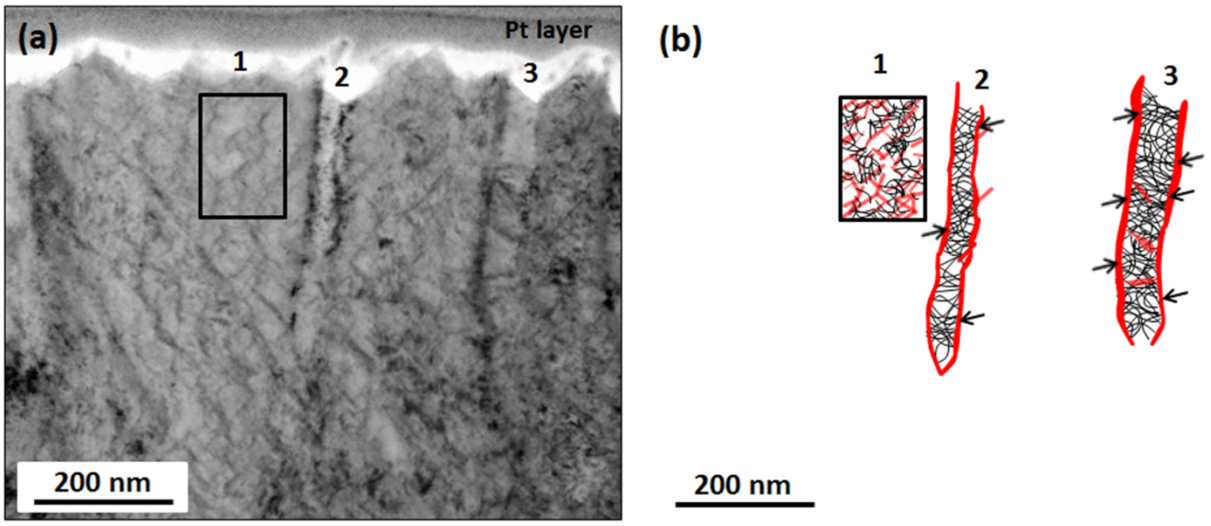

Figure 45. The TEM micrograph a) and associated sketch b), illustrating the dislocation and carbide configurations in the matrix and deformation lamellae. The black box indicated as 1 represents the neighbouring coarse lath martensite matrix, 2 and 3 represent the thin lath martensite deformation lamellae. In the sketch, the thick red rods and lines represent carbides while the black thin lines represent dislocations. The shown TEM micrograph was taken out from the cross-section of the gear tooth that was tested for 6.32 x 10^6 cycles by FIB in-situ lift out technique (paper V).

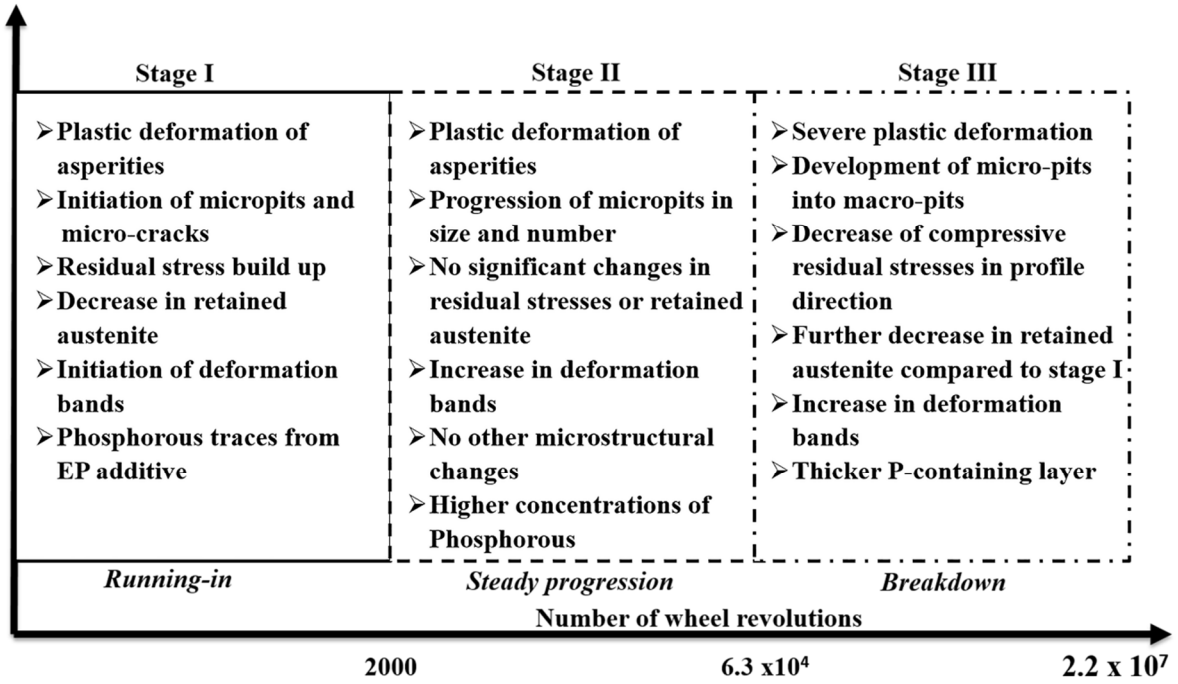

Figure 46. Schematic representation of the three stages of evolution of surface integrity characteristics (paper VI).

10 Conclusions

In the present study, the following concluding remarks can be highlighted.

Surface integrity characteristics of as-manufactured gears

- A methodology has been successfully developed to characterize the surface integrity characteristics of gears.
- All the surface characteristics; topography, residual stresses, microstructure and surface chemistry differ for gears finished by grinding, honing and superfinishing.
- Apart from the obvious differences in surface topography owing to finishing method, the residual stresses differed the most. The transformation of retained austenite during the finishing processes honing and superfinishing induced higher compressive stresses compared to the grinding of gears.

Running-in and efficiency testing

- The surface characteristics were clearly altered after running-in and efficiency testing, but were limited to a depth < 10 μm. The evolution of surface characteristics was strongly dependent on the initial state of the characteristics, in particular surface topography.
- Higher running-in load enhanced the smoothening of asperities via plastic deformation. However, it also gave more micropits. This trend continued also after identical efficiency tests. Still, the influence of running-in load was higher for ground gears that had higher initial surface roughness compared to the honed gears. The morphology of micropitting confirms that the micropits were associated with deformation of asperities in the sliding direction. Superfinished gears with smoother surface produced no micropits when tested. This suggests that roughness was of vital importance for the initiation and progression of micropitting.
- The initial residual stress state generated by different finishing methods played an influential role in the evolution along with the test conditions. For ground gears, running-in process increased the magnitude of surface compressive stresses in both profile and axial directions, but the profile direction compressive stress level decreased with prolonged testing i.e. the efficiency testing. However, the higher initial compressive stresses in honed gears tended to decrease more significantly in profile direction and only marginally in axial direction right from the start of running-in and after efficiency testing. These trends were enhanced by higher running- in loads for both the finishing methods grinding and honing. In the case of superfinished gears, the residual stresses remained almost unaltered. This again suggests that the changes in residual stresses resulted from the accumulated yielding of asperities. In addition, the deformation induced transformation of retained austenite contributed to the evolution of residual stresses in ground and honed gears.
- The concentrated stresses that acted on surface asperities gave rise to localized deformation that induced deformation bands into the microstructure. Hence, such deformation bands were seen only in ground and honed gears, indicating the significant

influence of roughness on such microstructure alteration. The bands appeared already after running-in and further developed with the efficiency testing. Most importantly, these bands were often found in connection with surface cracks and were promoted by higher running-in load.

- Phosphorous from EP additives was observed on all gears after running-in and efficiency testing. Also, the surface content of P was higher for ground gears followed by those for the honed and superfinished gears. This is attributed to the elevated contact stresses at asperity level.
- Overall, the results of this study showed that running-in process alters surface characteristics that are generated by a hard finishing process and presets the conditions for the usage/service. However, the influence of running-in was prominently seen only for the rough gear surfaces and this emphasise the roughness or topography as key characteristics that influences the performance of the gears.

Micropitting

- The SEM investigations revealed the first appearance of micropits on the tooth of the gear wheel that was tested for 2000 cycles. Then micropits progressed further with test cycles and developed into macro-pits at around 2.2 x 10^7 cycles.
- The micropitting initiated as a consequence of deformation of the asperities and associated microstructural changes; plastically deformed regions (PDR) and deformation bands. The PDR were seen already after 200 cycles, while deformation bands appeared after 2000 cycles. Hence, the actual initiation happened already during the initial 200 cycles.
- Detailed microstructural characterization by using TEM revealed that the deformation bands were nano-sized martensite laths with dislocations bulging out at the interface of martensite/ epsilon carbide precipitated at lath boundaries.
- The initial retained austenite content was decreased from 20 to 17vol% already after 200 cycles. This was responsible for an increase in compressive residual stresses during the initial 200 cycles.
- A tribofilm with P supposedly from EP additive was formed on asperities after initial 200 cycles and remained more or less unchanged until 20000 cycles when the coverage increased.
- The evolution of all the above mentioned characteristics indicates that the surface damage is a highly localized phenomena, which emphasise the importance of optimizing both surface topography and microstructure in order to avoid or at least to minimize the local impact.
- All in all, the current study showed that surface characteristics, in particular microstructural changes can occur within 2000 cycles, thus defining the running-in cycles from materials perspective.

11 Suggestions for future work

Some future recommendations based on the results obtained in this study are as follows.

- Knowing that the running-in period from materials prospective lasts for only 2000 cycles, the possibility of gear surface optimization within such short cycles can be investigated by varying different running-in parameters (load, speed, time and lubricant temperature).
- Further TEM analysis of deformation bands (for example intersected bands) could reveal additional information that might be helpful for better understanding of the micropitting mechanism in relation to microstructural changes.
- Further detailed TEM investigation is also needed to understand the true structure of the plastic deformed regions (PDR).
- Micropitting test on superfinished gears will be of interest in order to understand if there are any microstructural changes other than PDR and deformation bands.
- Synchrotron analysis locally around the deformation bands could reveal information regarding the local strains.

12 Acknowledgements

It gives me an immense pleasure to thank the many people who made this thesis possible.

First of all, I would like to thank my examiner, Professor Lars Nyborg for giving me the wonderful opportunity to work on this exciting project. His openness, invaluable guidance and suggestions are vital for completing the work presented in this thesis.

I gratefully acknowledge my supervisor Senior Lecturer Mats Norell for his support and encouragement throughout the thesis work, especially taking his extra time for never ending scientific discussions. Let me also express my special thanks to you, Mats, for taking care of me, professionally as well as socially.

I would like to thank Lennart Johansson at AB Volvo, Mats Henriksson at Scania CV AB and Professor Ulf Olofsson at KTH for their inputs and continuous engagement during the entire project. My special thanks goes in particular to Mario Sosa (twin PhD student at KTH) for helping me with the FZG gear testing, and for all the enthusiastic discussions on the running-in process.

I would also like to express my special thanks to Matti Näslund at Scania CV AB. I truly believe that without your encouragement and support gear testing at Scania would not have been possible. Thank you very much for sharing your knowledge and above all for your friendship.

Special thanks go to Rasha Alkaisee at AB Volvo for her support regarding stress measurements at Volvo Materials lab.

My deepest appreciation goes to senior researcher Xiaodan Zhang from Technical University of Denmark (DTU) for his wonderful collaboration. Thank you for enlightening and inspiring discussions related to deformation mechanisms. I really enjoyed working and writing an article with you.

My sincere thanks also go to research engineers Dr. Eric Tam, Dr. Yiming Yao and Roger Sagdahl at Chalmers University of Technology for their help with technical matters and issues related to experimental techniques. Without you people my work would have lasted longer.

I also benefited by outstanding work from Håkan Millqvist at Chalmers University of Technology who made tailored tool holders for residual stress measurements and XPS analysis.

I would also like to thank my current and former colleagues at the Department of Industrial and Materials Science for creating a friendly and motivating work environment.

Finally, I would like to express my deepest gratitude to my beloved wife (for all her patience during long working hours and for taking care of Saisha especially during the last months of this hectic journey), my parents, my brother and cousins (Nani and Chinnari Anna) for their endless support in every matter.

13 References

[1] K. Michaelis, B. Höhn, and M. Hinterstoißer, “Influence factors on gearbox power loss,” *Ind. Lubr. Tribol.*, vol. 63, no. 1, pp. 46–55, 2011.

[2] L. E. Alban, “Failures of gears,” in *Metals Handbook, Vol 11*, Ohio: ASM,1986, pp. 586–601.

[3] J. F. Kahles and M. Field, “Paper 4: Surface integrity—A new requirement for surfaces generated by material-removal methods,” *Proc. Inst. Mech. Eng. Conf. Proc.*, vol. 182, no. 11, pp. 31–45, Sep. 1967.

[4] U. Hindhede, “Spur gear fundamentals,” *Gear Technol.*, vol. 12, no. 6, pp. 36–48, 1989.

[5] P. Brechot, A. B. Cardis, W. R. Murphy, and J. Theissen, “Micropitting resistant industrial gear oils with balanced performance,” *Ind. Lubr. Tribol.*, vol. 52, no. 3, pp. 125–136, 2000.

[6] T. L. Krantz, “On the correlation of specific film thickness and gear pitting life,” *Gear Technol.*, no. February, pp. 52–62, 2015.

[7] Y. Ding and N. F. Rieger, “Spalling formation mechanism for gears,” *Wear*, vol. 254, no. 12, pp. 1307–1317, 2003.

[8] L. Faure, “Classification of types of gear tooth wear - Part 1,” *Gear Technol.*, no.November, pp. 32–38, 1992.

[9] L. Faure, “Classification of types of gear tooth wear - Part II,” *Gear Technol.*, no.January, pp. 34–40, 1993.

[10] S. R. Schmid, B. J. Hamrock, and Bo. O. Jacbson, Fundamentals of machine elements. Florida:Taylor and Francis Group, 2014.

[11] C. Hooke, “A review of the paper ‘A numerical solution to the elastohydrodynamic problem’ by D. Dowson and G.R. Higginson,” *Proc. Inst. Mech. Eng. Part C J. Mech. Eng. Sci.*, vol. 223, no. 1, pp. 49–63, 2009.

[12] A. V Olver, “Gear lubrication-a review,” *Proc. Inst. Mech. Eng. part J J Eng. Tribol.*, vol. 216, no. October 2001, pp. 255–267, 2002.

[13] H. Z. Jean Frene, Mihai Arghir, “Regimes of lubrication in lubricated contacts,” *Int. J. Surface Sci. Eng.*, vol. 4, no. 2, 2010.

[14] R. Errichello., “The Lubrication of Gears - Part II,” *Gear Technol.*,no.May, pp. 18–22, 1991.

[15] M. Sosa, "Running-in of gears-surface and efficiency transformation," PhD thesis, Royal Institute of Technology, Stockholm, 2017.

[16] A. Clarke, H. P. Evans, and R. W. Snidle, “Understanding micropitting in gears,” *Proc. Inst. Mech. Eng. Part C J. Mech. Eng. Sci.*, vol. 230, no. 7–8, pp. 1276–1289, 2015.

[17] I. V Kragelsky, M. N. Dobychin, and V. S. Kombalov., “Running-in and equilibrium and roughness,” *Friction and Wear*, Elsevier, 1982, pp. 297–316.

[18] J.D.Summer-Smith, *An introductry guide to industrial tribology*. UK: John Wiley and Sons Ltd, 1994.

[19] P. J. Blau and R. Komanduri, “Friction and wear transitions of materials: Break-in, Run-in, and Wear-in,” *J. Eng. Mater. Technol.*, vol. 112, no. 2, p. 254, 1990.

[20] S. M. Hsu, R. G. Munro, M. C. Shen, and R. S. Gates, “Boundary lubricated wear,” in

Wear - Materials, Mechanisms and Practice, England: John Wiley & Sons Ltd, 2014, pp. 37–70.

[21] R. Ismail, M. Tauviqirrahman, and D. J. Schipper, Topographical change of engineering Surface due to Running-in of Rolling Contacts, Netherlands: University og Twente, 2013.

[22] M. P. Cavatorta and C. Cusano, "Running-in of aluminum / steel contacts under starved lubrication Part I . Effects on scuffing," *Wear*, vol. 242, pp. 133–139, 2000.

[23] A. Stratmann, C. Hentschke, and G. Jacobs, "Formation of anti-wear films in Rolling bearings due to run-in procedures," in *Proceedings of the World Tribology Congress*, 2013, no. september, 2013, pp. 1–4.

[24] M. Mehdizadeh, S. Akbarzadeh, K. Shams, and M. M. Khonsari, "Experimental investigation on the effect of operating conditions on the running-in behavior of lubricated elliptical contacts," *Tribol. Lett.*, vol. 59, no. 1, p. 6, 2015.

[25] D. Flamand, L. Flamand, and D. Berthe., "Running-in of lubricated Hertizan contacts," in *The running-in process in tribology, proceedings of the 8th Leeds-Lyon Symposium on Tribology*, no. September, 1982, pp. 58–61.

[26] W. Wang, P.L. Wong, and Z. Zhang "Experimental study of the real time change in surface roughness during running-in for PEHL contacts," *Wear*, vol. 244, pp. 140–146.

[27] C. C. Chou, and J.F. Lin., "Tribological effects of roughness and running-in on oil-lubricated line contacts," *Proc. Inst. Mech. Eng. Part J, J. Eng. Tribol.*, vol. 211, no. 3, pp. 209–222, 1997.

[28] J. Sugimura, T. Watanabe, and Y. Yamamoto, "Effects of surface roughness pattern on the running-In process of rolling/sliding contacts," *Tribol. Ser.*, vol. 27, no. C, pp. 125–137, 1994.

[29] S. Andersson, "Initial wear of gears," *Tribol. Int.*, vol. 10, no. 4, pp. 206–210, Aug. 1977.

[30] S. Sjöberg, S. Bjorklund, and U. Olofsson, "The influence of manufacturing method on the running-in of gears," *Proc. Inst. Mech. Eng. Part J J. Eng. Tribol.*, vol. 225, no. 10, pp. 999–1012, 2011.

[31] V. Moorthy and B. A. Shaw, "An observation on the initiation of micro-pitting damage in as-ground and coated gears during contact fatigue," *Wear*, vol. 297, no. 1–2, pp. 878–884, 2013.

[32] B. R. Höhn, P. Oster, and S. Emmert., "Micropitting in case-carburized gears - FZG Micropitting Test," in *International Conference on Gears*, 1996, pp. 331–334.

[33] R. Errichello, "Morphology of Micropitting," *Gear Technol.*, no. December, pp. 74–81, 2012.

[34] A. V. Olver, "Paper XIII(iii)-Micropitting and asperity deformation," *Dev. Numer. Exp. Methods Appl. to Tribol.*, pp. 319–323, Jan. 1984.

[35] A. Oila and S. J. Bull, "Assessment of the factors influencing micropitting in rolling/sliding contacts," *Wear*, vol. 258, no. 10, pp. 1510–1524, 2005.

[36] S. Li and A. Kahraman, "Micro-pitting fatigue lives of lubricated point contacts: Experiments and model validation," *Int. J. Fatigue*, vol. 48, pp. 9–18, 2013.

[37] Y. Ariura, T. Ueno, and T. Nakanishi, "An investigation of surface failure of surface-hardened gears by scanning electron microscopy observations," *Wear*, vol. 87, no. 3, pp. 305–316, Jun. 1983.

[38] R. D. Britton, C. D. Elcoate, M. P. Alanou, H. P. Evans, and R. W. Snidle, “Effect of surface finish on gear tooth friction,” *J. Tribol.*, vol. 122, no. 1, p. 354, 2000.

[39] M. A. Muraro, F. Koda, U. Reisdorfer Jr., and C. H. da Silva, “The influence of contact stress distribution and specific film thickness on the wear of spur gears during pitting tests,” *J. Brazilian Soc. Mech. Sci. Eng.*, vol. 34, no. 2, pp. 135–144, 2012.

[40] L. Winkelmann, O. El Saeed, and M. Bell, “The effect of superfinishing on gear micropitting,” *Gear Technol.*, no. April, pp. 60–65, 2009.

[41] J. Zhang and B. A. Shaw, “The effect of superfinishing on the contact fatigue of case carburised gears,” *Appl. Mech. Mater.*, vol. 86, pp. 348–351, 2011.

[42] T. L. Krantz, M. P. Alanou, H. P. Evans, and R. W. Snidle, “Surface fatigue lives of case-carburized gears with an improved surface finish,” *J. Tribol.*, vol. 123, no. 4, p. 709, 2001.

[43] V. Moorthy and B. A. Shaw, “Contact fatigue performance of helical gears with surface coatings,” *Wear*, vol. 276–277, pp. 130–140, 2012.

[44] A. Batista, A. Dias, J. Lebrun, C. Le Flour, and G. Inglebert, “Contact fatigue of automotive gears: Evolution and Effects of Residual Stresses Induced by Surface Treatments,” *Fatigue Fract. Eng. Mater. Struct.*, vol. 23, pp. 217–228, 2000.

[45] D. P. Townsend and E. V. Zaretsky, “Effect of shot peening on surface fatigue life of carburized and hardened AISI 9310 spur gears,” *Nasa Technical Paper. 2047*, 1988.

[46] A. Oila, B. A. Shaw, C. J. Aylott, and S. J. Bull, “Martensite decay in micropitted gears,” *Proc. Inst. Mech. Eng. Part J J. Eng. Tribol.*, vol. 219, no. 2, pp. 77–83, Jan. 2005.

[47] A. Oila and S. J. Bull, “Phase transformations associated with micropitting in rolling/sliding contacts,” *J. Mater. Sci.*, vol. 40, no. 18, pp. 4767–4774, 2005.

[48] M. R. Hoeprich, “Analysis of micropitting of prototype surface fatigue test gears,” *Tribotest*, vol. 7, no. 4, pp. 333–347, Jun. 2001.

[49] V. C. Venkatesh and R. Krishnamurthy, “On some aspects of metallurgical changes during gear pitting,” *Tribology*, vol. 6, no. 5, pp. 195–199, 1973.

[50] P. H. Winter and D. P. Oster, “Influence of lubrication on pitting and micropitting resistance of gears,” *Gear Technol.*, no. March, pp. 16–23, 1990.

[51] A. B. Cardis and M. N. Webster, “Gear oil micropitting evaluation,” *Gear Technol.*, vol. 17, no. 5, pp. 30–35, 2000.

[52] R. Martins and J. Seabra, “Micropitting performance of mineral and biodegradable ester gear oils,” *Ind. Lubr. Tribol.*, vol. 60, no. 6, pp. 286–292, 2008.

[53] D.J. Whitehouse, *Handbook of surface and nanometrology*. Bristol: Institute of physics publishing, 2003.

[54] D.J. Whitehouse, *Surfaces and their measurement*. London: Hermes Penton Ltd, 2002.

[55] E. S. Gadelmawla, M. M. Koura, T. M. A. Maksoud, I. M. Elewa, and H. H. Soliman, “Roughness parameters,” *J. Mater. Process. Technol.*, vol. 123, no. 1, pp. 133–145, 2002.

[56] I. C. Noyan and J. B. Cohen, “The nature of residual stress and its measurement,” in *Residual Stress and Stress Relaxation*, Boston, MA: Springer US, 1982, pp. 1–17.

[57] G. Krauss, “Residual Stresses, Distortion, and Heat Treatment,” in *Steels-Processing, Structure, and performance,* Ohio: ASM International, 2015.

[58] E. Kula, and V. Weiss, *Residual Stress and Stress Relaxation*, vol. 1. Boston: Springer, 1982.

[59] K. Funatani and N. P. Co, "Residual Stresses during Gear Manufacture," in *Handbook of Residual stress and Deformation of Steel*, Ohio: ASM International, 2002, pp. 437–458.

[60] P. M. Kelly, "Crystallography of martensite transformations in steels," in *Phase Transformations in Steels*, vol. 2, Elsevier, 2012, pp. 3–33.

[61] Nishiyama.Z, "Crystallography of Martensite," in *Martensitic Transformation*, Elsevier, 1978, pp. 14–134.

[62] H. Bhadeshia. and H. H. Robert., "Formation of martensite," in *steels Microstructure and Properties*, vol. 11, Elsevier, 2017, pp. 135–177.

[63] T. Maki, "Morphology and substructure of martensite in steels," in *Phase Transformations in Steels*, Elsevier Ltd, 2012, pp. 34–58.

[64] G. R. Speich and W. C. Leslie, "Tempering of steel," *Metall. Trans.*, vol. 3, no. 5, pp. 1043–1054, 1972.

[65] H. Bhadeshia and H. H. Robert., "The tempering of martensite," in *Steels Microstructure and Properties*, Elsevier, 2017, pp. 237–270.

[66] K.H. Jack, "Structural transformations in the tempering of high-carbon martensitic steels," *J. Iron steel Inst.*, vol. 169, pp. 26–36, 1951.

[67] Y. Hirotsu and S. Nagakura, "Crystal structure and morphology of the carbide precipitated from martensitic high carbon steel during the first stage of tempering," *Acta Metall.*, vol. 20, no. 4, pp. 645–655, 1972.

[68] S. Q. A. Rizvi, "Additives and additive chemistry," in *Fuels and Lubricants handbook: Technology, Properties, Performance and Testing*, West conshohocken, PA: ASM International, 2003, pp. 199–245.

[69] P. Freeman, "Lubrication, friction and wear," *Nasa Space Vehicle Design Criteria*, 1962.

[70] A. N. Suarez, "The behaviour of antiwear additives in lubricated rolling-sliding contacts," PhD thesis, Luleå University of Technology, Luleå, 2011.

[71] K. Matsumoto, "Surface chemical and tribological investigations of Phosphorous-containing lubricant additives," PhD thesis, ETH, Switzerland, 2003.

[72] D. A. Rigney and J. P. Hirth, "Plastic deformation and sliding friction of metals," *Wear*, vol. 53, no. 2, pp. 345–370, 1979.

[73] G. E. Dieter Jr, "Plastic deformation of single crystals," in *Mechanical Metallurgy*, New York: Tata McGraw-Hill Education, pp. 78–116.

[74] W. Hosford, "Slip and crystallographic textures," in *Mechanical behaviour of Materials*, Cambridge University Press, 2009, pp. 113–136.

[75] S. Suwas and N. P. Gurao, "Deformation textures," in *Crystallographic Texture of materials*, London: Springer, vol. 88, no. 2, 2008, pp. 151–177.

[76] N. E. Dowling, *Mechanical behavior of materials engineering methods for deformation, fracture, and fatigue*. Boston: Pearson, 2013.

[77] S. Jonsson, *Mechanical properties of Metals and Dislocation Theory from an Engineer's Perspective*, Stockholm: Royal Institute of Technology, 2010.

[78] M.Clemens, "Gear manufacturing methods-forming the teeth," *Geartechnology.Com*,

pp. 41–48, 1987.

[79] D. R. Houser, “The effect of manufacturing microgeometry variations on the load distribution factor and on gear contact and root stresses,” *Gear Technol.*,no. July, pp. 51–60, 2009.

[80] G. P. Cavallaro, T. P. Wilks, C. Subramanian, K. N. Strafford, P. French, and J. E. Allison, “Bending fatigue and contact fatigue characteristics of carburized gears,” *Surf. Coatings Technol.*, vol. 71, no. 2, pp. 182–192, 1995.

[81] D. H. Herring, “Gear heat treatment : The influence of materials and geometry,” no. April, pp. 35–40, 2004.

[82] J. R. Davis, "Steels for gear*s"in Carbon and Alloy Steels, Ohio: ASM International*, 1996.

[83] F.-R. Group, “Research project No.345 efficiency test,” Frankfurt: FVA, 2002.

[84] W. Zhou, R. P. Apkarian, and Z. L. Wang, “Fundamentals of scanning electron microscopy,” in *Scanning microscopy and nanotechnology*, Springer, pp. 1–40, 2007.

[85] J. Goldstein, D. Newbury, D.Joy, C. Lyman, P. Echlin, E. Lifshin, L.Sawyer, *Scanning Electron Microscopy and X-Ray Microanalysis*, Springer, 2003.

[86] D. B. Williams, and C. B. Carter, *Transmission electron microscopy A Text book for Materials Science*. Springer, 2003.

[87] A.D. Roming, Jr., “Analytical transmission electron microscopy,” in *Metals Handbook, Vol 10, Ohio: ASM*, 1986.

[88] M.E. Fitzpatrick, A.T. Fry, P.Holdway, F.A. Kandil, J. Shackleton and L. Suominen,“Determination of residual stresses by X-ray Diffraction-Issue 2,” Feb. 2005.

[89] P. S. Prevéy, “X-ray diffraction residual stress techniques,” in *Meals Handbook, Vol.10, Ohio:ASM*, 1986, pp. 380–392.

[90] P. J. L. Fernandes and C. McDuling, “Surface contact fatigue failures in gears,” *Eng. Fail. Anal.*, vol. 4, no. 2, pp. 99–107, 1997.

[91] V. Hauk, “Lattice strain measuring techniques,” in *Structural Residual Stress Analysis by Nondestructive Methods*, Amsterdam: Elsevier, 1997, pp. 66–115.

[92] 1-7 ASTM E975-03, “Standard pratctice for X-ray determination of retained austenite in steel with near random crystallographic orientation.”

[93] J. F. Watts and J. Wolstenholme, *An introduction to surface analysis by XPS and AES*, UK: John Wiley & Sons, Ltd, 2003.

[94] G. Parrish, “Postcarburizing mechanical treatments,” in *Carburizing: Microstructures and Properties*, Ohio: ASM International, 1999, pp. 199–225.

[95] V. Vasilio, C. Gorgelsad, and K. Fritz, “Influence of the residual stresses induced by hard finishing processes on the running behaviour of gears,” *American gear manufacturers association fall technical meeting*, no. September, 2009.

[96] V. F. da Silva, L. F. Canale, D. Spinelli, W. W. Bose-Filho, and O. R. Crnkovic, “Influence of retained austenite on short fatigue crack growth and wear resistance of case carburized steel,” *J. Mater. Eng. Perform.*, vol. 8, no. 5, pp. 543–548, 1999.

[97] M. Andersson, M. Sosa, and U. Olofsson, “The effect of running-in on the efficiency of superfinished gears,” *Tribol. Int.*, vol. 93, pp. 71–77, 2016.

[98] H. K. Tönshoff, T. Friemuth, and C. Marzenell, “Properties of honed gears during

lifetime," *CIRP Ann. - Manuf. Technol.*, vol. 49, no. 1, pp. 431–434, 2000.

[99] B. A. Shaw, F. B. Abudaia, and J. T. Evans, "Characterization of retained austenite in case carburized gears and its influence on fatigue performance," *Gear Technol.*, vol. 1, no. May, pp. 12–16, 2003.

[100] M. Sosa, U. Sellgren, S. Björklund, and U. Olofsson, "In situ running-in analysis of ground gears," *Wear*, vol. 352–353, pp. 122–129, 2016.

[101] X. Zhang, N. Hansen, A. Godfrey, and X. Huang, "Structure and strength of sub-100 nm lamellar structures in cold-drawn pearlitic steel wire," *Mater. Sci. Technol. (United Kingdom)*, vol. 34, no. 7, pp. 794–808, 2018.

[102] X. Zhang, A. Godfrey, X. Huang, N. Hansen, and Q. Liu, "Microstructure and strengthening mechanisms in cold-drawn pearlitic steel wire," *Acta Mater.*, vol. 59, no. 9, pp. 3422–3430, 2011.

[103] X. Huang, S. Morito, N. Hansen, and T. Maki, "Ultrafine structure and high strength in cold-rolled martensite," *Metall. Mater. Trans. A Phys. Metall. Mater. Sci.*, vol. 43, no. 10, pp. 3517–3531, 2012.